Construction and Evaluation of Gas Feed-in System, Electrodes and Gas Exhaustion System applied to Low Pressure Plasma Coating Processes

Dissertation

approved for the degree of

Doctor in Engineering

– Dr.-Ing –

Faculty of Production Engineering

Department of Production Engineering

University of Bremen

by

Gustavo Simiema de Freitas Barbosa

Bremen, June 2018

Konstruktion und Evaluierung von Gaszuführungsystemen, Elektroden und Gasabsaugungssystemen für Niederdruckplasmabeschichtungsanlagen

Vom Fachbereich Produktionstechnik

der

Universität Bremen

zur Erlangung des Grades
Doktor-Ingenieur
Genehmigte

Dissertation

von

Gustavo Simiema de Freitas Barbosa

Bremen, Juni 2018

1. Referee

Prof. Dr. rer. nat. Bernd Mayer

Universität Bremen - Faculty of Production Engineering (FB4)

Wiener Straße 12 | 28359 Bremen - Germany

2. Referee

Prof. Dr. Jürgen Meichsner

Institute of Physics of the University of Greifswald

Felix-Hausdorff-Str- 6| 17489 Greifswald – Germany

Dissertation Defense Date: 25.06.2018

Eidesstattliche Versicherung

Hiermit versichere ich, Gustavo Simiema de Freitas Barbosa, dass ich diese Arbeit ohne unerlaubte fremde Hilfe angefertigt habe, keine anderen als die von mir angegebenen Quellen und Hilfsmittel benutzt habe und die den benutzten Werken wörtlich oder inhaltlich entnommenen Stellen als solche kenntlich gemacht habe.

____________________________	____________________________
Ort, Datum	Unterschrift

Abstract

Plasma polymerization is a technique used to deposit functional thin film coatings (nanometer until some micrometer thickness) on different materials surface. The thin film coating is deposited directly from a partially ionized precursor gas subjected to the effect of the plasma onto the surface of the substrate, which is placed in a low-pressure plasma chamber. This coating process regarding the achievement of the desired properties is in general well developed. The challenge is based on the scaling up process in respect to a large volume coater. Concerning this aspect only very few and rough information are available for constructors in respect to lay out of low-pressure plasma coater with the aim to achieve homogeneous coating deposition rate as well as homogeneous coating properties over all the products surfaces in contact with the plasma.

The aim of the present research work is mainly to investigate the potential of guiding the gas flow inside a large volume plasma polymerization-system and to investigate how this gas guiding directly influences the coating homogeneity as well as the coating properties. Thereby the creation of construction guidelines to support future developments under the frame of low-pressure plasma technology is part of the task.

To achieve this purpose, gas feed-in system, gas exhaustion system and electrode geometry were investigated. Taking into consideration that experimentally the local gas flow behavior cannot be directly measured inside a PECVD system computational fluid dynamics (CFD) simulations were carried out using the commercial software Ansys Fluent 16.0® to investigate the gas flow behavior. Additionally, to get more knowledge about the electric field created by the RF-electrode in combination with the powered electrode, electrostatic simulations were done using the commercial software Ansys Maxwell 16.0®.

Gas flow simulations showed clearly that the gas exhaustion system influences the local gas flow much more (in intensity and range) in comparison to the gas feed-in system. In this regard, a perforated polymeric plate was developed to reduce the influence of the gas exhaustion system and it was named under the frame of this work as “Baffle Plate”. Coating experiments exhibited a clear improvement in the coating deposition homogeneity due to the installation of the Baffle Plate.

The construction guidelines for gas feed-in systems and gas exhaustion systems were defined using gas flow simulations. To evaluate the simulation results, a non-uniformity coefficient was defined to define a construction border. For this work, the construction border was established at non-uniformity coefficient equals 5%. It means that construction layout which leads to non-uniformity coefficient higher than 5% will be not recommended for this application. From the analyzed parameters of the gas feed-in system, the pipe section area was the most relevant influencing the homogeneity of gas distribution. Regarding the gas exhaustion system, the simulation results showed that the distance between the Baffle Plate and the top of the chamber has a huge influence in the homogeneity of the gas exhaustion.

Coating experiments were performed to correlate the distribution of the coating deposition rate in addition to the coating properties with the local gas velocity and the local electric field. Therefore, the construction guidelines must be supplemented with hints how to handle the influence of the walls (chamber, electrodes and product holder systems).

The selected construction guidelines revealed to be useful for the development and construction of a new low-pressure plasma chamber of about 3 m^3. Following the knowledge acquired from this research work the realized coating showed on an area of 2 m^2 a standard deviation of the deposition rate less than 17%. With this it had been demonstrated, that especially for large volume PECVD-systems following the rules of the construction guidelines is essential.

Keywords: Low-pressure plasma; Plasma polymerization; Scale-up; Coating homogeneity; Construction guideline; Gas velocity; Computation fluid dynamics; Deposition rate;

Zusammenfassung

Die Plasmapolymerisation ist eine Verfahrenstechnik, die verwendet wird, um funktionelle Dünnfilmbeschichtungen (wenige Nanometer bis hin zu einigen Mikrometern Dicke) auf verschiedenen Materialoberflächen aufzubringen. Dabei wird die Beschichtung direkt aus der Gasphase, einem teilweise ionisierten Precursorgas, auf der Oberfläche des Substrats, dass in einer Niederdruckplasmakammer angeordnet ist, abgeschieden. Derartige Beschichtungsprozesse sind gut entwickelt und erlauben es bestimmte Schichteigenschaften gezielt zu erreichen. Die Herausforderung besteht in der Aufskalierung des Beschichtungsprozesses für großvolumige bzw. großflächige Anlagen. Für die Konstruktion von derartigen Niederdruck-Plasmabeschichtungsanlagen gibt es nur wenige, allgemeine Informationen für den Konstrukteur, wie er vorzugehen hat, um eine homogene Schichtabscheidungsrate sowie homogene Schichteigenschaften über alle Produktoberflächen zu erreichen.

Primäres Ziel der vorliegenden Forschungsarbeiten ist es, dass Potential von technischen Systemen zur Beeinflussung des Gasflusses in großvolumigen Plasma¬polymerisations¬anlagen zu untersuchen. Dabei liegt der Fokus auf deren Einfluss auf die Schichtabscheidehomogenität und der Homogenität der Schichteigenschaften. Hieraus sind Konstruktionsrichtlinien für zukünftige Entwicklungen im Rahmen der Niederdruckplasma¬technologie abzuleiten.

Um das Ziel zu erreichen, wurden das Gaszufuhrsystem, die Gasabsaugung und die Elektrodengeometrie untersucht. Dabei ist zu berücksichtigen, dass das lokale Gasströmungsverhalten in einem PECVD-System experimentell nicht direkt gemessen werden kann. Aus diesem Grund zur Untersuchung des Gasströmungsverhaltens CFD-Simulationen (Computational Fluid Dynamics) mit der kommerziellen Software Ansys Fluent 16.0® durchgeführt. Um ergänzende Informationen über das elektrische Gleichspannungsfeld der HF-Elektrode zu erhalten wurden Elektrostatiksimulationen mit der kommerziellen Software Ansys Maxwell 16.0® durchgeführt.

Die Gasflusssimulationen zeigten deutlich, dass das Gasabsaugungssystem den lokalen Gasfluss in einem großvolumigen Reaktor viel stärker (in der Intensität und der Reichweite) beeinflusst, als dass Gaszuführungssystem. Daher wurde ein neuartiges Absaugsystem in Form einer perforierte Polymerplatte entwickelt, um den Einfluss der Gasabsaugung zu homogenisieren. Sie wird im Rahmen dieser Arbeit als "Baffle-Plate"

bezeichnet. Beschichtungsexperimente zeigen mit dieser Vorrichtung eine deutliche Verbesserung der Beschichtungshomogenität.

Die Konstruktionsrichtlinien für das Gaszuführungssystem und das Gasabsaugungssystem wurden mit Hilfe von Gasfluss-Simulationen vorgenommen. Um eine Konstruktion bewerten zu können, wurde ein Uneinheitlichkeitskoeffizient definiert. Für diesen Koeffizienten wurde für diese Arbeit eine Konstruktionsgrenze (hier 5%) festgelegt. Dies bedeutet, dass das Konstruktionslayout, dass zu einem Ungleichförmigkeitskoeffizienten von mehr als 5% führt, für diese Anwendung nicht empfohlen wird. Für das Gaseinspeisungssystem war von den analysierten Parametern die Rohrquerschnittsfläche die relevanteste Größe, die die Homogenität der Gasverteilung beeinflusste. In Bezug auf die Gasabsaugung zeigten die Simulationsergebnisse, dass der Abstand zwischen dem Baffle-Plate und dem oberen Teil der Kammer einen großen Einfluss auf die Homogenität der Gasabsaugungsvorrichtung hat.

Um die Verteilung der lokale Abscheidungsrate sowie der Beschichtungseigenschaften mit der lokalen Gasgeschwindigkeit und dem lokalen elektrischen Feld zu korrelieren wurden Beschichtungsexperimente durchgeführt. Daraufhin wurden die Konstruktionshinweise um Angaben zum Umgang mit den Wänden (Kammerwänden, Elektroden und Warenhaltesysteme) ergänzt.

Die erstellten Konstruktionsrichtlinien erwiesen sich bereits als Nützlich bei der Entwicklung und Auslegung einer neuen Niederdruck-Plasmaanlage mit Volumen von ca. 3 m³. Durch die Anwendung der Erkenntnisse aus dieser Forschungsarbeit konnte die Beschichtung nicht nur übertragen werden, sondern es wurde auf einer Fläche von ca. 2 m² eine Standardabweichung der Abscheidungsrate von weniger als 17% realisiert. Damit konnte demonstriert werden, dass insbesondere für großvolumige PE-CVD – Anlagen die Befolgung der Konstruktionsrichtlinien von hoher Bedeutung ist.

Stichwörter: Niederdruckplasma; Plasmapolymerisation; Aufskalierung; Beschichtungshomogenität; Konstruktionsrichtlinien; Gasgeschwindigkeit; Gasfluss-Simulation; Abscheiderate

Publication List

Published

(a) Barbosa, Gustavo Simiema de Freitas, Vissing K., Mayer B. (2016) Creation and Evaluation of Construction Guidelines Using CFD for Low Pressure Plasma Gas Feed-in Systems to Homogenize the Precursor Gas Flow. OJFD;06(04):391–405

(b) Barbosa, Gustavo Simiema de Freitas, Vissing K., Mayer B. (2018) Introduction of a New Baffle-Plate Concept to Control the Gas Flow Behavior in a Large Volume PECVD Chamber. OJFD;08, 141-160

Table of Contents

Abstract .... **V**

Zusammenfassung .... **VII**

Publication List .... **IX**

Table of Contents .... **X**

List of Abbreviations .... **XII**

List of Figures .... **XIII**

List of Tables .... **XVII**

1. Motivation and Objective **1**

1.1. Motivation 1

1.2. Objective 3

2. Theoretical part **4**

2.1. Plasma Polymerization 4

2.1.1. Organosilicon plasma coating 5

2.2. Capacitive coupled radio frequency (CCRF) plasmas 7

2.2.1. Sheath formation 8

2.2.2. Geometry of a RF-Discharge device 10

2.3. Coating properties 15

2.4. Coating characterization 16

2.4.1. Reflectometry analysis for the measurement of coating thickness 17

2.4.2. Nanoindentation 18

2.4.3. Contact angle measurements 21

2.5. Plasma Modelling 25

2.5.1. Computational fluid dynamics (CFD) 25

2.5.1.1. Governing Equations 27

2.5.1.2. Knudsen number 28

2.5.2. Electrostatics 29

3. Simulation and Experimental Part 32

3.1. Gas feed-in system 33

3.1.1. CFD simulation 37

3.1.2. Experimental pressure measurements 40

3.1.3. Results and Discussion 41

3.2. Gas exhaustion system 48

3.2.1. CFD Simulation 53

3.2.2. Experiment with installed Baffle Plate 67

3.2.3. Electric field Simulation 73

3.3. Electrode assembly 76

3.3.1. CFD simulation 78

3.3.2. Electric field simulation 80

3.3.3. Experiments 81

4. Construction of a new low-pressure plasma chamber 86

4.1.1. CFD simulation 90

4.1.2. Electric field simulation 92

4.1.3. Experiment 92

5. Conclusions 96

6. Outlook 103

7. Acknowledgements 105

8. References 106

List of Abbreviations

Abbreviation	Definition
AFM	Atomic Force Microscope
AOES	Actinometric optical emission spectroscopy
CALC	Calculated
CCP	Capacitively Coupled Plasmas
CCRF	Capacitive coupled radio frequency
CFD	Computational Fluid Dynamics
DC	Direct-current
EEDF	Electron energy distribution function
EXP	Experimentally measured
FTIR	Fourier transform infrared spectroscopy
GC-MS	Gas chromatography with mass spectrometric detection
HMDSO	Hexamethyldisiloxane
PDE	Partial Differential Equation
PECVD	Plasma Enhanced Chemical Vapor Deposition
RF	Radio Frequency
SFE	Surface Energy
TEOS	Tetraethoxysilane
TMOS	Tetramethoxysilane
TMS	Trimethylsilane
XPS	X-Ray Photoelectron Spectroscopy

List of Figures

Figure 1 Potential species for thin film coating formation. Reproduced from[17] 4

Figure 2 Deposition mechanism of HMDSO with different O_2/HMDSO ratio. Adapted from [29–31] 6

Figure 3 Maxwellian Electron Energy Distribution Functions (EEDF) for plasmas of different average electron energy. Reproduced from [16].. 7

Figure 4 Schematic of the sheath and pre-sheath adjacent to a surface in contact with a plasma phase. Adapted from [16] 10

Figure 5 Illustrative averaged potentials and instantaneous plasma potentials V_p(t) (solid curves) and excitation electrode voltages V(t) (dashed curves), assuming purely capacitive RF sheath behavior, for three different capacitively coupled excitation electrodes geometries. Adapted from [41,42]. 12

Figure 6 Illustration of the different sheath length for the case with asymmetric electrode, which the powered electrode has the smallest area in comparison to the grounded electrode 13

Figure 7 Sketch of the low-pressure plasma chamber used for this thesis 14

Figure 8 Ocean Optics NanoCalc 2000. Reproduced from [58] 18

Figure 9 Typical load–displacement curve. Reproduced from [60]. 19

Figure 10 Deformation pattern of an elastic–plastic material during and after indentation. Reproduced from [60] 20

Figure 11 Measuring head used for the hardness measurements 21

Figure 12 Illustration of contact angles formed by sessile liquid drops on a smooth homogeneous: Reproduced from [64] 22

Figure 13 Representation of the surface tension caused by the unbalanced forces of liquid molecules at the surface. Reproduced from [64] 23

Figure 14 Gas flow regime based on the Knudsen number.. 28

Figure 15 Examples of electric fields in different situations. Reproduced from [90]. 30

Figure 16 Small chamber used for LPCVD (Low Pressure Chemical Vapor Deposition) developed by Applied Mateirals,Inc. Reproduced from [96] 33

Figure 17 Spargers for bubble column reactor: (A) sieve plate sparger; (B) multiple ring sparger; (C) spider; (D) pipe sparger. Adapted from [97,98] 34

Figure 18 Eligible gas feed-in configurations and desired requirements 35

Figure 19 a) Gas feed-in distributor model under analysis, b) Gas feed-in distributor position inside the PECVD chamber. ... 36
Figure 20 Pipe profiles under analysis (front view) ... 38
Figure 21 System model with XY symmetry plane... 39
Figure 22 Pressure measurement details: (a) Sketch of the pipe with measurement position (b) Pipe connection with vacuum gauge (view from inside the chamber) (c) Handheld vacuum gauge ... 41
Figure 23 Influence of the pipe section area in the distribution homogeneity (a) Gas flow distribution through holes and (b) Non-uniformity coefficient obtained for the different pipe section values considered. The results are shown via the points; the lines connecting the points in the plot are only to support guiding the eyes and are not modelled fits. ... 42
Figure 24 Pressure contour and velocity contour a) 10 mm x 10 mm b) 30 mm x 30 mm.. 44
Figure 25 Influence of different parameters on the homogeneity of gas flow distribution ... 45
Figure 26 Comparison of pressure values obtained through experiments and simulations (a) & (b) Pipe section 10 mm x 10 mm; (c) & (d) Pipe section 30 mm x 30 mm ... 47
Figure 27 Gas simulation result showing the two dissimilar influence zones of the gas feed-in and of the gas exhaustion ... 49
Figure 28 (a) Samples used in the experiment (b) Experimental setup ... 50
Figure 29 Coating deposition rate distribution (a) top plane (b) middle plane (c) bottom plane ... 52
Figure 30 Average of deposition rate - Experiment current setup ... 53
Figure 31 Model of the experiment setup (a) Isometric view (b) Front view (c) isometric view of a quarter of the model ... 54
Figure 32 Gas simulation results of the experiment- Current setup ... 56
Figure 33 Eligible gas exhaustion configurations and desired requirements ... 58
Figure 34 Baffle plate model a) radial distribution b) linear distribution ... 59
Figure 35 Gas flow simulation results for two different baffle plates assembled (a) radial distribution of the holes (b) linear distribution of the holes ... 60
Figure 36 (a) Pressure contour [simulation] (b) Scheme of the low-pressure chamber showing the positions where the pressure was measured ... 61

Figure 37 Comparative of calculated and measured pressure values (a) Pressure inside the low-pressure chamber (b) Pressure in the gas exhaustion (c) Pressure difference between the inside chamber and the gas exhaustion 62

Figure 38 Representation of the low-pressure plasma chamber with different distances between the Baffle Plate and the top chamber 63

Figure 39 Influence of the distance from the Baffle Plate to the top of the chamber on the non-uniformity coefficient. The results are shown via the points; the lines connecting the points in the plot are only to support guiding the eyes and are not modelled fits. 64

Figure 40 Gas flow simulation results showing pressure contour and velocity contour for two different distances between Baffle Plate and top of the chamber 65

Figure 41 Influence of different parameters in the homogeneity of the gas exhaustion through the holes of Baffle Plate The results are shown via the points; the lines connecting the points in the plot are only to support guiding the eyes and are not modelled fits. 66

Figure 42 Scheme of the experiment setup with the baffle plate installed 68

Figure 43 Detail of one hole of the Baffle Plate a) just the Baffle Plate b) Baffle Plate direct in contact with the perforated grid 68

Figure 44 Gas simulation results of the experiment- Current setup with Baffle Plate installed 69

Figure 45 Comparative of coating deposition rate with and without the Baffle Plate installed 71

Figure 46 Comparative of the average of deposition rate - Experiment current setup and with Baffle Plate installed 72

Figure 47 Comparative average of the surface energy [Wu method] – With and without Baffle Plate 72

Figure 48 Electric field calculation results for the current setup 75

Figure 49 Scheme of the experiment with one additional electrode (sides open) 76

Figure 50 Scheme of the experiment with one additional electrode (sides closed) 77

Figure 51 Gas flow simulation results – Experiment Metallic Plate open sides (a) XY plane (b) ZY plane 78

Figure 52 Gas flow simulation results – Experiment Metallic Plate closed sides (a) XY plane (b) ZY plane 79

Figure 53 Electric field calculation results for the Experiment - Metallic Plate (a) Plane XZ (side view) (b) Plane YZ (front view) (c) Plane XY (top view) 80
Figure 54 Setup of the experiment - Metallic Plate (a) open sides (b) closed sides................ 82
Figure 55 Coating deposition rate distribution (a) open sides (b) closed sides....................... 83
Figure 56 Image of the coating process – Metallic plate with closed sides, showing local plasma concentration on the top corners.. 84
Figure 57 Comparative average (a) deposition rate (b) surface energy.................................. 85
Figure 58 Plain metallic product placed on a Polycarbonate-holder...................................... 86
Figure 59 Model of the gas feed-in system.. 87
Figure 60 (a) Model of the low-pressure plasma chamber with triangular shape RF-Electrode (b) Electric field simulation for the triangular shape RF-electrode... 88
Figure 61 Model of the trapeze RF-electrode.. 88
Figure 62 Model of the Baffle Plate 89
Figure 63 Model of the complete low-pressure plasma chamber 90
Figure 64 Gas flow simulation – New low-pressure plasma chamber (a) gas streamlines b) velocity contour (middle plane) (c) velocity contour on product plane 91
Figure 65 Electric field simulation results for the new low-pressure plasma chamber model92
Figure 66 Setup of the experiment – One product for each side of the trapeze electrode.... 93
Figure 67 Coating deposition rate distribution (a) left side (b) right side 93
Figure 68 Coating thickness results for both plain products 94
Figure 69 Surface energy results for both plain products 95
Figure 70 Elastic modulus results for both plain products 95

List of Tables

Table 1 Coating process used.. 16

Table 2 Pressure range values in vacuum technology [88]... 29

Table 3 Pipe technical layout under simulation analysis 38

Table 4 Parameters used for experimental and simulation approach 39

Table 5 Boundary conditions 40

Table 6 Knudsen number using 200 sccm of N_2 for two different pipe section areas:

6 mm x 6 mm and 30 mm x 30 mm.. 46

Table 7 Boundary conditions for the gas flow simulation of the experiment 55

Table 8 Baffle Plate technical layout under simulation analysis... 64

1. Motivation and Objective

1.1. Motivation

Plasma polymerization is a thin film coating technique used for the modification of surface properties of different materials, e.g. metals, polymers and composites [1]. For instance, tailored coatings permit the enhance of mechanical, chemical, electrical and optical properties of surfaces [2–6]. Therefore, this technique is very useful for different range of industrial fields, such as aircraft, aerospace, automotive, packaging, food, textile and medical devices.

The formation of the functional thin film coatings can be achieved through different processes, such as chemical vapor deposition, sputtering and plasma enhanced chemical vapor deposition (PECVD) [7]. Concentrating on the PECVD processes, the substrate is placed in a low-pressure chamber supplied with precursor gases and subjected to the effects of the plasma discharge. Due to the plasma, the precursor gases are fragmented. Those fragments are able to react and form a thin film coating onto the surface of the substrate as well as on every surface positioned inside or near the plasma region [8]. Plasma parameters like pressure, precursor gas flow, discharge power, self-bias and at least reaction time are responsible for these film formations. Therefore, it is very important to control the gas velocity inside the plasma chamber, especially for processes with a low self-bias, to ensure a high deposition rate as well as good coating properties all over the products surface. The management of the gas flow inside the chamber is possible through the control of the gas feed-in and at least the gas exhaustion system. Especially for small plasma coaters (in semiconductor industry), some patents about this topic can be found [9–14]. They created different gas feed-in systems integrated to the electrode (called showerhead) for different applications. The opening area ratio and/or the hole density distribution over the plate area can be tailored to reach the desired coating properties. Furthermore, some gas feed-in solutions are established where tubes or perforated pipes are applied or even perforated rings [15]. Regarding the gas exhaustion, normally the gas is pumped out in most of the cases in a radial way.

Additionally, the local gas flow behavior and the local electric fields are also important parameters concerning deposition rate and coating performance. For instance, in

capacitive coupled plasmas (CCP) powered by radio frequency (RF) generator, lighter electrons will be accelerated much faster than heavy ions, gaining energy and heating up. Nevertheless, the ions and neutrals will remain close to ambient temperature. When the electrons are not in thermal equilibrium with the ions and neutral is called "Nonthermal plasma". The electrons with high energy can ionize and fragmentize the precursor gas producing ions, free electrons and radicals [16]. Since the electrons are much lighter than the ions, every surface in contact with the plasma will start to charge up negatively with respect to the plasma. The surfaces will continue to charge negatively until the electron flux is reduced by repulsion balancing the ions flux. It is important to keep in mind that, due to the potential difference between the plasma and the surface, an electric field accelerating the ions toward the surface is generated. Thus, the ions play an important role in the film coating formation [17,18]. Therefore, it is very important to control the electric field distribution inside the chamber to know how and where to place the products to be coated and also to understand how to build the electrodes in order to achieve high and homogeneous deposition rates as well as good coating properties.

The domain over the gas flow behavior and over the electric field distribution is even more challenging when the scaling up is desired either to process many products in one batch or to coat one part with larger dimensions. In this perspective, the design of the plasma chamber is crucial to achieve high and homogeneous deposition rates as well as good quality of the formed thin film. Hence, the gas exhaustion system, gas feed-in system and the electrodes must be carefully designed. From the state of the art, there are some patents issued regarding gas distribution systems for small plasma chambers for semiconductor applications [9,10,19,20]. However, concerning large volume plasma chambers, normally interesting in other industries, there is limited information either due to lack of knowledge or due to confidential issues. Especially for these cases, the improvement of the cost effectiveness is very important. It is expected that all products processed in one batch show the same surface properties and often also a homogeneous coating thickness distribution as well. Hence, the local gas flow behavior and the local electric field are key factors to enable the scaling up of plasma polymerization processes. Apart from the product geometry and the electrode design, there are two main influences on the gas flow distribution inside a large volume chamber: (i) gas feed-in system and (ii) gas exhaustion

system. They must be carefully designed to guarantee an evenly gas flow through the products and consequently accomplish reasonable coating properties.

As pointed out above the prediction of the gas flow behavior and the prediction of the electric field distribution inside the plasma chamber are of industrial and economic interests. Thus, a better understanding of the plasma chamber construction and its influence on the coating deposition rate is very important for future developments of new plasma polymerization systems. Therefore, the use of simulation tools in response to the gas flow and the electric field was planned. The simulation results were matched with the coating validation, e.g. surface energy, reflectometry and nanoindentation.

Taking into consideration all these aspects, my research guiding to this thesis focuses on the investigation of the influence of the gas feed-in system, gas exhaustion system and electric field distribution on the local deposition rate through simulations and practical experiments. Based on the knowledge acquired, general guidelines are presented. These can be useful for constructors and scientists, showing how to move forward by building gas feed-in, gas exhaustion systems and electrodes in respect to them.

1.2. Objective

This thesis focuses on the prediction of the gas flow behavior and the electric field distribution inside a low-pressure plasma chamber using simulation tools in agreement with coating experiments. The knowledge developed intends to support the construction of specific electrode configurations in combination with gas feed-in and gas exhaustion systems for low-pressure plasma polymerization applications. The following objectives were determined:

- Improve the scientific understanding of a large (~1m^3) low-pressure plasma chamber taking into consideration the gas flow along with the electric field to achieve homogeneous coating deposition rate as well as homogeneous coating properties
- Create guidelines for the construction of gas feed-in systems, gas exhaustion systems and electrodes systems to support future developments of large volume plasma coaters

2. Theoretical part

In section 2.1 a brief explanation about plasma polymerization showing the influence of the gas mixing ratio (O_2/HMDSO) on the properties of the deposited thin film coating was depicted. Section 2.2 describes the generation and sustenance of the plasma with focus on the applied method (Capacitive Coupled Radiofrequency), explaining the formation of the sheath region and the influence of the ratio of the powered electrode on the grounded electrode area on the formation of the self-bias. Section 2.3 describes the properties of the coating used in this thesis. Section 2.4 introduces different methods used in this thesis to characterize thin film coatings. Finally, section 2.5 describes the methods used for the performed simulations: Computational Fluid Dynamics (CFD) and Electrostatics.

2.1. Plasma Polymerization

Plasma polymerization is a useful technique to deposit polymeric thin films onto surfaces of different substrates, e.g. metals, polymers and composites, in order to enhance the surface properties under the stimulus of a plasma [18,21]. The plasma forms different species with unlike masses, kinetic energies and charges. Due to these differences, different thin film properties are generated due to different energies delivered to the surface. Michelmore and coauthors showed a very visible sketch of the potential species inside a plasma correlating with the electron energy, as depicted in Figure 1 [17]:

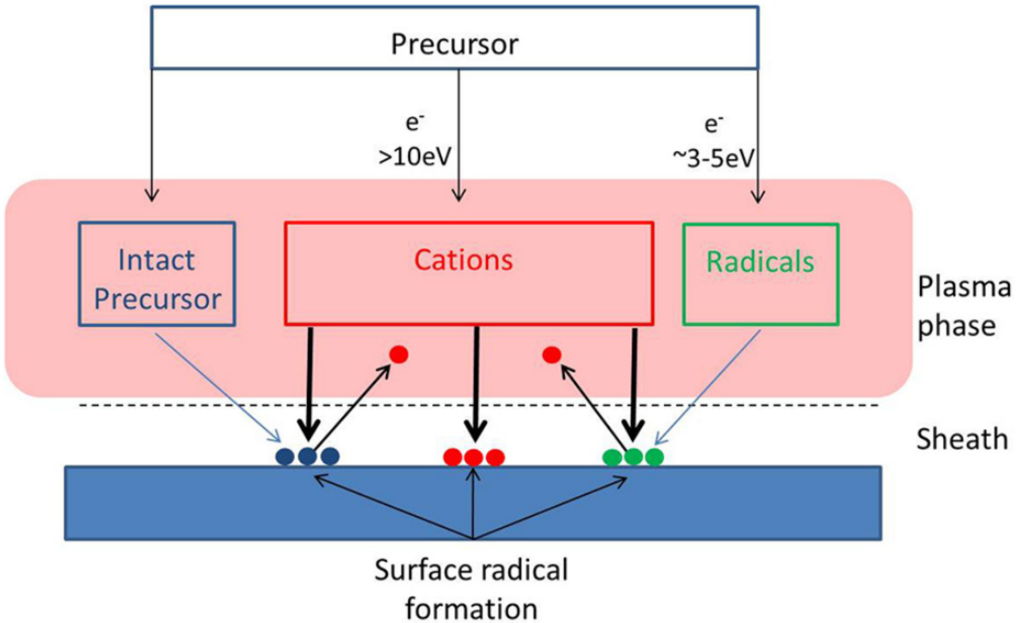

Figure 1 *Potential species for thin film coating formation. Reproduced from[17]*

Figure 1 shows that the ions play a main role in the formation of the thin film coating illustrated by the larger red box (cations) in comparison to the blue and green boxes (intact precursor and radicals respectively). This can be explained by the electric field constituted between the borders of the plasma and the surface. This electric field will accelerate the positive ions toward the surface with enough energy to start chemical reactions and thus grow the film coating. The region where the electric field forms the so-called sheath will be explained in more detail in chapter 2.2.

2.1.1. Organosilicon plasma coating

Currently, many organosilicon compounds are used as PE-CVD precursors instead of the hazardous silane (SiH_4), which is gaseous at room temperature. There is a variety of organosilicon precursors such as hexamethyldisiloxane (HMDSO), tetraethoxysilane (TEOS) and tetramethoxysilane (TMOS) [22–24]. Among them, HMDSO is most commonly used due to its high vapor pressure, low toxicity and low cost [25].

With the help of those precursors it is possible to create a lot of different coating properties (e.g. barrier coatings, corrosion protection coatings, primer coatings, easy-to-clean and release coatings) [8,26,27]. Noborisaka and coauthors [28] reported for example on the importance of the selection of the right precursor gas mixture for the coating formation. The appropriate mixture ratio of the precursor gases trimethylsilane and oxygen (TMS and O_2) was investigated to obtain polycarbonate films as alternative to conventional windows glasses. The results revealed that hardness and transparency properties could be tailored by changing the gas mixture ratio.

There are different diagnostic techniques already used to study organosilicon containing plasmas, such as Fourier transform infrared spectroscopy (FTIR), actinometric optical emission spectroscopy (AOES) and X-Ray Photoelectron Spectroscopy (XPS) showed in the work of Lamendola and coworkers [29]. Fracassi and coauthors applied a cold trap in the gas effluent and analyzed the by-products formed in plasmas fed with HMDSO, oxygen and argon using gas chromatography-mass spectrometry (GC-MS). Their findings, under the experimental conditions employed, indicated that the activation of HMDSO is mainly due to electron collisions instead of by reaction of oxygen. Nevertheless, the oxygen is responsible

for the control over the chemistry of the plasma [30]. The main conclusions of these works were schematized in Figure 2.

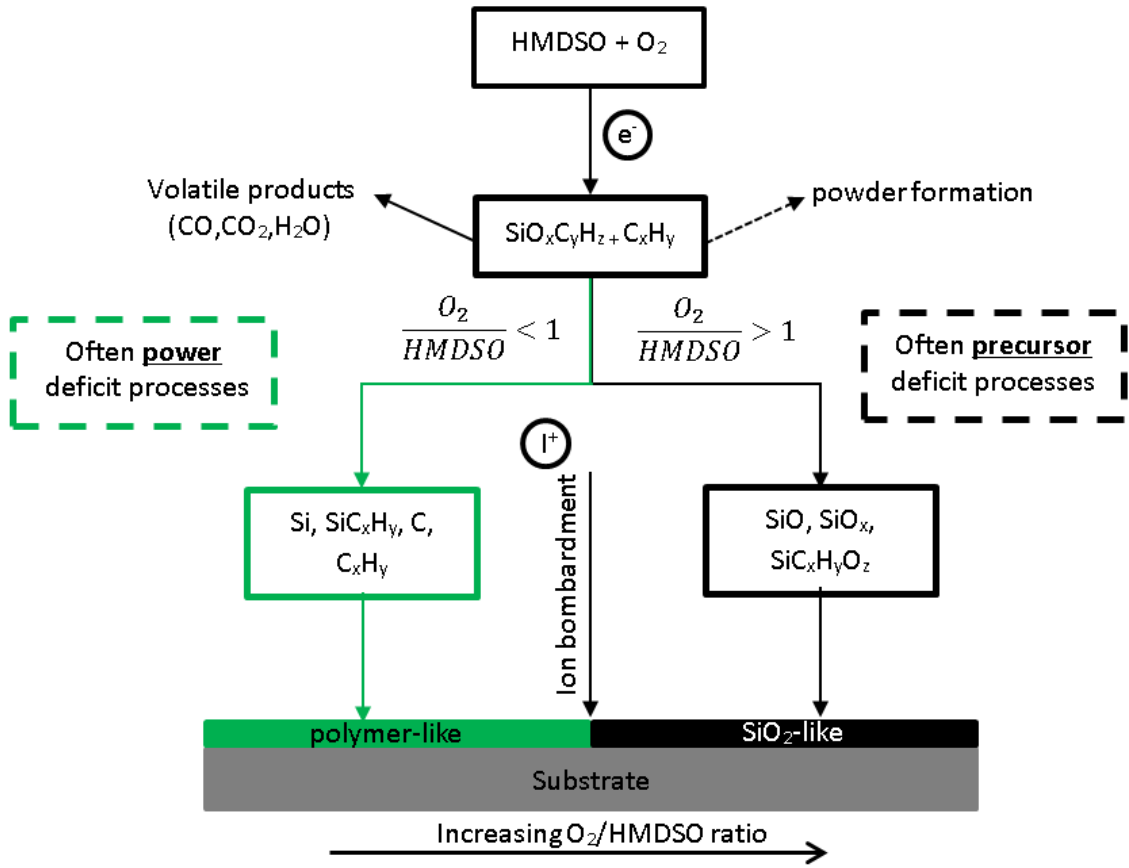

Figure 2 *Deposition mechanism of HMDSO with different O_2/HMDSO ratio. Adapted from [29–31]*

The fragmentation of the HMDSO molecule does not occur completely. The electrons gain energy from the RF electric field and, due to the collisions, they distribute this energy with other species in the plasma. Eventually, highly depending on the working pressure, powder can be formed because of the gas phase polymerization reactions. Considering the electron-molecule collision frequency constant, commonly named Maxwellian distribution, typical from the electron energy distribution function (EEDF) plots can be seen in literature, as depicted in Figure 3:

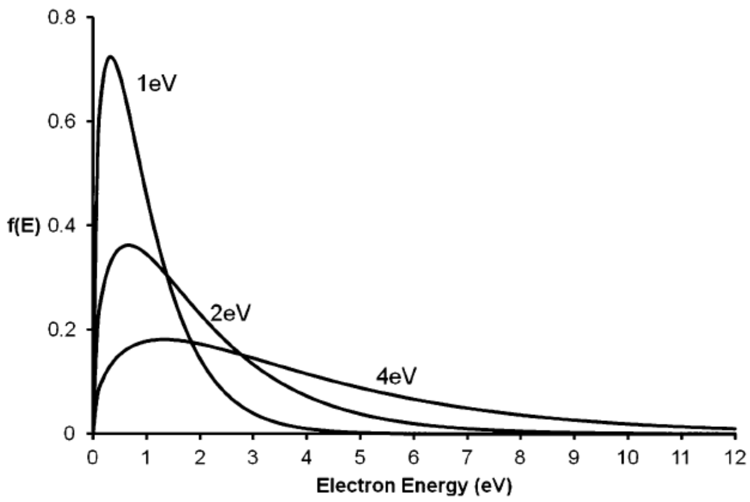

Figure 3 *Maxwellian Electron Energy Distribution Functions (EEDF) for plasmas of different average electron energy. Reproduced from [16]*

Figure 3 shows that, even in the case with an average electron temperature of 4 eV most of the electrons have an energy lower than 5 eV. It means that preferably Si-C (4.5eV) and C-H (3.6 eV) bonds will be broken since they exhibit weaker bonding energy than Si-O (8.3 eV) bonds. Therefore, the carbonated radicals and the formed methyl groups, depending on the composition of the feed gas, are directly deposited and they experience oxidation reactions or also reactions with hydrocarbons. The O_2/HMDSO ratio will rule the coating properties. If this ratio increases, the thin film coating will be more SiO_2-like. Bernd Jacoby showed on his doctoral dissertation the results of the XPS analysis of the samples coated with HMDSO as precursor gas changing the O_2 flow rate. He plotted the O/Si and C/Si ratios for different O_2 flow rates. He concluded that, by increasing the O_2 flow rate, the carbon content was reduced and the oxygen content increased [32].

2.2. Capacitive coupled radio frequency (CCRF) plasmas

Plasmas can be generated by different methods. The most widely used method is the electrical breakdown of a neutral gas in the presence of an external electric field [33]. Direct-current (DC) discharges, RF and microwave discharges are commonly employed to sustain the plasma.

A very usual configuration applied to PECVD process is the so-called capacitive coupled RF plasmas (CCRF) [34,35]. The CCRF system is driven by a RF power supply, usually combined with an impedance matching network, and both, in combination with the reactor

and electrodes, sustain the discharge. A range of frequencies can be used. The most often used frequency is 13.56 MHz, which is a fixed value in international standards. Normally the CCRF discharges operate at low pressure between 1 and 10^4 Pa; nevertheless it can also be applied at atmospheric pressure [36]. The main advantage of this system is the possibility to coat temperature sensitive materials and to build large and individual electrode systems.

2.2.1. Sheath formation

As already introduced in chapter 2.1, in the case of a surface in contact with the plasma, it will be bombarded with ions and electrons as described by David Bohm in 1949 [37]. The flux of each species will be unequal since electrons are lighter and hotter than positively charged ions. In this scenario, the flux of electrons to the surface is initially much higher than the flux of the ions. Therefore, the surface charges up to negative potential relative to the bulk plasma until a certain value, the electrical charge equilibrium is reached. At this point the surface will held a potential called “floating potential”, since the potential floats to a value enough to maintain an equal flux of positive and negative species. This value is usually about 10 Volts negative in comparison with the plasma [37]. The bulk plasma is normally at equipotential and is named “plasma potential”. The potential difference between the floating potential and the plasma potential is called “sheath potential”. This is the magnitude of the energy barrier which an electron must overcome to reach the surface. It is also the potential through which a positive ion is accelerated onto the surface.

Bohm showed that the presence of the surface in the plasma results in the formation of a sheath region adjacent to the surface where the density of charged particles decreases [37]. In fact, there are two distinct regions; the sheath, where the density of the positive ions (n_i) is higher than the density of electrons (n_e), and a pre-sheath, where the densities are the same but decrease slightly compared to the bulk plasma [17]. In this pre-sheath region, ions are accelerated. They enter the sheath at the Bohm velocity, u_b

$$u_b = \sqrt{\frac{kT_e}{m}}$$

where T_e is the electron temperature, k is Boltzmann’s constant and m is the particle mass.

The flux of ions, J_i, is given by:

$$J_i = exp\left(-\frac{1}{2}\right) n_i \sqrt{\frac{kT_e}{m}}$$

where n_i is the ion density in the plasma phase and the *exp* (−1/2) term describes the ion density decrease in the pre-sheath.

Therefore, the surface has the effect of increasing the flux of positive ions through the pre-sheath/sheath regions to the surface. The increase in flux above the normal thermal flux, J_t, can be mathematically described by:

$$\frac{J_i}{J_t} = \sqrt{2\pi} exp\left(-\frac{1}{2}\right) \sqrt{\frac{T_e}{T_i}}$$

where T_i is the temperature of the ions in the plasma phase, usually close to ambient temperature. Therefore, for a typical electron temperature of ∼3 eV, the flux of ions is increased by a factor of ∼15 [16].

Michelmore and coauthors [16] summarized very well in a scheme the concentration variation of ions and electrons, as well as the increase in the ion velocity inside the plasma bulk, pre-sheath and sheath regions, as showed in Figure 4. Right side of Figure 4 shows potential in y-axis and distance in x-axis. This distance can range from millimeters to centimeters and in this specific case the x-axis represents 0 V.

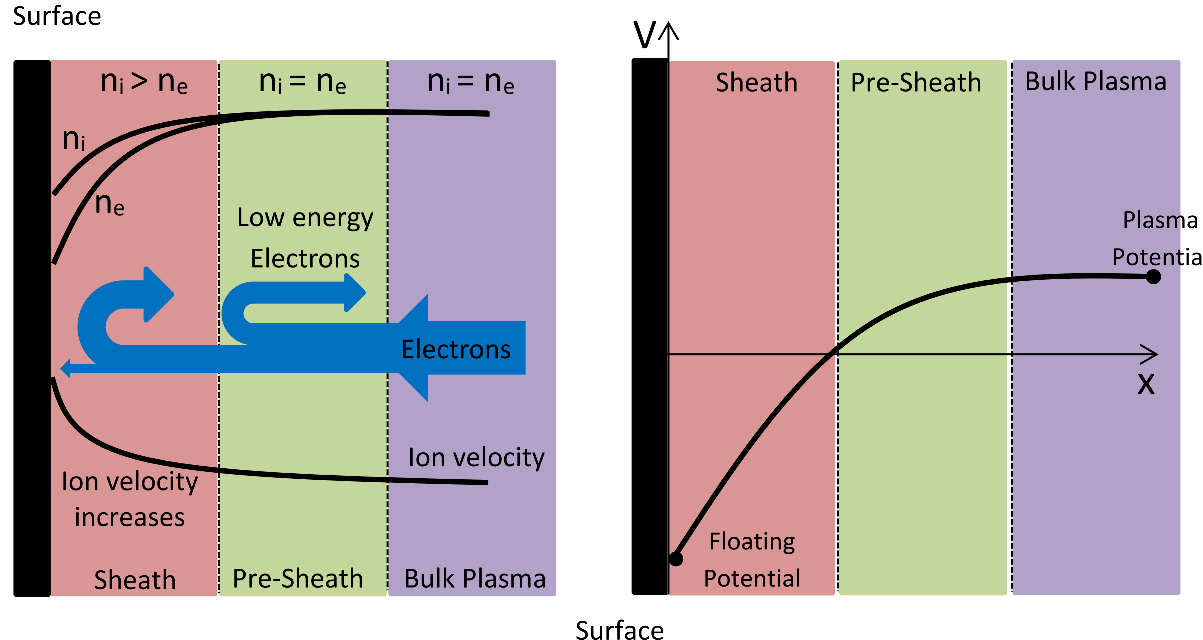

Figure 4 Schematic of the sheath and pre-sheath adjacent to a surface in contact with a plasma phase. Adapted from [16]

Because the sheath is a region over which a negative potential is dropped, electrons are quickly expelled from the sheath. This electron density loss results in a reduction of electron impact excitation reactions in that region, since the electrons are active species in these excitation/fragmentation/ionization processes. Since such reactions lead to fluorescent emission from excited species, the sheath region does not glow as much as the plasma bulk. So the substrate is surrounded by a comparatively dark space, which may be a few µm to a few mm in size depending on the plasma conditions [38].

2.2.2. Geometry of a RF-Discharge device

The RF generator supplies a sinusoidal waveform to the powered electrode, and the plasma potential rises and falls in phase with it. Normally the RF systems have a variable capacitor between the RF generator and the plasma. In order to guarantee maximum power transfer into the plasma, the input impedance of the plasma must be equal to the output impedance of the generator, normally 50 Ω, which is the standard the industry has settled on for measuring and transferring high-frequency electrical power [39]. Varying the value of this capacitor the effective impedance of the load (plasma + capacitor) can be made equal to 50 Ω. However, the presence of this blocking capacitor introduces the constraint that no net

current can flow during one RF cycle. It means that the total net charge flow per RF cycle to both electrodes must be zero [40]. In other words, to keep a steady state, ions and electrons must reach the surfaces in the same rate at which they are formed.

In the case of capacitive coupled plasma systems, the geometry of the electrodes, especially the area ratio of the powered electrode to grounded electrode strong influence on the potential distribution inside the plasma chamber. To realize a specific coating for determined application is very important to keep in mind those influences. Figure 5 shows different construction situations that can be performed regarding electrode areas, the time average plasma potential (V_p) and excitation voltage for capacitive coupled radio frequency plasma, respectively.

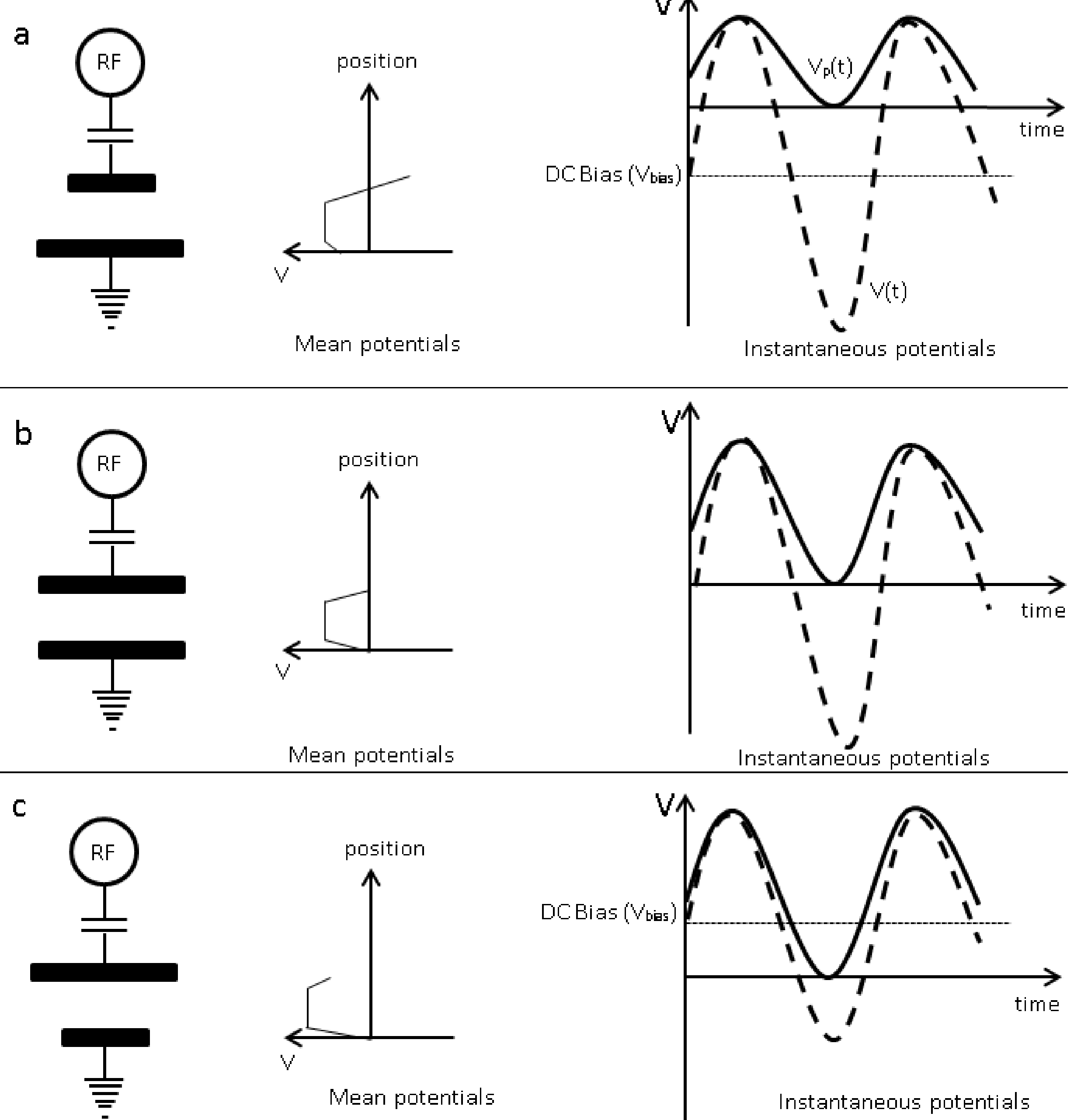

Figure 5 *Illustrative averaged potentials and instantaneous plasma potentials $V_p(t)$ (solid curves) and excitation electrode voltages V(t) (dashed curves), assuming purely capacitive RF sheath behavior, for three different capacitively coupled excitation electrodes geometries. Adapted from [41,42].*

The first reactor geometry represented in Figure 5a corresponds to the asymmetric one with the smallest electrode coupled to the RF generator. During the positive RF half cycle a high negative charge accumulates on the powered electrode, while during the negative RF half cycle only a smaller positive ion current flows due to the much lower ion mobility compared to the electron mobility. Negative charges accumulate on the electrode

during a complete cycle, since the blocking capacitor prevents the flow of current in the external circuit. In subsequent RF cycles, a steady state is reached, since low energetic electrons are repelled by the formed potential. Therefore, the RF signal oscillates around a DC potential, the DC bias potential (V_{bias}), which is negative with respect to the plasma potential, V_p. In this case, where $A_{RF} < A_{grounded}$, the main potential drop (higher sheath potential) is obtained at the powered electrode, as depicted in Figure 6. The DC bias potential, $V_{bias,}$ can be several hundred volts depending on the ratio of the powered to the grounded electrode area and on the applied RF. Ions will be accelerated toward the powered electrode through a maximum potential of V_p+V_{bias} [43].

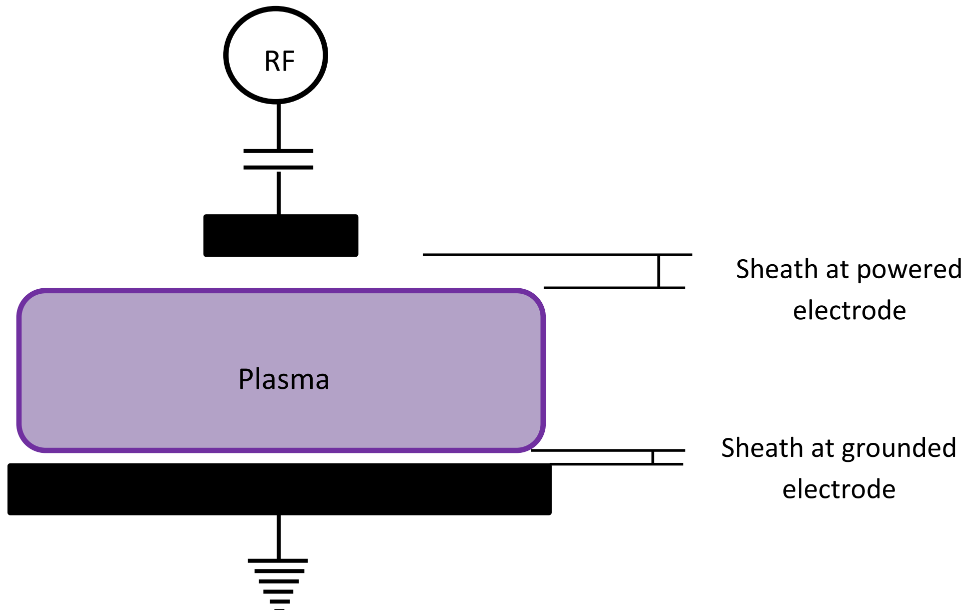

Figure 6 *Illustration of the different sheath length for the case with asymmetric electrode, which the powered electrode has the smallest area in comparison to the grounded electrode*

The highest possible negative V_{bias} value, which occurs for highly asymmetric systems, is ½ of the peak-to-peak voltage, and since the plasma cannot be more negative than ground its mean potential is at least close to ground. With this arrangement, strong ion bombardment is experienced only by the small electrode. As a function of the substrate position, therefore, it is possible to conduct contemporaneously in the same plasma environment, processes with high (on RF electrode) and low (on floating or ground surfaces) contributions of positively charged particles bombardment. When the area of the electrodes is the same (Figure 5b), symmetric geometry, RF oscillates around ground and the plasma potential is about ¼ of the peak-to-peak voltage. This configuration was the starting point for this research thesis since release coating is desired. It means that the thin film must be

polymer-like (Si, SiC_xH_y, C, C_xH_y). As depicted in Figure 2, the kind of ions plays an important role on the final characteristics of the thin film coating. Thus, it is mandatory to run the process in a 0 Bias form to avoid high ions bombardment, as shown in Figure 5b, since in this configuration the sheath potential is much lower than the case showed in Figure 5a with negative Bias. Consequently the electric field is lower leading to lower ion bombardment energy. The geometry of Figure 5c is very uncommon among real systems. In this case, if the positive Bias is very high, it implies in an energy barrier for ions which will certainly lead to different coating properties.

In the frame of my research, a large volume plasma reactor, about $1m^3$ volume, developed by Fraunhofer IFAM with symmetric electrode configurations is used. It is operated with a capacitive radio-frequency generator (13.56 MHz). In Figure 7 the used plasma system setup is shown schematically with its most important components. Basically, it has a “U-form” electrode, represented by the blue geometry, connected to the RF-Generator. To keep the symmetry, the “U-form” grounded counter electrode is formed by the door, the back wall and the perforated grid. This grid has also a protection function: avoid plasma to burn inside the exhaustion system and therefore to preserve the integrity of the chamber.

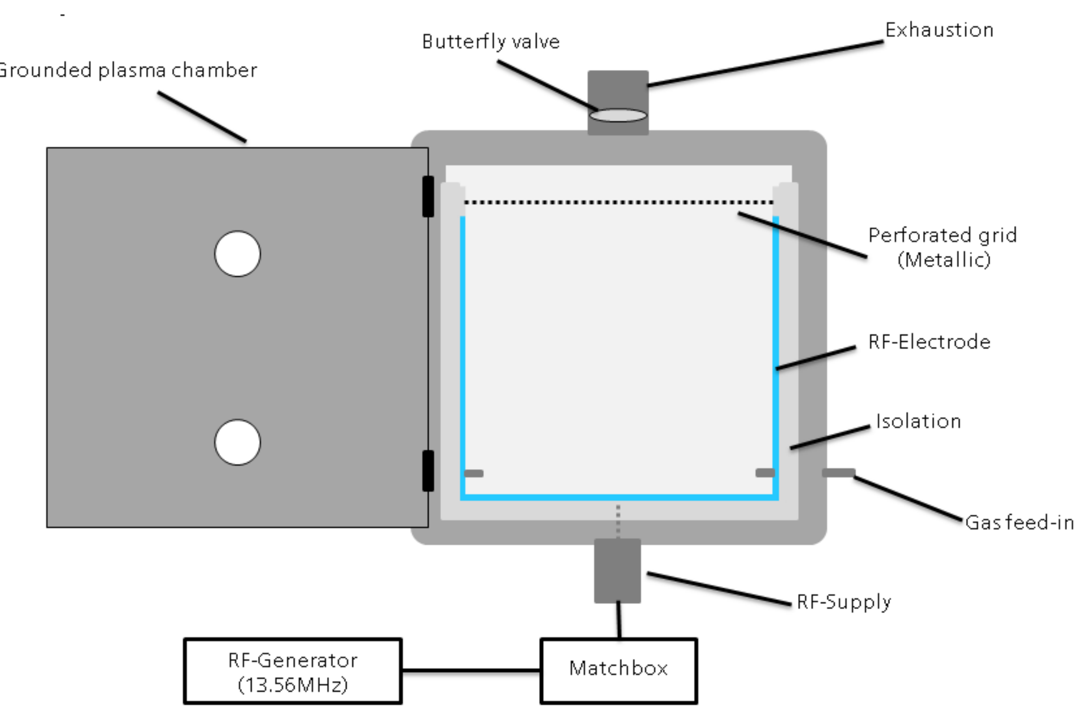

Figure 7 *Sketch of the low-pressure plasma chamber used for this thesis*

To regulate the process pressure, an adjustable butterfly valve is installed in the gas exhaustion. During the process, gas is continuously introduced via the gas feed-in system and the butterfly valve ensures a constant process pressure together with the exhaustion system. The power is generated by the RF-generator, coupled via the Matchbox with the electrode. The Matchbox works to compensate the unsteady ohmic resistance of the plasma and at the same time, the RF-generator is protected against backscattered power.

2.3. Coating properties

The coating process used under the frame of this thesis is shown in Table 1 and it will be the same performed in all experiments. The idea of this coating, commercially known as "Release$^{PLAS©}$", is to enhance the processes where a mold is needed or applications where a barrier (low surface energy) to attachments (i.e. dirty, insects) is desired [44]. Current industrial applications which use carbon fibers, especially for the aircraft industry, release agents are applied in the mold surface before the lamination. Due to this release agent application, additional steps are required in the production process. The mold must be cleaned before other lamination can be started and also the demolded product must be cleaned before moving to the next stage. Either the mold or the parts can be damaged during the demolding process. This is a drawback in a market where the costs must be minimized. In this context, a coating with "release" properties is very welcome. The Release$^{PLAS©}$ coating shows the following advantages:

- Protect the mold and the molded part
- Facilitate the demolding of the part
- Chemically stable
- Avoid additional processing steps on the mold and on the molded part

The coating process is divided in 4 steps, each one with a defined purpose. The first one uses oxygen as precursor gas and is denominated "Activation". In this step the surface energy is increased to facilitate the deposition of the primer in the step 2. Still in Step 1, some surface bonds can be broken which allows a better attachment of the next coating. The second step is the deposition of a hard coating, mainly a SiO_x-characteristic, which works as a barrier coating. This is important to protect the substrate from corrosion and to

optimize the coating adhesion. The third step is an adapter coating, which is softer than the primer coating. In the step 4 the final release coating is deposited. Here is the amount of HMDSO higher than oxygen and the desired polymeric coating with release properties is deposited. The deposited coating show a polymer-like characteristic due to the more content of HMDSO in the gas mixing ratio (HMDSO+O_2) [45].

Table 1 *Coating process used*

	Activation (1500W)	Primer (1500W)	Adaption Coating (1500W)	Release Coating (2200W)
Hexamethyldisiloxane	-	20 sccm	32 sccm	92 sccm
Oxygen	400 sccm	198 sccm	95 sccm	53 sccm

To realize such a polymeric coating, with low polar part, a Self-Bias free process is necessary [46]. Otherwise, the ion bombardment on the surface of the mold to be coated would be very intense, due to a negative Bias potential. More methyl components would be broken in small products and exhausted from the vacuum pump. It leads to a SiO_x characteristic coating, losing the “release” properties.

2.4. Coating characterization

There are different methods to characterize the deposited thin coating on the surfaces. The selection of the technique will mostly depend on the desired information. For example, to have information about the topography of the coating, an Atomic Force Microscope (AFM) is normally used [47]. In the case of optical properties of the coating, Ellipsometry and Reflectometry can be employed depending on the required information [48–50]. Fourier Transform Infrared Spectrophotometer (FTIR) is mainly used to estimate the structure of organic compounds [51]. Regarding mechanical properties, nanoindentation is a technique often employed [52,53]. Another very important technique is the contact angle measurements in order to calculate the surface energy and identify its wettability [54–56]. In the frame of this work, special attention will be given to the following coating characterization techniques: reflectometry, nanoindentation and contact angle measurements. The first one was implemented to identify the coating deposition

homogeneity and the last two techniques with the aim of confirm the desired coating properties (elastic modulus, hardness and surface polarity).

2.4.1. Reflectometry analysis for the measurement of coating thickness

To test the thickness and reflectivity of thin layers, several optical methods are commonly used due to quickness, precision, and for being a non-destructive testing technique. The optical reflectometry is a fast and contactless method. It measures thin film interference (i.e. the amount of light reflected from a thin film over a specified wavelength range). With this method the thickness is not measured directly but is deduced from the reflectance spectrum with the help of a mathematical algorithm. For thin layers a regression analysis (fit algorithm) that allows the determination of the thickness of more than one layer in a layer stack even with nanometer resolution is used [57].

In the current work, the measurements were done with the Ocean Optics NanoCalc 2000 model as depicted in Figure 8. It is a quick and easy way to measure thickness between 50 and 5000 nanometers for reflective coatings deposited on different substrates.

The NanoCalc series tool is a specialized equipment for measuring thin films. These are versatile and reconfigurable systems that apply spectroscopic reflectometry to determine the thickness of thin films in a wide range of substrates [58]. The equipment has a resolution of up to 0.1 nm and can measure slightly defective and rough surfaces. As a disadvantage, the use of the equipment presumes that the operator knows the optical behavior or constants of the substrate and of the coating. Thus, the method is limited to measuring coatings that are already well known and that have optical constants available in the software interface.

Figure 8 shows the NanoCalc 2000 along with the sample holder. The sample holder, located on the bottom right corner of Figure 8, is just a simple metal disc with a support that holds the tip of the optical measurement device. In order to perform the measurement, the tip should be at the same distance from the substrate during the measurement as it was in the reference measurement.

Figure 8 *Ocean Optics NanoCalc 2000. Reproduced from [58]*

The computer takes the substrate reflectivity measurements for all the specified wavelengths, usually from 250 nm to 800 nm, and compares them to a previously selected model of base substrate and coating to fit the thickness.

The equipment has models for many coatings and for many different substrates in its internal library. For instance, aluminized foil and silicon wafers were used as substrates in this research. The thickness of the coatings could be measured with good precision and reliability.

2.4.2. Nanoindentation

Nanoindentation techniques are commonly applied for the characterization of mechanical properties of thin films at nanoscale. This technique uses indentation load–displacement data, acquired during one cycle of loading and unloading, to measure hardness and elastic modulus of a material.

During a typical depth-sensing test, loading initiates both elastic and plastic deformation under the indenter, while unloading is dominated by recovery of the elastic deformation. To simplify the modelling, is assumed that deformation during loading is both elastic and plastic as the permanent hardness impression arises. During unloading, it is

assumed that only the elastic displacement is recovered. The analysis is simplified due to the elastic nature of the unloading curve [59–61].

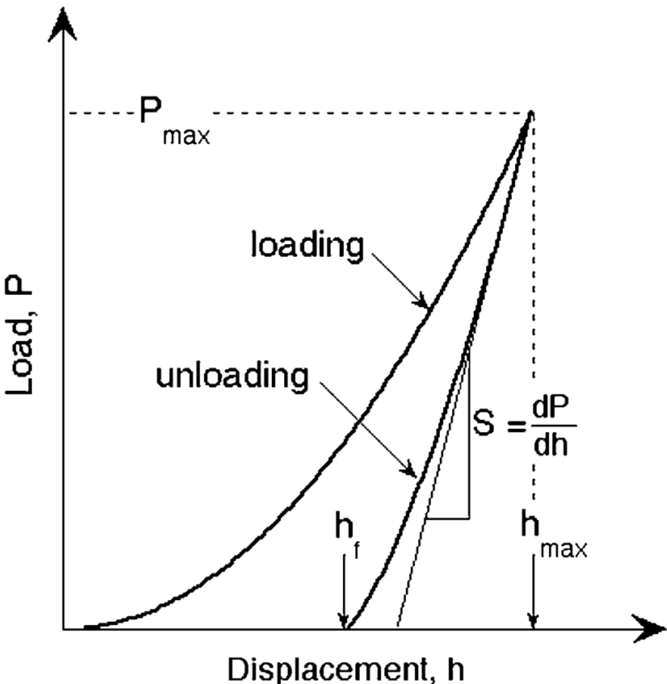

Figure 9 *Typical load–displacement curve. Reproduced from [60].*

Figure 9 shows a typical load–displacement curve, where the parameter P defines the load and h the displacement relative to the initial undeformed surface. Three important values must be measured from the P– h curves: the maximum load (P_{max}), the maximum displacement (h_{max}), and the elastic unloading stiffness ($S = \frac{dP}{dh}$), defined as the slope of the upper portion of the unloading curve during the initial stages of unloading (also called the contact stiffness). Additionally, the permanent depth of penetration after the indenter is fully unloaded, called final depth (h_f), must be also measured.

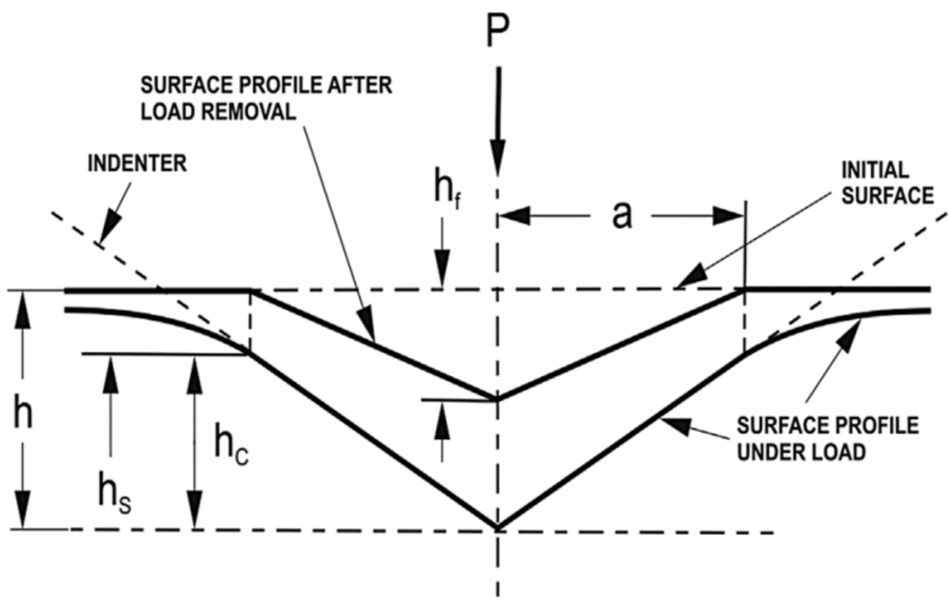

Figure 10 *Deformation pattern of an elastic–plastic material during and after indentation. Reproduced from [60]*

The deformation pattern of an elastic–plastic material during and after indentation is depicted in Figure 10. It also shows the parameters used in the subsequent equations. Based on studies from the early 1970s, there is a relationship between the initial unloading contact stiffness and the reduced modulus (E_r) according to the following equation,

$$S = \frac{2}{\sqrt{\pi}} E_r \sqrt{A},$$

where *A* is the projected contact area. In order to determine the measured stiffness (*S*) from the experiment, the slope ($S = dP/dh$, P is the load, and h is the displacement) of the upper portion of the unloading curve (Figure 9) is used and it depends on the analyzed material, e.g., within a range of 60–95%.The reduced modulus is given by

$$\frac{1}{E_r} = \frac{(1-\upsilon^2)}{E} + \frac{(1-\upsilon_i^2)}{E_i},$$

which includes elastic deformation of the specimen and the indenter. In this context, *E* and υ are the elastic modulus and Poisson's ratio of the specimen, and E_i and υ_i are the same parameters for the diamond indenter, e.g., a Berkovich indenter (E_i = 1141 GPa and υ_i = 0.07).

The hardness is determined from the measured data by the equation

$$H = \frac{P_{max}}{A},$$

where P_{max} is the peak indentation load [60].

The nanoindentation measurements of the plasma polymeric films were carried out at room temperature using a Tribometer - Universal Material Tester, model UMT3-MT-NH2. Figure 11 shows an image of the nanoindenter. The thickness of the tested films was about 1 μm, and a Berkovich indenter with a radius of curvature of 200 nm was used.

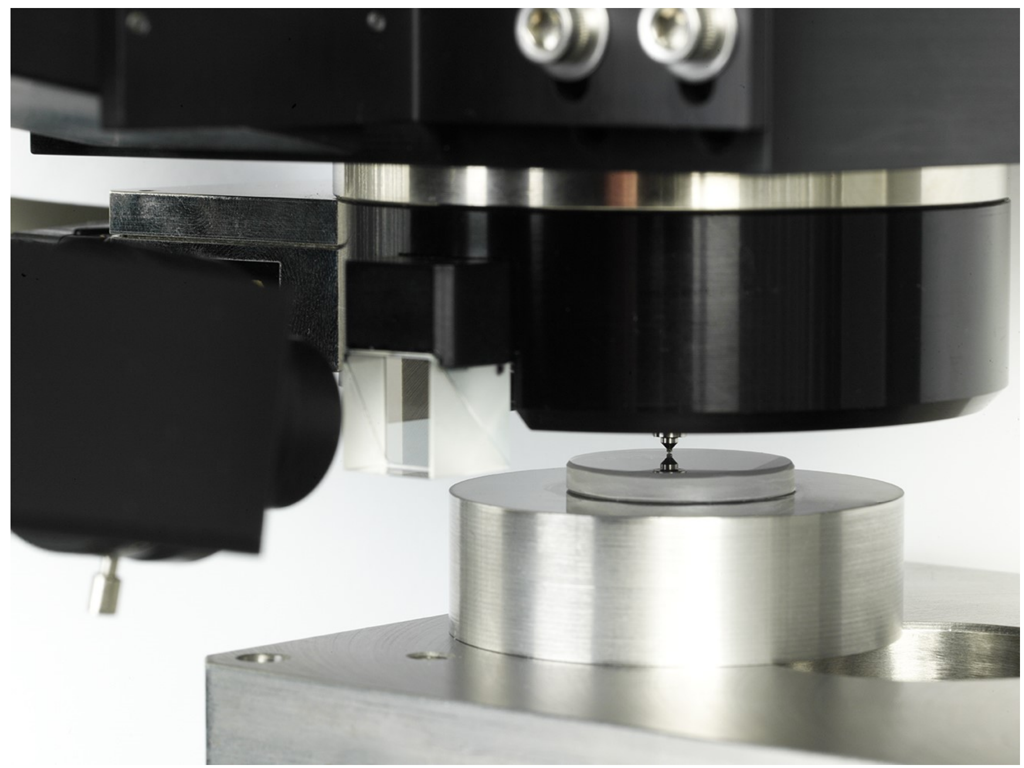

Figure 11 *Measuring head used for the hardness measurements*

2.4.3. Contact angle measurements

One of the important properties commonly analyzed within the plasma polymerization coatings is the wettability of the coated surface. It indicates the degree of wetting when a solid and liquid interact. Depending on the application, different degree of wettability can be tailored: from hydrophobic characteristic (low wettability), i.e. large contact angle ($> 90°$) to hydrophilic characteristic (high wettability), i.e. small contact angle($< 90°$). Beside that topic, the contact angle for a specific coating gives also an

information about the surface chemistry. So, it can be used to characterize the local homogeneity of a coating.

Figure 12 shows a liquid drop resting on a horizontal flat solid surface. The resulting angle between the juncture of the liquid-solid interface and the liquid-vapor interface is the contact angle. From the geometric point of view, the contact angle can be measured by applying a tangent line from the contact point along the liquid-vapor interface in the droplet profile. It can be observed an interface where solid, liquid, and vapor co-exist, and it is referred as the “three-phase contact point”. Small contact angles are observed when the liquid spreads on the surface (left image from Figure 12), while a large contact angle is observed when the liquid beads on the surface (right image from Figure 12). In other words, a contact angle less than 90° indicates that wetting of the surface is favorable, and the fluid will spread over a large area on the surface; while contact angles greater than 90° generally means that wetting of the surface is unfavorable so the fluid will minimize its contact with the surface and form a compact liquid droplet. As an example, a perfect wetting of the surface is achieved when the contact angle is 0°, when the droplet spreads completely over the surface. The opposite case, for superhydrophobic surfaces, water contact angles are usually greater than 150°, showing almost no contact between the liquid drop and the surface. This behavior is commonly named as the “lotus effect” [62,63].

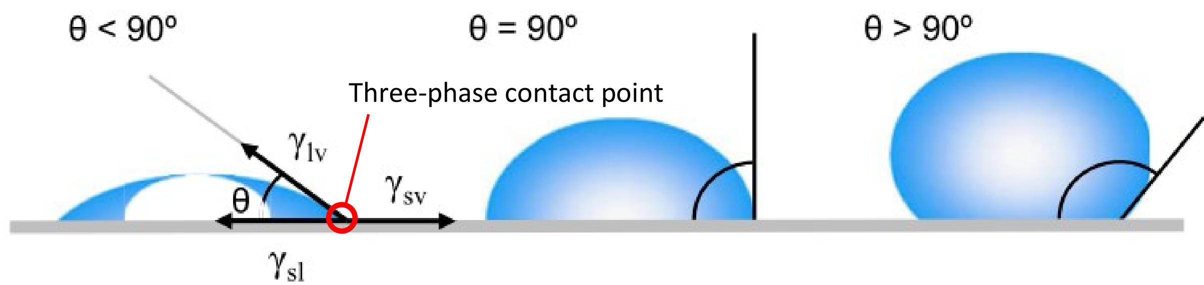

Figure 12 *Illustration of contact angles formed by sessile liquid drops on a smooth homogeneous: Reproduced from [64]*

In an ideal condition is expected that the surface tension of the liquid determines the shape of a liquid droplet. Taking into consideration a pure liquid, the molecules interact with

each other in the bulk in a way that each molecule is pulled in the same manner in all directions by neighboring molecules. These interactions result in a net force of zero. Nevertheless, the molecules at the surface do not have neighboring molecules in all directions to provide a balanced net force. As a result, they are pulled inward by the neighboring molecules (Figure 13) creating an internal pressure. Consequently, the liquid spontaneously contracts its surface area to maintain the lowest surface free energy, which is in a spherical format. Spheres have the minimum surface area for a fixed volume. In practice, external forces such as gravity deform the droplet, thus the contact angle is a compromise between surface tension and external forces (usually gravity). This intermolecular force to contract the surface is called the surface tension, and it is responsible for the shape of liquid droplets. From the theory point of view, the contact angle is expected to be characteristic for a given solid-liquid system in a certain environment [65].

Figure 13 *Representation of the surface tension caused by the unbalanced forces of liquid molecules at the surface. Reproduced from [64]*

The well-known Young´s equation describes the balance at the three phase contact of solid-liquid and gas [66]. The contact angle of a liquid drop on an ideal solid surface is defined by the mechanical equilibrium of the drop under the action of three interfacial tensions:

$$\gamma_{lv} cos\theta_Y = \gamma_{sv} - \gamma_{sl}$$

where γ_{lv}, γ_{sv}, and γ_{sl} represent the liquid-vapor, solid-vapor, and solid-liquid interfacial tensions, respectively, and θ_Y is the contact angle. The aforementioned equation is usually referred to as Young's equation, and θ_Y is Young's contact angle [64].

There are some assumptions for the Young´s equation: the topography should be smooth and chemically homogenous. With the help of the contact angle measurement it is possible to determine the surface free energy (SFE) of the solid and identify the polar and dispersive part. These values are very important to know because they can be used to judge if the desired properties for a specific application were attended (e.g. a coating with a function to facilitate the release of the molded part shows a polar part around 1 mN/m). Surface free energy of the solid corresponds to surface tension of the liquid, thus it has the same unit “mN/m”.

There are different methods to determine the SFE of a solid surface, for instance: Owens-Wendt, Kaelble and Wu [67–69]. Under the frame of this work the Wu method was used. The method according to Wu uses the contact angle with at least two liquids, one mainly polar and the other dispersive, to calculate the surface free energy of a solid. Thereupon, the surface free energy is divided into a polar part and a disperse part. In the Wu calculation a harmonic mean of the disperse part and the polar part is used:

$$\gamma_{sl} = \gamma_{sv} + \gamma_{lv} - 4\left[\frac{\gamma_{sv}^{d}\gamma_{lv}^{d}}{\left(\gamma_{sv}^{d} + \gamma_{lv}^{d}\right)} + \frac{\gamma_{sv}^{p}\gamma_{lv}^{p}}{\left(\gamma_{sv}^{p} + \gamma_{lv}^{p}\right)}\right]$$

And if combined with Young´s equation, Wu´s equation can be written as

$$\left[\frac{\gamma_{sv}^{d}\gamma_{lv}^{d}}{\left(\gamma_{sv}^{d} + \gamma_{lv}^{d}\right)} + \frac{\gamma_{sv}^{p}\gamma_{lv}^{p}}{\left(\gamma_{sv}^{p} + \gamma_{lv}^{p}\right)}\right] = 0.25\gamma_{lv}(1 + cos\theta_{Y})$$

Wu method for calculating surface energy is mostly used for polymers with low surface energy (up to 40 mN/m) [70]. Water, diiodomethane and ethylene glycol are often used for the measurements.

In this work, the contact angle measurements were performed using the equipment G2 from the company "Krüss". For this purpose, drops in a rate of 0.2 µl/s, with a total volume of 6 µl, were deposited on the sample surface and the contact angle was measured. This process was performed at 5 different positions of a sample with three liquids each (water, ethylene glycol and diiodomethane). The used samples were quartz glasses.

2.5. Plasma Modelling

Plasma process modelling is quite complex due to many reasons. For instance, there are electrostatic interactions between electrons and ions, the sheath formation and the influence of the plasma on the thermochemical properties of the material under its exposure. Besides that, in the case of reactive plasmas, there are countless reactions among charged particles and neutral species with mostly unknown rate constants. There are some commercial software packages available in this direction with good achievements, especially for small plasma chambers applied in the semiconductor industry. However, they are not yet suitable for large volume chambers and for complex reactive plasma applications [71,72]. Normally, as the reaction information is not complete available, especially regarding the cross section of the species formed, it is necessary to reduce the number of reactions in the model which culminates in limited success in the prediction of measured data [73,74]. In addition, very high computational efforts are still required.

In this work, the modelling effort was therefore restricted to computational fluid dynamics (CFD) simulations to evaluate the gas flow behavior, i.e. the steady-state condition before plasma ignition of the existing PECVD chamber and for the suggestion of new electrodes geometries for different applications. Furthermore, some basic electrostatic simulations were performed to get more hints over the electric field distribution inside the plasma chamber.

2.5.1. Computational fluid dynamics (CFD)

For the design of PECVD chambers, fluid dynamic is very significant. Since the process requires the supply of precursor gases, which through the influence of the plasma will fragmentize and react with the product surface forming the thin film coating, it is very helpful to predict and have control over its behavior. Moreover, coating inhomogeneity may be attributed to adverse gas flow conditions or nonuniform gas velocity close to the substrates to be coated [31], especially in the case where self-bias does not occur (V_{bias}=0). Furthermore, the gas residence time inside the chamber is also one important parameter because it can lead to different degree of fragmentation, resulting in nonuniform coating properties [75]. In this scenario, fluid simulation is an important tool, since it gives the

chance to the person in charge of the process to optimize the chamber together with the constructor, tailoring the project for each application with less risk of rework.

Different authors deal with CFD applied to PECVD processes. Collins et all [76] used CFD in combination with a one-dimensional simulator to study the deposition of silicon nitride from an N_2-SiH_4-NH_3 gas composition, through a small single-wafer chamber. Crose and coauthors developed a multiscale computational fluid dynamics model combining gas flow simulations (macroscopic level) with Monte Carlo model (microscopic level describing the thin film growth) for solar cells applications [77]. Da Silva and Morimoto used CFD model to predict the velocity and temperature curves inside a small plasma chamber for doped and undoped silicon oxide deposition [78].

Unlike the aforementioned authors, the idea of this thesis is to use CFD simulations for a large plasma chamber (~1m^3) in order to create guidelines for future constructions regarding gas feed-in systems, gas exhaustion systems and electrode geometry looking toward to homogeneous deposition rates as well as good coating properties. Effects like the formation of new gases (e.g. CO_2 and H_2O through plasma combustion) and the loss through the deposition process itself are neglected. This is possible because the used plasma process works with a precursor surplus.

Basically, fluid flows are governed by partial differential equations (PDEs) which represent conservation laws for the mass, momentum, and energy. Computational Fluid Dynamics (CFD) is a technique to replace such PDE systems by a set of algebraic equations, which can be solved using computers. Through mathematical modeling (partial differential equations), numerical methods (discretization and solution techniques) and the embedded tools in the software (solvers, pre- and post-processing utilities) the user can have access to qualitative and quantitative prediction of fluid flows.

2.5.1.1. Governing Equations

In this work Ansys Fluent 16.0® was used for the gas flow simulations. This software solves the Navier-Stokes equations for transport of mass, momentum, species, and energy when it calculates laminar flow with heat transfer. Additional transport equations are solved when the flow is turbulent or when radiative heat transfer is included. Under the frame of this work, the continuity, energy and momentum equations employed are standard and therefore will be presented only briefly. For a more detailed description of the flow field equations, please refer to the Fluent user manual [79].

In a general form, the equation for conservation of mass, or continuity equation, can be written as follows [80,81]:

$$\frac{\partial \rho}{\partial t} + \nabla(\rho \vec{V}) = 0$$

where ρ represents the gas density and $\vec{V}$ the local velocity.

Transport of momentum is calculated by the following form:

$$\frac{\partial \rho}{\partial t}(\rho \vec{V}) + \nabla(\rho \vec{V}\vec{V}) = -\nabla \mathrm{p} + \nabla(\bar{\bar{\tau}}) + \rho \vec{g} + \vec{F}$$

where p is the static pressure, $\bar{\bar{\tau}}$ is the stress tensor, and $\rho \vec{g}$ and $\vec{F}$ are the gravitational body force and external body forces, respectively.

Finally, the energy equation can be written as:

$$\frac{\partial}{\partial t}(\rho h) + \nabla(\rho h \vec{V}) = \nabla[(k + k_t)\nabla \mathrm{T}] + S_h$$

where h is the sensible enthalpy, k is the molecular conductivity, k_t is the conductivity due to turbulent transport and the source term S_h includes any volumetric heat sources defined.

Detailed information about the used boundary conditions and model used under the frame of this work will be described in chapter 3.

2.5.1.2. Knudsen number

On fluid dynamics the Knudsen (Kn) number is an important parameter to evaluate and classify the gas flow behavior. The Kn is defined as the ratio between the molecular mean free path and the characteristic dimension of the flow geometry [82–84]:

$$Kn = \frac{\lambda}{L}$$

where λ is the mean free path and *L* is the characteristic dimension or characteristic length of the flow system.

Based on the Kn the degree of rarefaction of the gas and the validity of the continuum flow assumption can be determined.

According to the Knudsen number the gas flow can be divided in 4 regimes [82–84], as illustrated in Figure 14. For $Kn \leq 0.001$, called continuum flow regime, the continuum hypothesis is suitable and the flow can be analyzed using the Navier-Stokes equations with conventional no-slip boundary conditions. For $0.001 \leq Kn \leq 0.1$, named slip-flow regime, rarefaction effects start to influence the flow. To use the Navier-Stokes equations tangential slip-velocity boundary conditions must be provided along the walls of the flow domain. When the gas becomes more rarefied, $0.1 \leq Kn \leq 10$, the flow is characterized as transient. For this regime, as the continuum assumption of the Navier-Stokes equations begins to break down, alternative simulation techniques such as particle based direct simulation Monte Carlo (DSMC) approaches must be adopted. For the $Kn \geq 10$, the continuum assumption is completely broken, the regime can then be described as a free molecular flow.

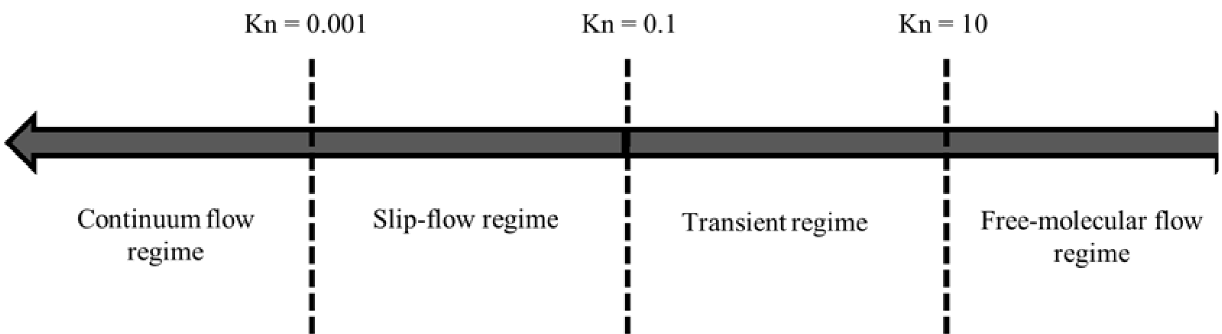

Figure 14 *Gas flow regime based on the Knudsen number*

The pressure range values in vacuum technology are presented in Table 2. According to the model configuration, different Kn values can occur for different regions of the PECVD chamber depending on the variations of the pressure and on the characteristic length values. For instance, different Kn values can occur when the pressure inside the gas feed-in distributor is much higher than the pressure inside the chamber. A further reason for different Kn values is when the characteristic length of the gas feed-in distributor is much smaller than the characteristic length of the chamber.

Most of all low-pressure PECVD applications work within the medium vacuum range [85]. For the PECVD chamber condition investigated in this work the Kn value is 0.03. It is in the range of the slip-flow regime ($0.001 \leq Kn \geq 0.1$), which enable the use of the continuum hypothesis to simulate the gas flow behavior analyzed using the Navier-Stokes equations with conventional no-slip boundary conditions [86]. For plasma coating the mean free path is important regarding the sustaining of the plasma. If the mean free path is much larger than the sheath or the relevant dimensions of the chamber or of the product, there will be very few excitation/ionization and the plasma will not sustain [87]. For instance, as a condition for sustaining plasma, there is a relationship between pressure and distance between the electrodes:

$$p.d > 0.5 \text{ (cm . Torr)}$$

where “*p*” is the pressure and “*d*” is the distance between the electrodes.

Table 2 *Pressure range values in vacuum technology [88]*

Vacuum range	Pressure in mbar	Molecules / cm^3	Mean free path
Ambient pressure	1013	2.7×10^{19}	68 nm
Low vacuum	300 – 1	$10^{19} – 10^{16}$	0.1 – 100 µm
Medium vacuum	$1 – 10^{-3}$	$10^{16} – 10^{13}$	0.1 – 100 mm
High vacuum	$10^{-3} – 10^{-7}$	$10^{13} – 10^{9}$	10 cm – 1 km

2.5.2. Electrostatics

For the fragmentation of the precursor gas a radiofrequency generator is used. As showed in Figure 7, there is a “U form” electrode connected to the RF-generator. Additionally, the door, perforated grid and back of the chamber build the grounded counter-electrode. In practice, it means that an electric field is generated inside of the chamber due

to the potential difference between these electrodes. The effect of this electric field is also investigated on this work through the software Ansys Maxwell®.

Basically, the electrodes of the plasma reactor are considered as a simple capacitor with a non-usual geometry and therefore the Gauss´s law can be used to determine the electric field between them. The integral form of Gauss´s law is written as follows:

$$\oint_S \vec{E}\,\hat{n}\,da = \frac{q_{enc}}{\varepsilon_0}$$

The left side of this equation is a mathematical description of the electric flux – the number of electric field lines – passing through a closed surface "*S*", whereas the right side is the total amount of charge contained within that surface (q_{enc}) divided by a constant called the permittivity of free space (ε_0). The only sources of the electrostatic field are the charges of the charged particles [89].

The visualization of the electric field of a charged object is very helpful to understand its influence on the region close to it. The most used visual representations of an electric field are either field lines that show the direction of the field at each point in space or arrows. For the first approach, the strength of the field is characterized by the spacing of the lines, where closer lines represent a strong field. In the case of arrows, the strength of the field is characterized by the length of the arrow. Some examples of electric field are shown in Figure 15.

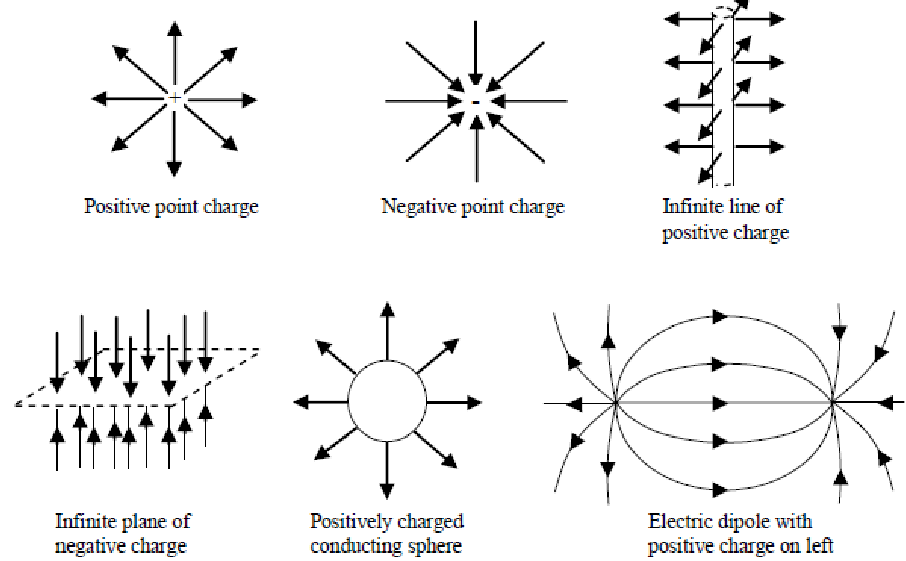

Figure 15 *Examples of electric fields in different situations. Reproduced from [90].*

Fleish [90] listed on his book some rules of thumb that support the understanding and also allow to sketch the electric fields produced by charges:

- Electric field lines must originate on positive charge and terminate on negative charge
- The net electric field at any point is the vector sum of all electric fields present at that point
- Electric field lines can never cross, since that would indicate that the field points in two different directions at the same location (if two or more different sources contribute electric fields pointing in different directions at the same location, the total electric field is the vector sum of the individual fields, and the electric field lines always point in the single direction of the total field)
- Electric field lines are always perpendicular to the surface of a conductor in equilibrium

The boundary conditions and model used for the electric field calculations in this work will be explained in detail in the section 3.2.3.

3. Simulation and Experimental Part

The construction of low-pressure plasma chambers requires special attention for the development of gas feed-in systems and gas exhaust systems to perform homogenous coating deposition in all samples surfaces with the same coating properties. Additionally, if it is desired to use the same chamber for different samples with different geometries and dimensions, the electrode setup must be well defined to allow the customization of the low-pressure plasma chamber as well as to attend the desired coating properties and deposition rates.

In the case of small reactors, for instance applied in the semiconductor industry, as the flat sample is placed very close and plan parallel to the gas feed-in system, the influence zone of the supplied gas covers basically all the surface of the material to be coated [91–93]. It means that if the precursor gas flow is not homogeneous over the product surface, different deposition rates can occur. This kind of application deals with special flat products, which means high costs, and failure in the process, like inhomogeneous deposition rate, is highly undesired. One example of such reactor is shown in Figure 16. To homogenize the precursor gas supply, a perforated plate is used as gas distributor. This plate is perforated in an organized manner and positioned below the gas feed-in supply system. The idea is to achieve a homogeneous pressure difference between the upper and the lower region which allows an even gas distribution over the product to be coated. In this context, Guensuk and coauthors investigated the influence of the opening area ratio of a showerhead structure (perforated plate) over the film thickness homogeneity in a small vertical flow coater applied for Dynamic Random Access Memory (DRAM) manufacturing [94]. They found out that the optimization of the opening area ratio can change the film deposition profile as well as improve the film thickness homogeneity. However, the optimization depends also on the desired coating properties, since a change of the hole opening area leads not just to a change in the local supply of the precursor gas but also to a change of the local plasma density and local temperature. Sansonnens and coauthors investigated the film thickness uniformity likewise for a showerhead-type reactor, used for deposit thin solid films as amorphous silicon or silicon oxide on photovoltaic solar cells and transistors for flat screen production. In this case, the gas is supplied from the top electrode (showerhead is integrated

to it) and pumped out through the side of the reactor [95]. They showed that the showerhead-type gas-feed in system improves the coating thickness homogeneity.

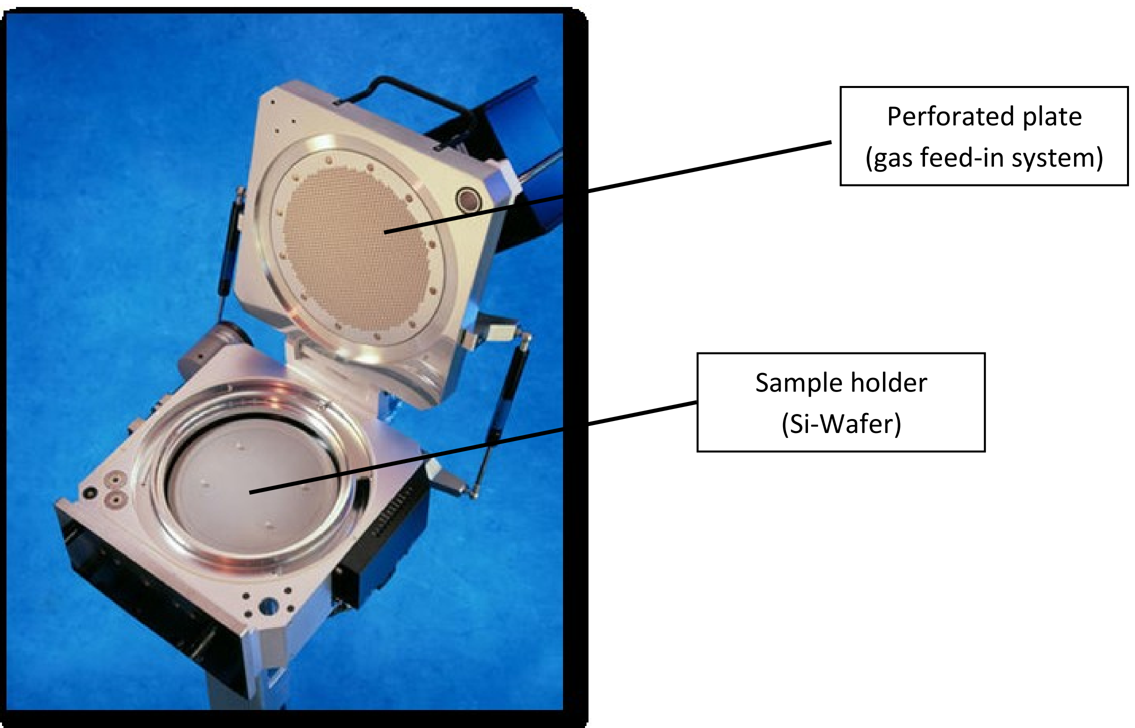

Figure 16 *Small chamber used for LPCVD (Low Pressure Chemical Vapor Deposition) developed by Applied Mateirals,Inc. Reproduced from [96]*

Regarding the current thesis, the idea is to work with a large plasma-chamber with a volume order of ~1m^3 (Figure 7). It is expected that different gas influence zones are generated inside the plasma area. One influence zone is created due to the gas feed-in system and the other one due to the gas exhaustion system. There are naturally other gas disturbances related to geometric reasons, i.e. geometry of the electrode and the shape and size of the products to be coated. They also need special attention – but they are not part of this research work.

3.1. Gas feed-in system

There are different solutions to supply and distribute gas already applied in different industries. Kulkarni and coauthors investigated different sparger geometries for bubble column application, as depicted in Figure 17 [97,98]. They compared theoretical models with experiments and later on with CFD calculations to define layout constructions for straight and ring pipe spargers. It was found out that the non-uniformity increases with an increase in the free area and the length of the pipe sparger. Bahroun and coauthors investigated

ways to enhance the barrier property of coatings applied inside PET beverage bottles. In this case, they used CFD tool to develop the gas feed-in system, which consisted of a tube with diameter smaller than the bottle neck diameter. This tube was installed passing through the bottle neck until close to the bottom of the bottle where the precursor gas is supplied [99]. Therefore, the gas feed-in system is developed according to each application and depends also on the process requirements. If the homogeneity of the gas flow is not important like in activation processes [100], then simple solutions (one tube, one hole) are already suitable. However, for sensitive process where the homogeneity of the gas flow is highly required, special attention must be paid to the construction of gas feed-in systems.

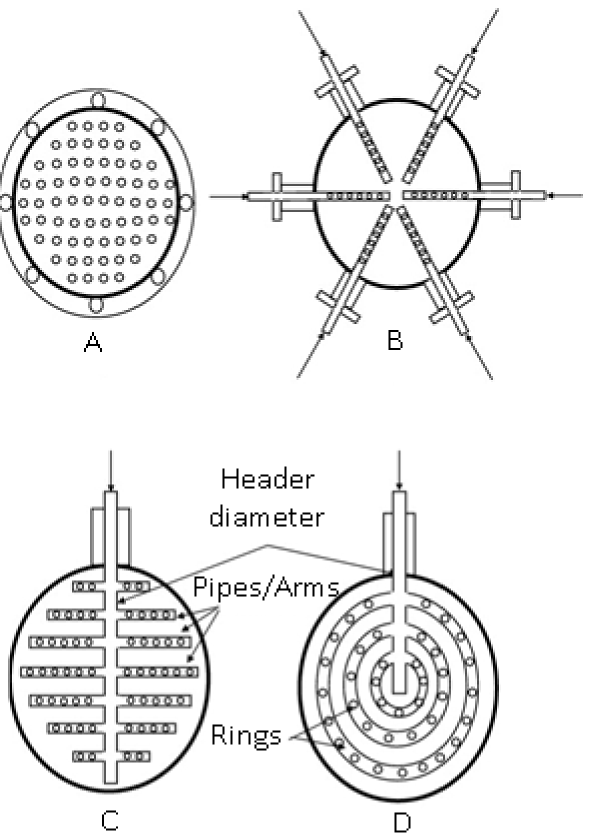

Figure 17 *Spargers for bubble column reactor: (A) sieve plate sparger; (B) multiple ring sparger; (C) spider; (D) pipe sparger. Adapted from [97,98]*

Under the frame of this research thesis, some eligible configurations were listed and the desired requirements were defined and schematized in Figure 18. The red “x” means out of requirement, the green mark means that the requirement is satisfied and the circle blue mark stays for cases where the requirement is partially satisfied. It means that the construction cannot be applied in plasma processes where coating deposition rate homogeneity is required but could be applied, for example, to plasma activation process. For

the aim of this work, is mandatory a configuration that allows a very homogeneous gas distribution to the chamber along with applicability in plasma coating process. If these two requirements can be fulfilled together with versatility, low construction cost and short construction time then it would be the optimal one. The pipe with open sides, both square section and circle section, as they present one inlet and one outlet makes the application in the plasma coating process unfeasible. It will feed the precursor gas just in one position. Thus a larger volume of the chamber will have poor gas supply. The showerhead configuration shows a very good homogeneity of gas distribution and applicability to plasma coating process, but the costs to build it and the time to modify the standard plasma coater make it unfeasible. The perforated pipe configuration with closed sides and circle section satisfies almost all the requirements except the plasma applicability. Due to the cylindrical geometry, its installation is more complicated and this geometry might lead to local plasma formation. Finally, the perforated pipe with square section satisfies all the established requirements and therefore was selected to be developed in this research work. Furthermore, construction guidelines were developed [101] in order to make it easier for researchers or constructors to take decision in future developments.

			Requirements				
Description	Sketch	Profile	Homogeneity of gas distribution	Versatility	Construction cost	Construction time	Plasma applicability
Pipe (open sides)	Inlet → Outlet	□	✗	✓	✓	✓	○
	Inlet → Outlet	○	✗	✓	✓	✓	○
Perforated Pipe (closed sides)	Outlet / Inlet	□	✓	✓	✓	✓	✓
	Outlet / Inlet	○	✓	✓	✓	✓	○
Showerhead Plate (integrated into the electrode)	Outlet / Inlet	⁞⁞⁞	✓	✓	✗	✗	✓

Figure 18 *Eligible gas feed-in configurations and desired requirements*

A perforated pipe (in one surface) with a rectangular section was selected because it is easier to construct and to install in comparison to a cylindrical one. Different cross-sections are possible and the pipe itself can be placed easily on an electrode without creating local plasmas (like tubing may do). The solution with holes distributed in one

surface was used since it gives the chance to distribute the gas evenly in the length of the chamber. Besides that, the perforated pipe is versatile, it can be used even if it is decided to divide the chamber in small volumes through parts holders or additional electrodes with the aim for coating more parts. Other solutions as showerhead or perforated plate would require further work to adapt for new configurations using the same plasma coater.

The selected pipe is closed at both ends. At the bottom of the gas feed-in distributor the gas inlet is centrally placed. The rectangular pipe contains equally spaced perforations to provide the gas flow into the PECVD chamber. The sketch of the gas feed-in distributor model is shown in Figure 19a and the PECVD chamber model is presented in Figure 19b.

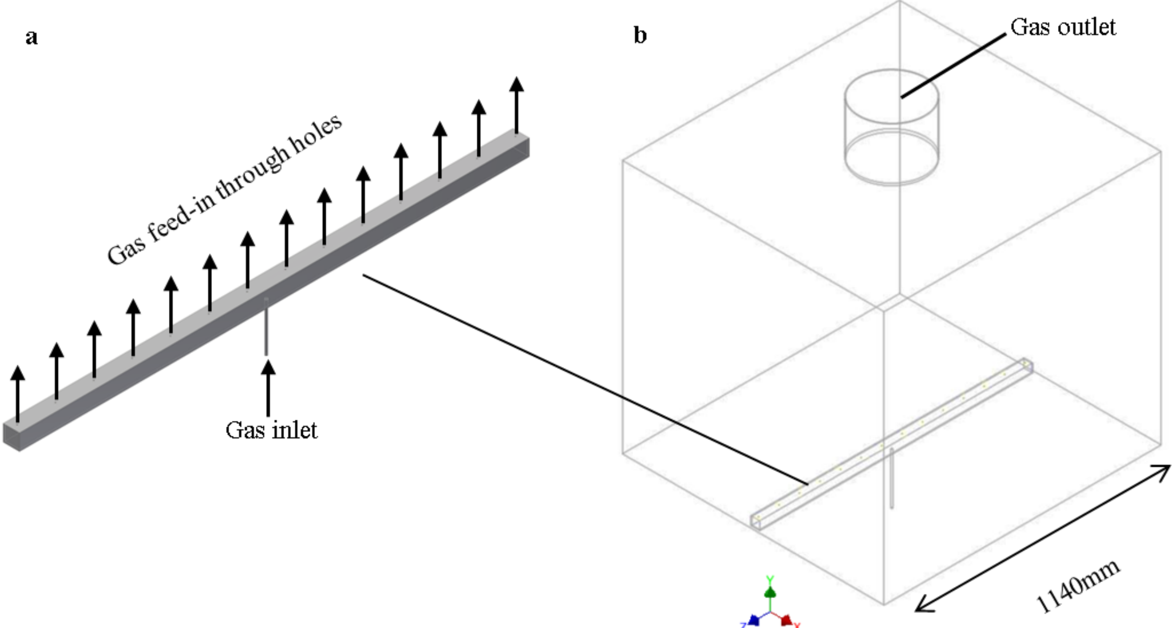

***Figure 19** a) Gas feed-in distributor model under analysis, b) Gas feed-in distributor position inside the PECVD chamber.*

The objective is to determine and evaluate conditions that influence the gas flow homogeneity inside the PECVD chambers and therefore also inside the gas feed-in distributor. Hence, a condition to achieve a homogenous gas flow at every feed-in hole is related to a constant gas pressure along the whole length of the gas feed-in distributor. However, the pressure distribution can be mainly influenced by one of the following two scenarios: (i) due to the gas friction with the internal surface of the pipe the pressure decreases in the direction of the flow, or (ii) the velocity of the gas is reduced caused by the

loss of the gas which is flowing via the holes into the PECVD chamber, i.e. the momentum of the gas is reduced and the pressure rises in the direction of the flow [15,102].

Consequently, a proper balance between these two influence conditions on the pressure is crucial to obtain an equal gas feed-in along the length of the distributor. Further aspects influence the gas flow within this simple construction model as the geometry parameters. The cross section of the pipe and the number and diameter of the holes, the length of the pipe, and the flow rate are among the parameters which can strongly cause changes in the gas flow [103,104]. For this reason, predicting the precursor gas flow inside the gas feed-in system is very useful for the construction design and consequently to improve the process performance.

Taking into consideration that the local gas flow behavior cannot be experimentally directly measured inside a PECVD system, computational fluid dynamics (CFD) simulations are valuable tools to determine the gas flow behavior inside gas feed-in system in low pressure environments. The objective was to predict the gas flow behavior inside the gas feed-in system for achieving a homogeneous gas supply through the investigated pipe holes and afterwards to compare the calculated pressure with the experimentally measured ones to validate the simulation results.

3.1.1. CFD simulation

CFD simulations were performed applying the software package Ansys Fluent 16.0®. First of all, gas flow simulations were performed for five distinct pipe section areas (Figure 20), keeping constant other reference parameters as presented in Table 3, the resulting curve was named as reference curve. Secondly, the same CFD simulations were performed varying the values of some parameters as shown in Table 3 under the changed parameters column. For each simulation one parameter was varied while the others were kept constant. The pipe was placed on the bottom of the PECVD chamber, as illustrated in Figure 19, considering a chamber volume of 1 m^3.

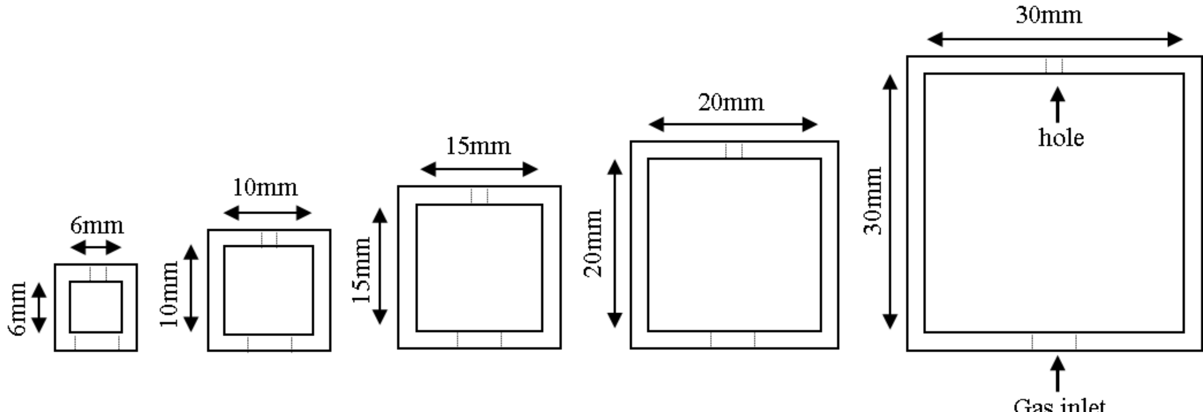

Figure 20 *Pipe profiles under analysis (front view)*

Table 3 *Pipe technical layout under simulation analysis*

Pipe section [mm x mm]	Reference parameters		Changed parameters: Flow rate [sccm]	Number of holes	Hole Diameter [mm]	Pipe length [mm]	*Aspect ratio
6x6	Flow rate [sccm]	200	300	-	-	-	-
10x10	Number of holes	14	-	28	-	-	-
15x15	Hole diameter [mm]	2	-	-	3	-	-
20x20	Pipe length [mm]	1000	-	-	-	2000	-
30x30	Aspect ratio	1	-	-	-	-	2

*Refers to the pipe section aspect ratio keeping constant the equivalent section area

The local gas velocity could not be determined experimentally and in order to validate the simulations with available experimental data, the pressure values were calculated via the CFD simulations to obtain a pressure curve. Considering those cases where experimental and simulation data could be compared, further simulations were performed varying some of the parameter values to acquire the pressure curve. Hence, for the pipe section cases of 10mm x 10mm and 30mm x 30mm the simulations were carried out varying the gas flow rate from 100 to 600 sccm in intervals of 100 sccm, and different number of pipe holes were considered. These parameters and all the respective values are presented in Table 4.

Table 4 *Parameters used for experimental and simulation approach*

Pipe section [mm x mm]	Flow rate [sccm]	Number of holes	Hole diameter [mm]	Pipe length [mm]
10x10	100, 200, 300, 400, 500 and 600	14	2	1000
		7	2	1000
30x30	100, 200, 300, 400, 500 and 600	14	2	1000
		7	2	1000

The 3D models were created using one symmetry plane (Figure 21) to minimize the simulation time, keeping a proper mesh resolution. For all carried out CFD simulations carried out the boundary conditions were defined to reproduce the conditions of the experiment (Table 5). The number of elements in each model was approximately 2,500,000. Grid independence tests were performed to determine the greatest mesh refinement. The mesh was refined inside the pipe, inner holes, gas inlet and gas outlet. The solutions were converged when all the residuals were smaller than 10^{-5} for the continuity and momentum equations and smaller than 10^{-6} for the energy equation.

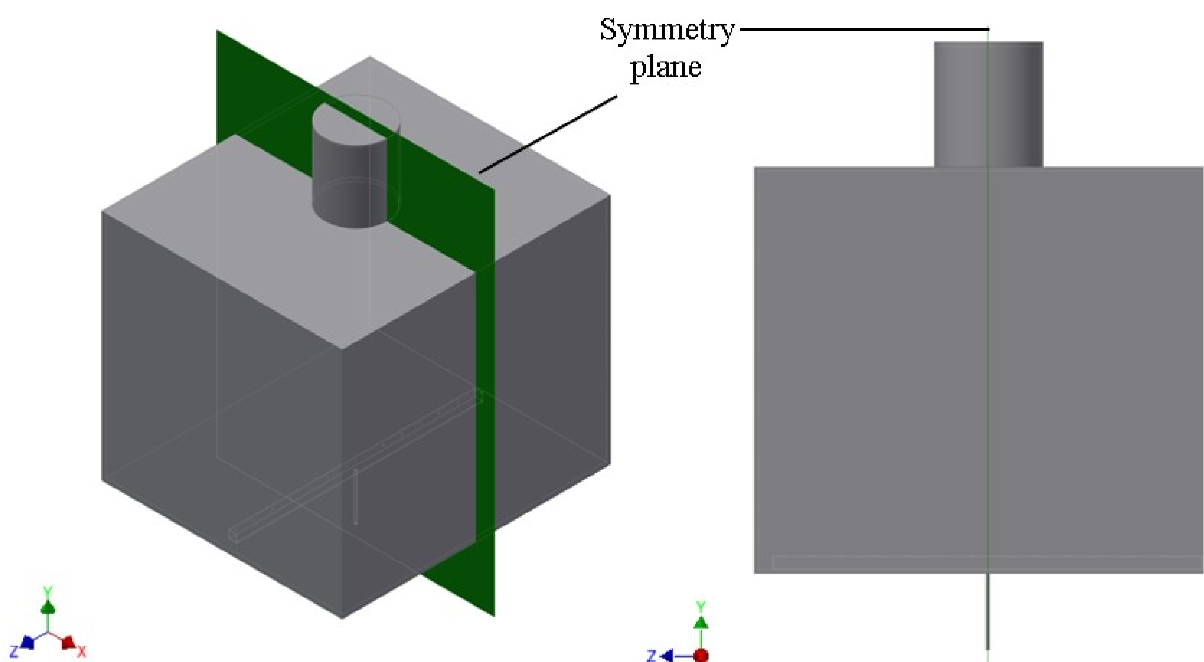

Figure 21 *System model with XY symmetry plane*

Table 5 *Boundary conditions*

Model	Boundary conditions	Values
Laminar flow with low pressure boundary slip	Gas Temperature	298.15 [K]
	Wall Temperature	298.15 [K]
Ideal gas	Mass flow rate of N_2 (inlet)	*variable [kg/s]
Steady state	Pressure (outlet)	0.03 [hPa]

*Different flow rates were applied according with the objective desired. The unit [sccm] was converted to [kg/s].

3.1.2. Experimental pressure measurements

Experiments were conducted inside a 1m^3 PECVD chamber for two different pipe section area values and for pipes containing 7 and 14 holes (Table 4), leading a total of four pipe configurations (i.e. four pressure measurement trials were performed). For all cases 2mm holes were manually drilled using a drilling machine. For each trial the nitrogen gas was used as working gas. The gas flow rate varied from 100 to 600 sccm and the pressure value on the gas outlet was kept equal to 0.03 hPa.

The pressure was measured in one of the closed sides of the pipe using a handheld vacuum gauge (Pfeiffer TPG202) and compared to the previous simulations predictions. The experiment setup is shown in Figure 22.

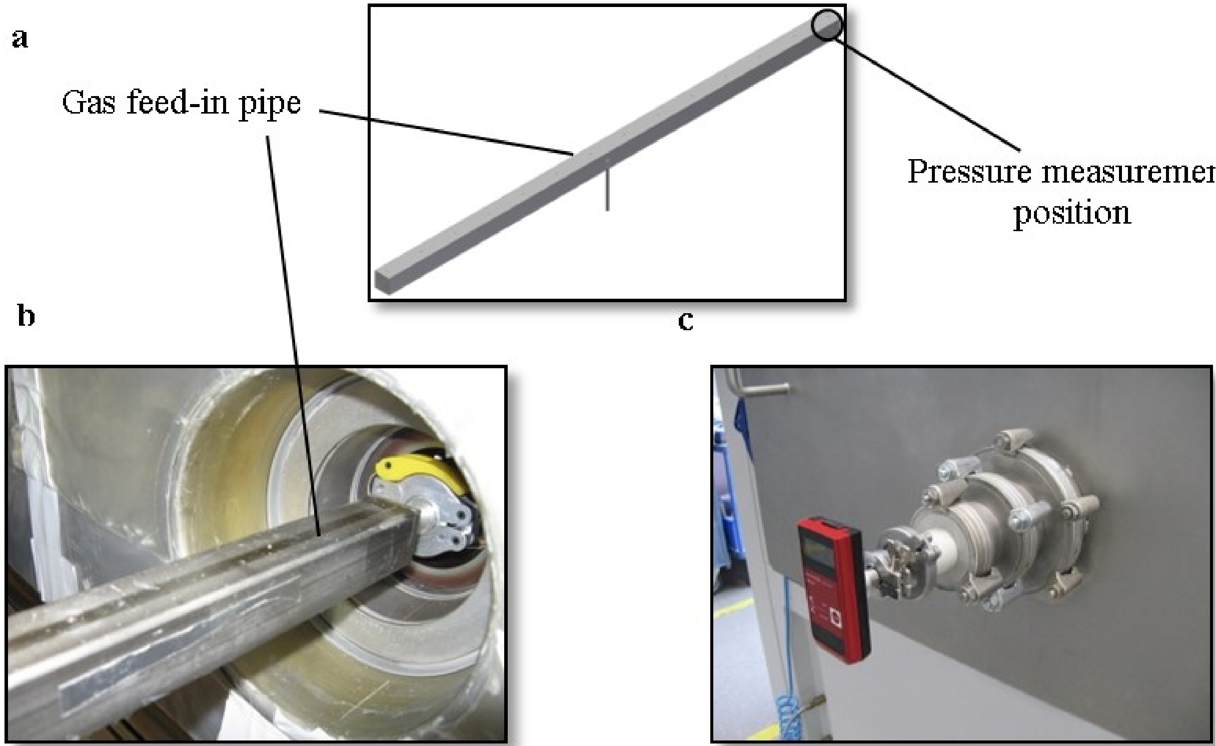

Figure 22 *Pressure measurement details: (a) Sketch of the pipe with measurement position (b) Pipe connection with vacuum gauge (view from inside the chamber) (c) Handheld vacuum gauge*

3.1.3. Results and Discussion

First CFD simulations were performed to understand the effect of the pipe sectional area (Figure 20) on the gas flow distribution through the pipe holes.

In order to compute the homogeneity of gas flow distribution through the holes, one dimensionless coefficient Φ was used [105]. Its definition is given as follows:

$$\Phi = \frac{\text{Standard deviation of flow rate}}{\text{Average flow rate per hole}}$$

The homogeneity of the gas flow distribution is inversely proportional to the value of Φ (i.e. the smaller is Φ, the more homogeneous is the gas flow distribution).

Figure 23a presents the flow rate in each hole for different pipe section areas. The pipe image on the top left side highlights the gas inlet from the middle of the pipe. Part b of Figure 23 shows the nonuniformity coefficient for different pipe section areas and emphasizes through the dash dot line the construction border that was recommended.

The flow rate tends to decrease from the gas inlet to the sides of the pipe, i.e. the holes closer to the gas inlet discharge more gas, as depicted in Figure 23a. It indicates that the friction effects may predominate. Further evidence from these effects are displayed in Figure 24a and Figure 24b, where the pipe with smaller section area, and thus more pressure drop, presented more pressure gradient than the pipe with larger section area.

Under the frame of this research thesis, the acceptable values of the dimensionless coefficient Φ was defined in the range Φ < 5%, because within this scale the gas feed-in inhomogeneity is negligible, i.e. the gas velocity through the holes is still similar. Therefore, this value is applied in this work as construction border value (Figure 23b).

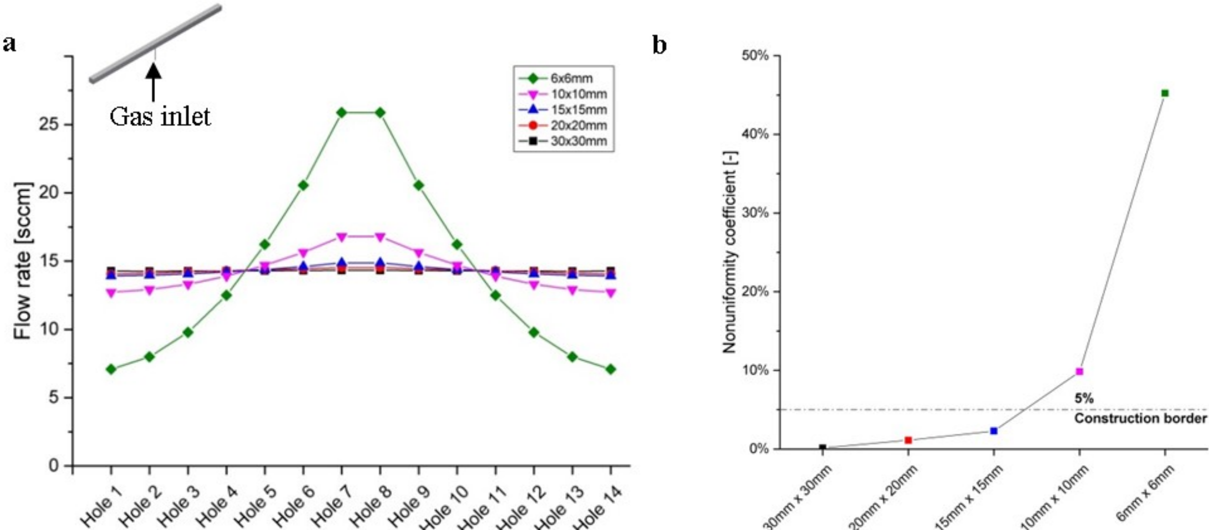

Figure 23 *Influence of the pipe section area in the distribution homogeneity (a) Gas flow distribution through holes and (b) Non-uniformity coefficient obtained for the different pipe section values considered. The results are shown via the points; the lines connecting the points in the plot are only to support guiding the eyes and are not modelled fits.*

In the Figure 23a it can also be observed that there is a cross point between holes 10 and 11. Additionally, it is noteworthy that since only the cross-section area was changed, all plots display the same behavior. Because the difference of flow rate between the holes is a consequence of the pressure drop, the cross point suggests that the mean pressure inside the pipe is always achieved in the same distance from the inlet for all the configurations under analysis.

The results of the pressure contour and velocity contour for two different pipe section areas and gas flow rate of 200 sccm are depicted in Figure 24. Figure 24a refers to

the pipe with 10 mm x 10 mm section area. The left image from Figure 24a show the pressure contour inside the chamber (blue) and inside the pipe (gradient color). The right image from Figure 24a shows the velocity contour inside the chamber (blue gradient) and inside the pipe (gradient color). Likewise, Figure 24b shows the pressure contour (left) and velocity contour (right) for the pipe with 30 mm x 30 mm section area. For instance, regarding the pressure, both Figure 24a (left) and Figure 24b (left) present a homogeneous blue color inside the chamber. Nevertheless Figure 24a (left) shows a gradient color inside the pipe (10mm x 10mm). The same pattern is not observed inside the 30 mm x 30 mm pipe in Figure 24b (left). Concerning velocity contour, Figure 24a (right) and Figure 24b (right) show a blue gradient inside the chamber. This is a hint of how much of the chamber gas volume is influenced by the gas feed-in system and by the gas outlet (gas exhaust system). Similarly, Figure 24a (right) presents a gradient color inside the 10 mm x 10 mm pipe. Figure 24b (right) shows also a color gradient inside the 30mm x 30mm pipe but slighter in comparison with Figure 24a (right). These plots contours are a visual representation of the nonuniformity coefficient of Figure 23b. For example, for the smaller section area pipe (10 mm x 10 mm) higher pressure and velocity gradient are found inside the pipe resulting in a higher nonuniformity coefficient in comparison with the bigger one (30 mm x 30 mm).

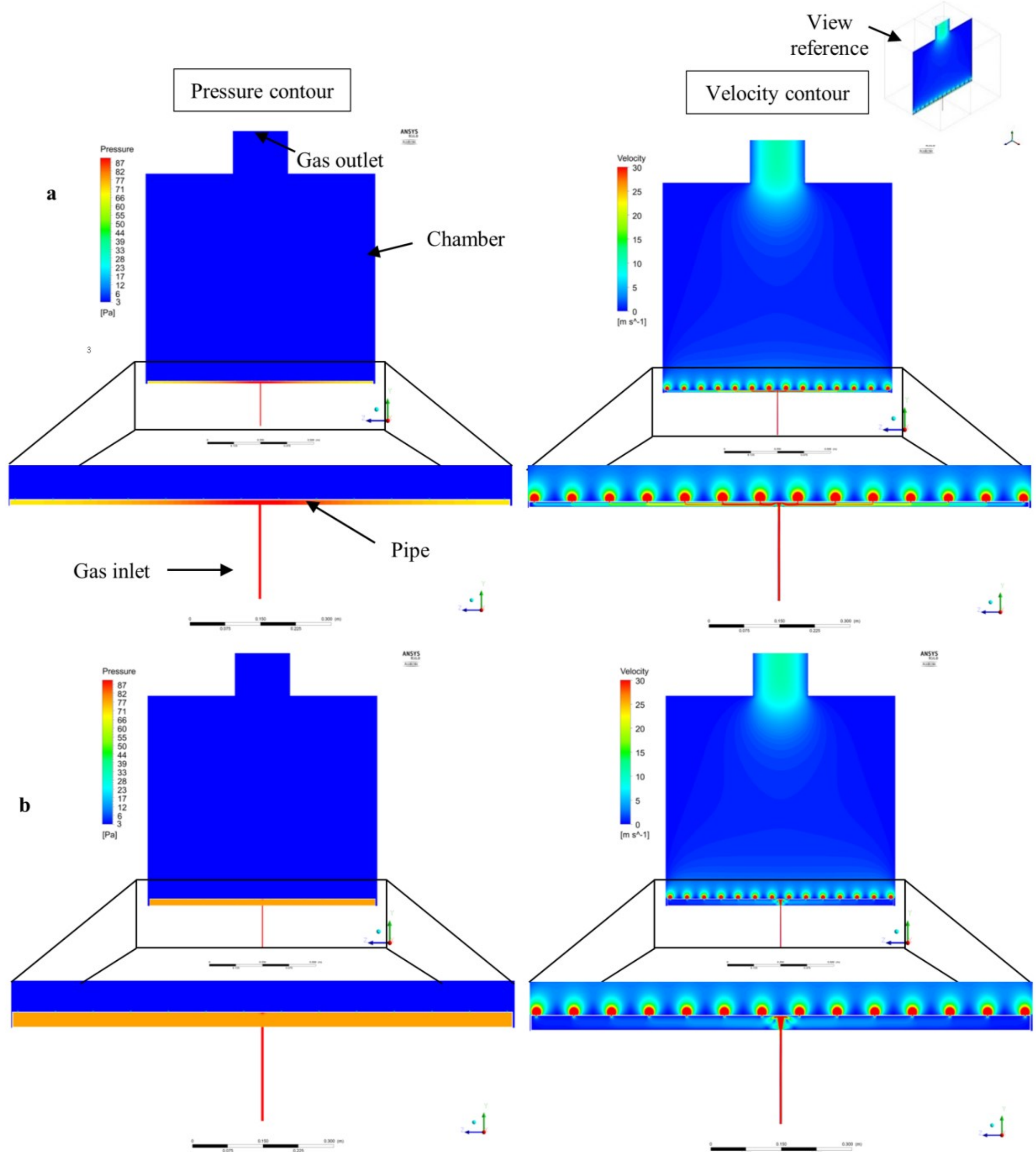

Figure 24 *Pressure contour and velocity contour a) 10 mm x 10 mm b) 30 mm x 30 mm*

Aiming at evaluating the influence of further parameters on the homogeneity of the gas flow distribution, additional simulations were done using the parameters as presented in Table 3. In Figure 25 is plotted the nonuniformity coefficient in a logarithmic scale for five different pipe section areas: 6 mm x 6 mm, 10 mm x 10 mm, 15 mm x 15 mm, 20 mm x 20 mm and 30 mm x 30 mm in diverse parameters arrangement. For each case, one parameter was changed keeping the others constant. The parameters varied were: flow rate, pipe length, number of holes, hole diameter and aspect ratio of the pipe section. It is observed that with an increase of the gas flow the homogeneity of the gas distribution

increases. The pipe section aspect ratio does not lead to a significant impact in the homogeneity. Thus, the influence of the section area on the homogeneity of the gas distribution is more relevant. Increasing the values of the length of the pipe, the pipe diameter and the number of holes, the homogeneity of the gas flow distribution decreases like found by Kulkarni and coauthors [15]. They investigated the technical layout of straight and ring pipe spargers for bubble column application. The pipe section dimensions of 30 mm x 30 mm and 20 mm x 20 mm are in a safe area regarding the homogeneity of the flow distribution (i.e. under the Φ based construction border).

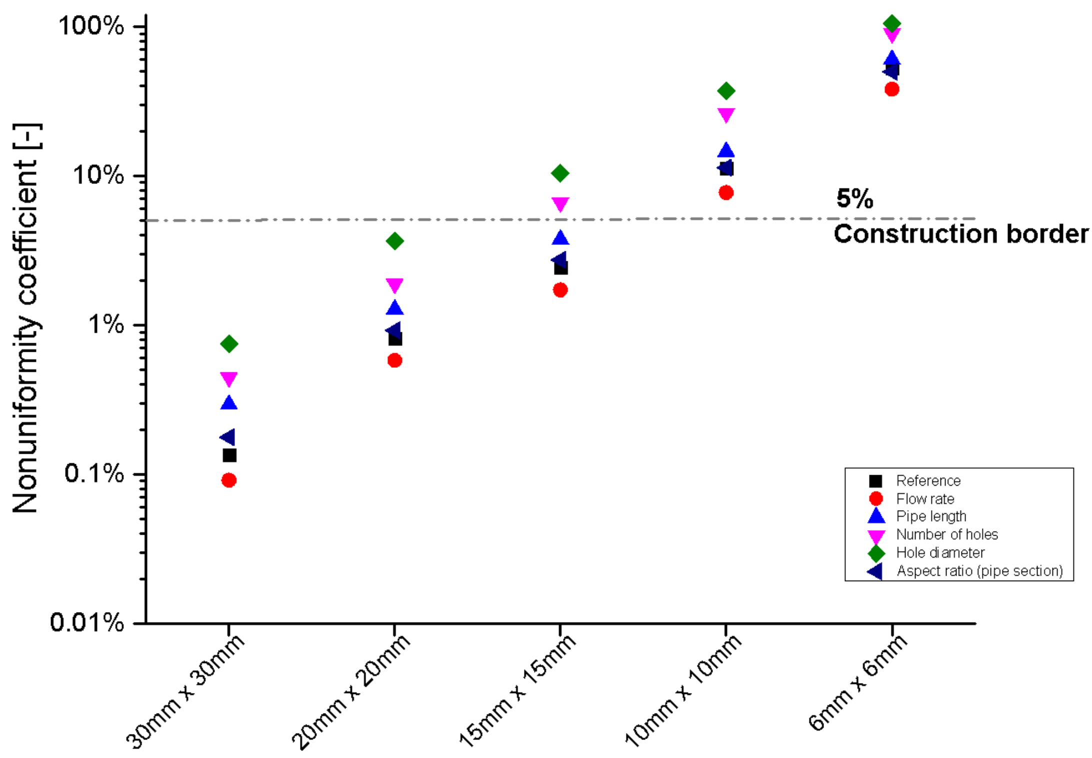

Figure 25 *Influence of different parameters on the homogeneity of gas flow distribution*

The gas flow regime of the setup under analysis was classified in terms of calculated Kn values. Based on the CFD calculations of pressure, the gas and PECVD chamber parameters the Kn values for the pipe section area of 6 mm x 6 mm and 30 mm x 30 mm were obtained. For the CFD calculation, the low pressure boundary slip condition was applied in order to consider the slip-velocity conditions [83,84]. From the analysis, the current work showed to be in the range of the slip-flow regime ($0.001 \leq Kn \geq 0.1$) as depicted in Table 6.

Table 6 *Knudsen number using 200 sccm of N_2 for two different pipe section areas: 6 mm x 6 mm and 30 mm x 30 mm*

Pipe section area (mm x mm)	Pressure (mbar)*	Mean free path (mm)	Characteristic length (mm)	Kn
6x6	1.42	0.07	6	0.012
30x30	0.78	0.13	30	0.004

*Pressure (mbar) calculated using the CFD software

Considering that the local gas flow behavior inside a PECVD chamber cannot be experimentally directly measured, the measurement of pressure values is employed to validate the simulations. The pressure inside the pipe (measured at one side of the pipe) and the pressure calculated with the CFD software in both cases changing the gas flow rate are plotted in Figure 26. Figure 26a shows in detail the experimentally measured (Exp) and calculated (Calc) pressure values for the pipe with 10 mm x 10 mm section area and 7 holes. Figure 26b, right beside shows the results for a pipe with 14 holes. Likewise, Figure 26c and Figure *26*d display the measured and calculated pressure values for the pipe with 30 mm x 30 mm section area.

The simulations agree with experimental findings leading to a maximum error of 10%. For instance, concerning the 10 mm x 10 mm pipe section area with 7 holes and flow rate of 200 sccm the internal measured pressure in one side of the pipe was 1.4 hPa and the calculated one was 1.3 hPa. This variance could be attributed to the fact that the drilled holes were not perfectly with 2 mm diameter due to the manual preparation process, especially for the pipe with larger section area. Thus more holes would mean a statistical average that is closer to the model.

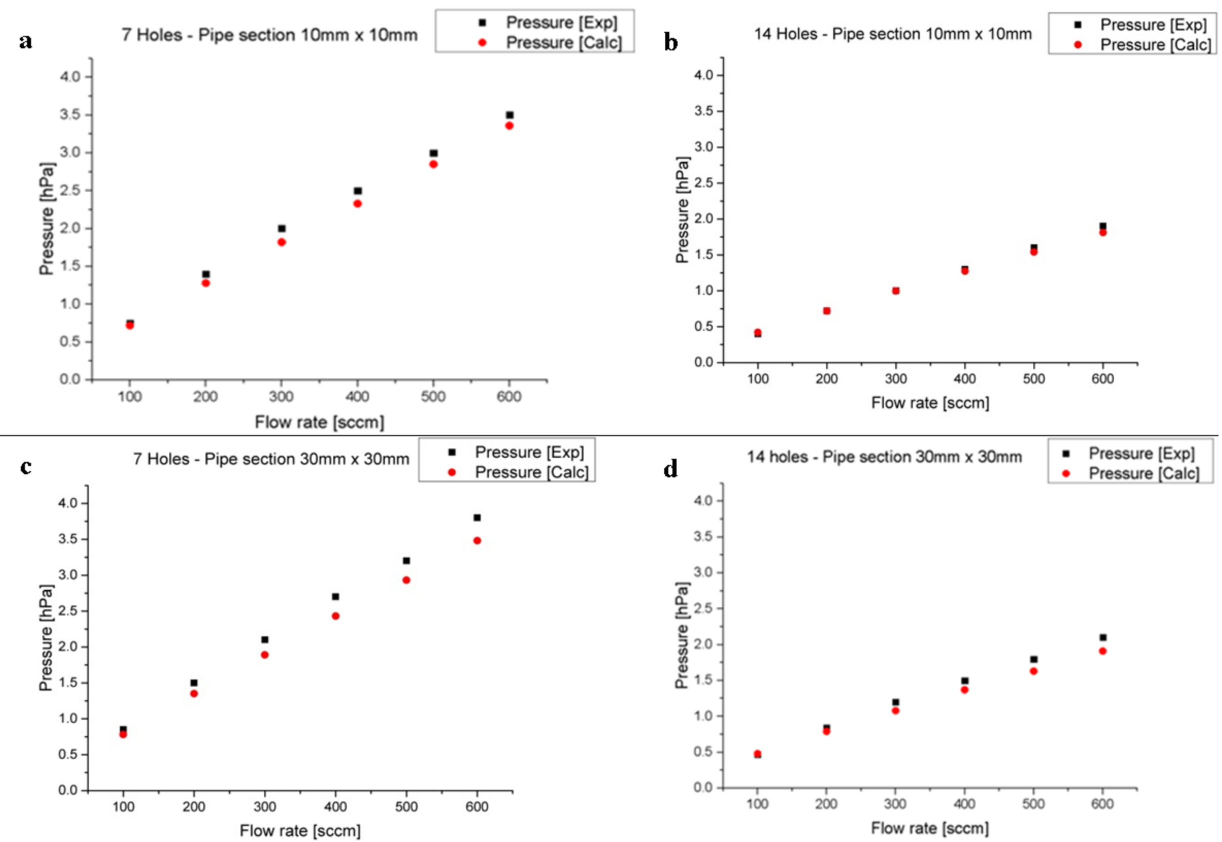

Figure 26 *Comparison of pressure values obtained through experiments and simulations (a) & (b) Pipe section 10 mm x 10 mm; (c) & (d) Pipe section 30 mm x 30 mm*

The main conclusions extracted from the results are:

a) From the analyzed parameters the pipe section area is the most relevant one influencing the homogeneity of gas distribution.

b) By decreasing the pipe section area, the pressure gradient increases, resulting in a nonhomogeneous gas distribution through the holes. For instance, the nonuniformity coefficient for the 30 mm x 30 mm pipe section area is 0.1% and for the 6 mm x 6 mm one 45%.

c) Taking the construction border (Φ <5%) into consideration the results show that the pipe section area above 20 mm x 20 mm are in a safety area regarding the homogeneity of gas distribution. It means that pipes with section area larger than 20 mm x 20 mm allow more flexibility to change other layout parameters, like hole diameter and pipe length, keeping the nonuniformity coefficient under 5%.

d) The pressure values from the CFD simulations are in good agreement with the obtained experimental data.

The knowledge acquired with the CFD calculations in agreement with experimental pressure measurements are very helpful for researchers and constructors to develop new gas feed-in systems for low-pressure plasma chambers.

3.2. Gas exhaustion system

Figure 27 shows a gas simulation result from the current setup of the low-pressure plasma chamber used for this research with a smaller scale bar range. The influence zone of the gas feed-in system is depicted in Figure 27 and it represents a small fraction of the plasma chamber volume. The gradient color, which means velocity gradient, extends over approximately 5cm from the pipe holes. Nevertheless, it is very important to have it in mind before an experiment or a complete construction project of a low-pressure plasma chamber is done. From the gas exhaustion system point of view, its influence zone is much larger than the one from the gas feed-in system. The gradient color is much more intense in the region of the exhaustion system in comparison to the gas supply region. Having this picture in mind, in a coating process is expected to see a similar pattern which would represent a gradient in the deposition rate.

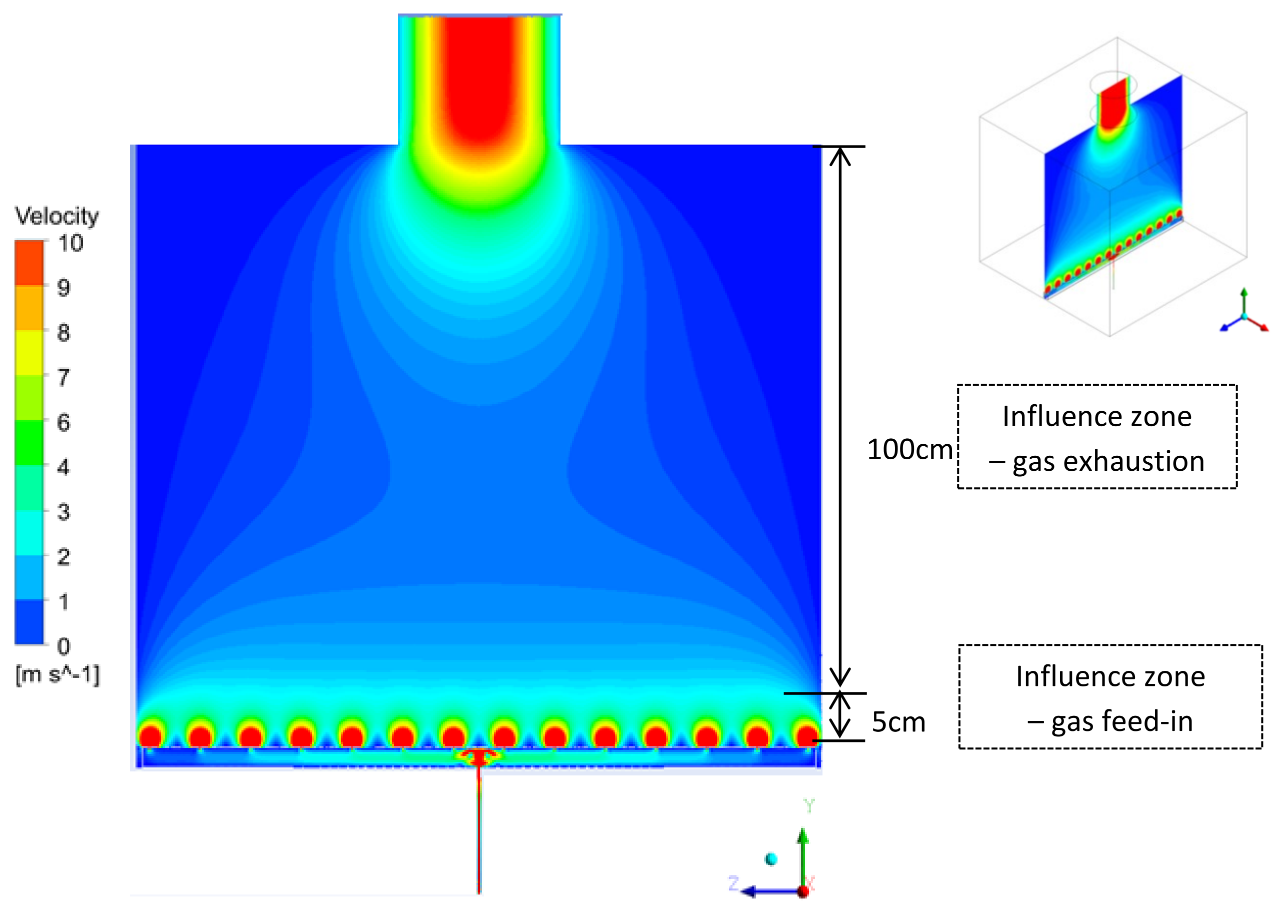

Figure 27 *Gas simulation result showing the two dissimilar influence zones of the gas feed-in and of the gas exhaustion*

To verify the current condition of the low-pressure plasma chamber regarding the deposition rate distribution, an experiment was planned, as showed in Figure 28. The experiment consisted in coating Si-Wafers equally distributed in the volume of the chamber and in floating potential (i.e. the samples were not direct in contact with the electrodes). To perform it, the Si-wafers were fixed on a quartz glass (Figure 28) and this assembly was fixed to a nylon wire and hanged at the perforated grid. A total of 25 nylon wires were used, each one with three assemblies of Si-wafers + Glass equally spaced. As shown in Figure 28 there is a “U” form electrode system, which is connected to the RF-generator and the other “U” is formed with the grounded electrodes. Hence, the area ratio of powered electrode to grounded electrode is equal one, which means a Self-Bias free process.

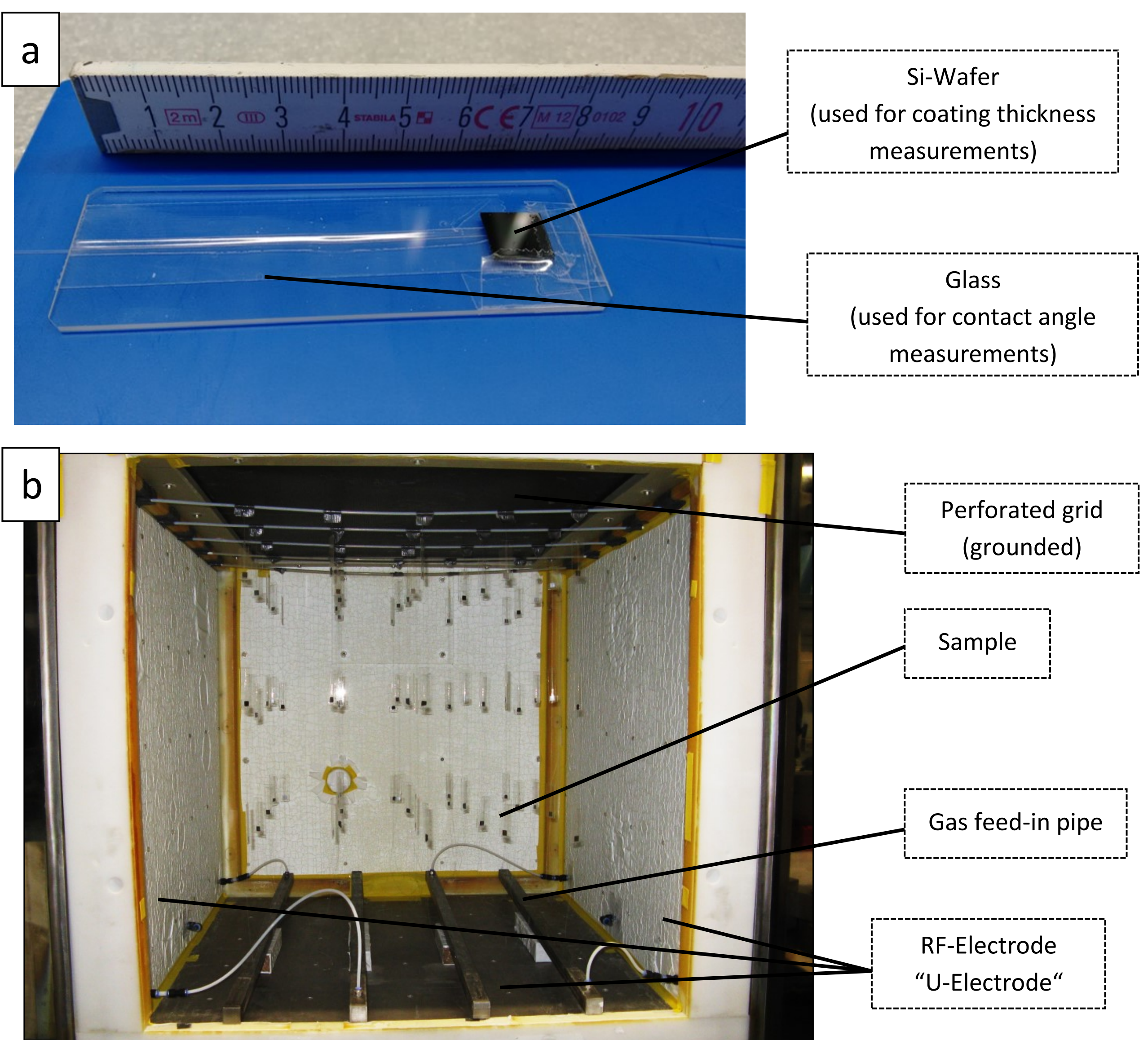

Figure 28 *(a) Samples used in the experiment (b) Experimental setup*

The coating process used was the same as shown in Table 1 and it will be the same in all performed experiments under the frame of this research thesis.

Figure 29 shows the results of the calculated deposition rate based on the measurements of the coating thickness distribution over the Si-Wafers and interpolated using the software Origin. The deposition rate was calculated dividing the measured coating thickness by the coating deposition time.

$$Deposition\ rate\ = \frac{Coating\ thickness}{deposition\ time}\left[\frac{nm}{min}\right]$$

The calculated deposition rate was plotted using a color contour graphic. This kind of plot was used to make easier the understanding in a way that a 3D experiment is showed in a 2D graphic. In this case, low deposition rate and high deposition rate are represented in blue and red, respectively.

The results are showed in three different planes: top plane (Figure 29a), middle plane (Figure 29b) and bottom plane (Figure 29c). Each plane contains 25 samples. Their positions are represented by the black points in each image.

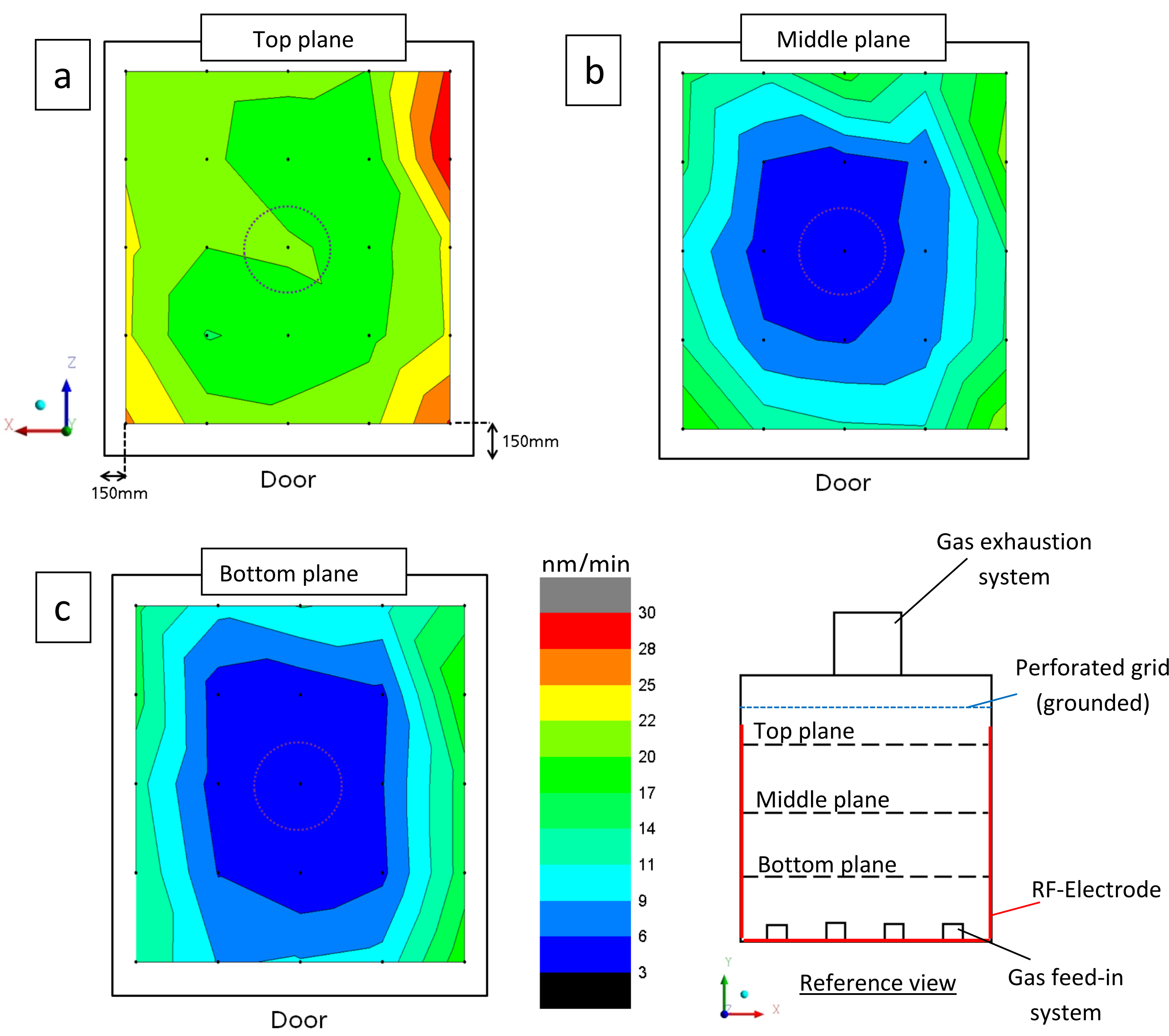

Figure 29 *Coating deposition rate distribution (a) top plane (b) middle plane (c) bottom plane*

In all three planes (bottom, middle and top plane), high deposition rates on the edges (close to the electrodes) and low deposition rates in the middle were observed. A high difference can be seen between the middle chamber and in their edges. These results suggest that there is a not homogeneous gas flow inside the chamber. Additionally, Figure 30 shows clearly that the deposition rate increases from bottom plane to the top plane while in the bottom and middle plane was practically the same. Furthermore, very high standard deviations can be observed, especially in the bottom and middle plane. Since there is no literature available to compare these values, as coating deposition is process and chamber dependent, the values obtained are the reference starting points for new improvements in

the standard low-pressure plasma chamber focusing on reducing the inhomogeneity. In this experiment, the top plane showed the lowest inhomogeneity and it was calculated by the following equation:

$$Inhomogeneity(\%) = \frac{Standard\ Deviation\ of\ deposition\ rate}{Average\ of\ deposition\ rate}$$

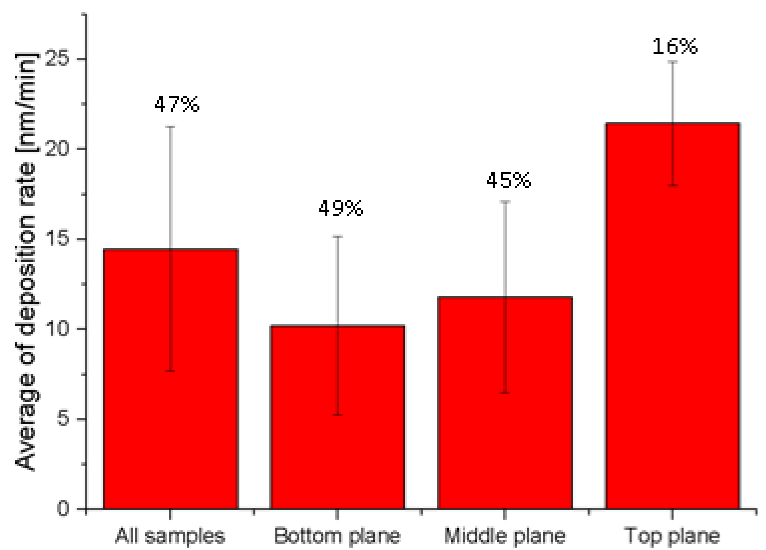

Figure 30 *Average of deposition rate - Experiment current setup*

To get a better understanding about the reasons why the current setup showed the aforementioned pattern, gas flow simulations were performed.

3.2.1. CFD Simulation

The CFD simulations were performed applying the software package Ansys Fluent 16.0®. A quarter of the model was used. It allows shorter simulation time and mesh refinement at important regions (gas feed-in holes and gas exhaustion region). Moreover, they require relatively less modelling effort (e.g. pre-processing) when compared to a full model analysis. Figure 31 (part a and b) show the full model of the experiment setup and part c of Figure 31 shows the quarter of the experiment setup model which was used for the gas flow simulation. It can also be seen that the metallic perforated grid (grounded) was not included in the gas simulation due to process limitation of the computer used. As the name already suggests, perforated grid, is a metallic grid completely perforated with 1 mm diameter holes in sequence. It means that by adding the perforated plate to the simulation

the number of elements to be calculated would jump from less than 10^6 to more than $20*10^6$ which makes unfeasible the calculation.

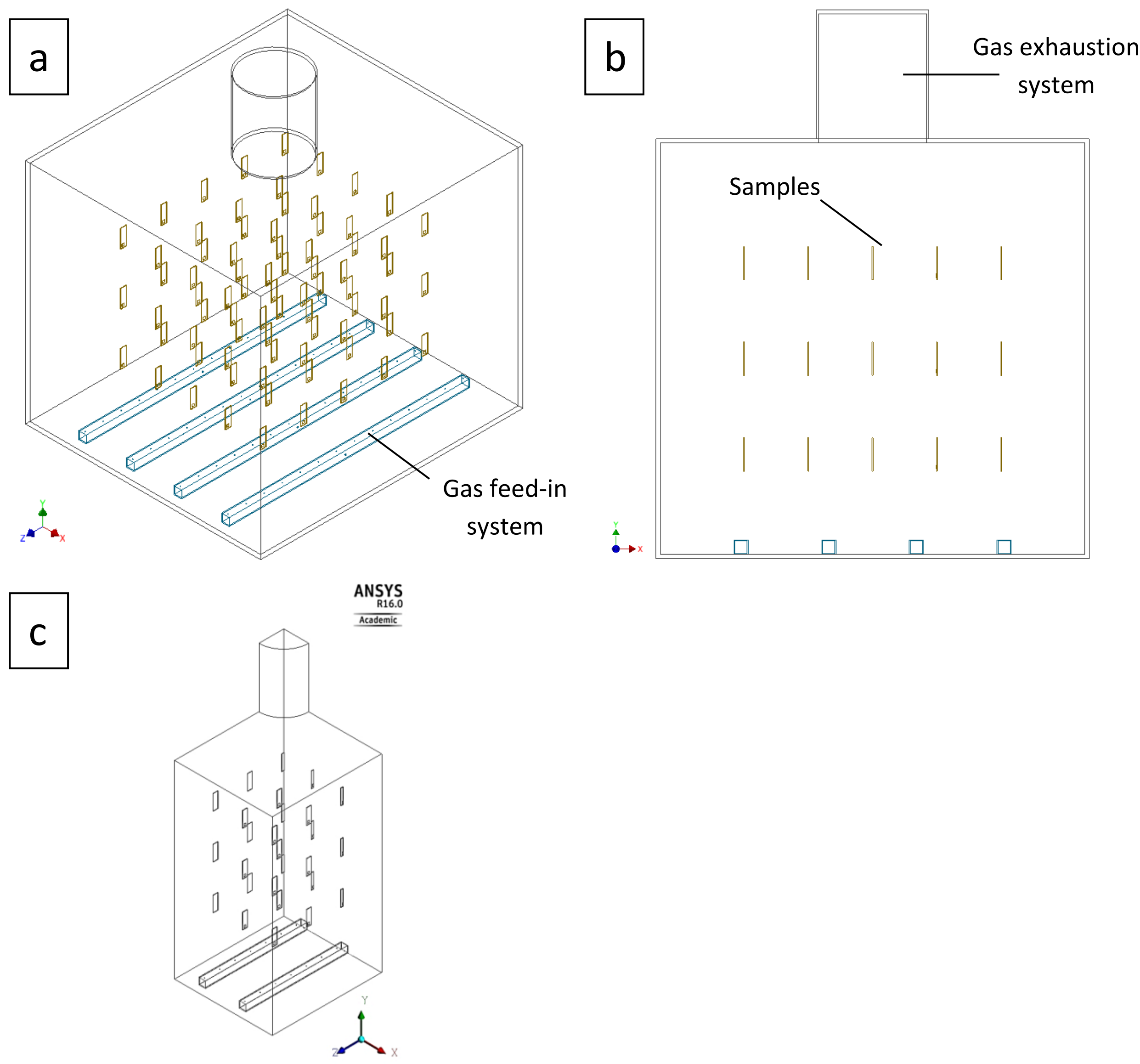

Figure 31 *Model of the experiment setup*
(a) Isometric view (b) Front view (c) isometric view of a quarter of the model

For all CFD simulations carried out the boundary conditions were defined to reproduce the conditions of the experiment (Table 7). The number of elements in each model was approximately 3,000,000. Grid independence tests were performed to determine the greatest mesh refinement. The mesh was refined in the gas feed-in pipe, inner holes and close to the gas exhaustion system. The solutions were converged when all the residuals

were smaller than 10^{-5} for the continuity and momentum equations and smaller than 10^{-6} for the energy equation.

Table 7 *Boundary conditions for the gas flow simulation of the experiment*

Model	Boundary conditions	Values
Laminar flow with low pressure boundary slip	Gas Temperature	298.15 [K]
Ideal gas	Wall Temperature	298.15 [K]
Steady state	Mass flow rate of N_2 (inlet)	2.76E-06 [kg/s]
	Pressure (outlet)	0.015 [hPa]

The results from the gas flow simulation of the experiment setup are depicted in Figure 32, where part a represents the top plane, part b middle plane and part c bottom plane. To make the results more visual, the simulation result for the quarter model was mirrored in the two symmetry planes. From Figure 32 is observed that the gas obtains high velocity in the middle, represented by the red color, and low velocity near to the walls represented by the dark blue color. It is also showed that the gas velocity increases toward the gas exhaustion system, from bottom plane to top plane. Additionally, the samples influenced the gas flow inside the chamber characterized by the lower velocities closed to them in comparison to the neighbor region.

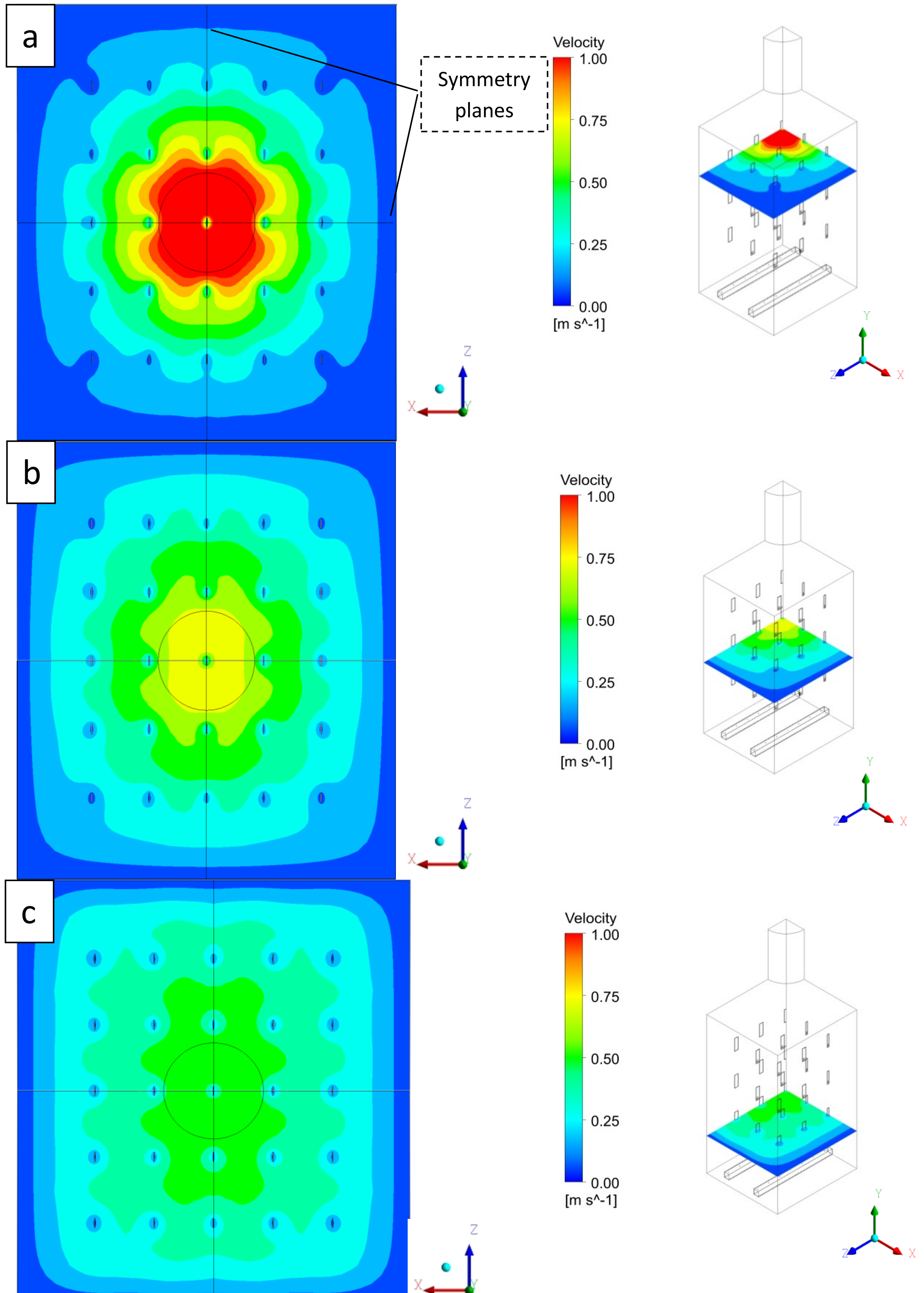

Figure 32 *Gas simulation results of the experiment- Current setup*

Based on the experimental and on the gas simulation results the following hypotheses are formulated:

- The gas exhaustion system is influencing the coating deposition rate
- Higher velocities (in the chamber middle) lead to lower deposition rates and lower velocities (near to the walls) lead to higher deposition rates. Nevertheless, it cannot explain why the top plane showed higher deposition rates as it showed higher gas velocity average
- The gas flow plays a role in the homogeneity of the coating deposition rate
- The gas feed-in system is apparently not influencing the coating deposition rate for the current setup

With the aim of verify the previous hypotheses, it was necessary to create new solutions to modify the gas flow inside the chamber by reducing the influence of the gas exhaustion system. In this context, three eligible configurations were considered and the desired requirements were defined and schematized in Figure 33. The red “x” means out of requirement and the green mark means that the requirement is satisfied. Mandatory is a configuration that allows very homogeneous gas exhaustion from the chamber along with applicability in plasma coating process. If these two requirements can be fulfilled together with versatility, low construction cost and short construction time then it would be the optimal one. The standard condition of the plasma-coater is a large (260 mm diameter) central exhaustion flange with a perforated metallic grid installed under it. One idea is to substitute this single flange for more flanges and distribute them in an organized way on the top of the plasma chamber. This construction can homogenize the gas exhaustion once the low pressure inside the plasma chamber is taken into consideration. This is a different situation from the gas feed-in where inside the pipe a high pressure is generated. It means that the dimensions of the flanges must be carefully designed so as to reduce the pressure drop and not to jeopardize the vacuum pump capacity. However this solution offers very low versatility, high construction cost and high construction time. Other alternative evaluated was the installation of perforated pipes (without the bottom surface) between the perforated metallic grid and the central exhaustion flange. These kinds of pipes would be manufactured in a plate with the aim to let the gas exhaustion just through the pipe holes. This solution can achieve homogeneous gas exhaustion as well with relative low construction

cost. Nevertheless, it requires time to construct and it is not versatile. Any future change would imply in time and money cost. Lastly, a solution with a thin perforated plate installed over the perforated metallic grid was evaluated and it satisfies all the defined requirements. As the plate is thin, the pressure drop will not be significant which allows a larger range of holes diameter. Therefore, the hole diameter can be tailored taking into consideration the vacuum pumping capacity to achieve the desired working pressure. Moreover, this configuration allows quick modifications, has low cost and short construction time. Therefore, this idea was selected to be developed in this research work.

Through the development of gas feed-in systems, was shown in the previous section (3.1) that the pressure inside the gas feed-in pipe must be homogeneous and higher than the chamber pressure to achieve an even gas supply through the pipe holes. The same principle was applied for the gas exhaustion system with the aim to remove the gas evenly from the low-pressure chamber and to allow a homogeneous gas flow distribution inside it.

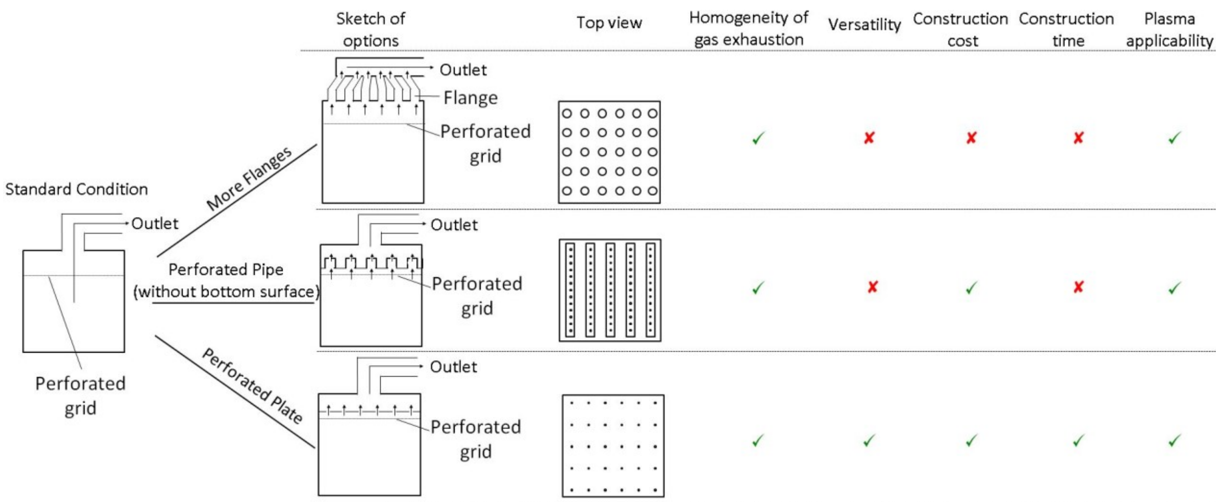

Figure 33 *Eligible gas exhaustion configurations and desired requirements*

In this context, a perforated plate was developed. It was named Baffle Plate. It is similar to ideas used in other applications, i.e. control the fluid flow for instrumentation accuracy requirements [106]. The idea is to create comparable effect, like the installation of more flanges, but in a simpler manner from the construction point of view. This effect can be achieved by the Baffle Plate where the holes will act as smaller “exhaustion systems” without huge modifications in the low-pressure plasma chamber and it avoids high investments. The challenge is to develop this Baffle Plate in a way that all the holes will show the same pressure difference between the regions under and above the holes what will

imply in homogenous gas exhaustion from each hole. Thereupon, it is very important to define the influence of the Baffle Plate layout constructions on pressure loss through the holes. The constructor needs to take into consideration the desired work pressure and the pump suction capacity by developing the Baffle Plate. This is very important since the control over the gas residence time, which can be achieved through the control over the working pressure by installation of the Baffle Plate, can reduce the powder formation.

The first step was to use the support of the simulation tool (Ansys Fluent 16.0®) to achieve the desired configuration. Figure 34 shows two different configurations of the baffle plate, which were used in the gas simulation. Part a from Figure 34 shows a baffle plate with a radial distribution of the holes and part b shows a baffle plate with a linear distribution of the holes. Both of them have the same number of holes, which is 30, and same hole diameter (18 mm).

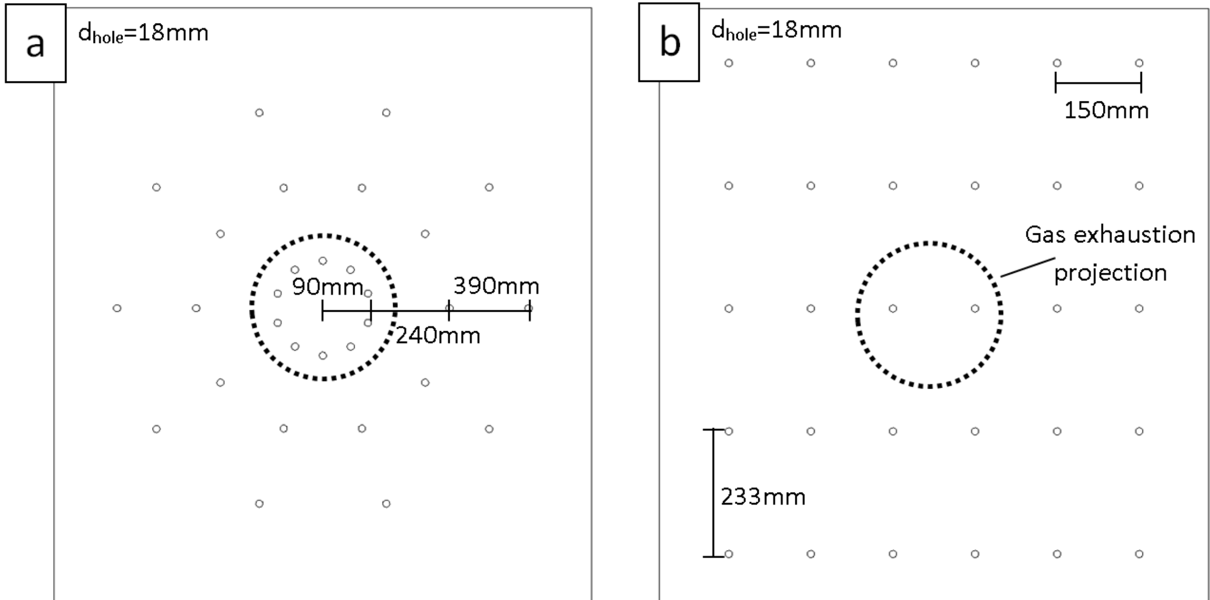

Figure 34 *Baffle plate model a) radial distribution b) linear distribution*

The simulations with the baffle plate assembled were done in the same way as for the current setup of the low-pressure plasma chamber. Just a quarter of the model was used for the simulation and to make the velocity distribution more visual, the results were mirrored with the symmetry planes. Figure 35 shows the gas simulation results for two different baffle plate configurations. Figure 35a represents the baffle plate with radial distribution of the holes and Figure 35b represents the baffle plate with linear distribution of the holes. For the case where the holes were radially distributed (Figure 35a) it can be seen

that in the middle the velocity is still much higher than on the borders, although in reduced scale in comparison with the Figure 32b where no Baffle Plate is installed. This is characterized by the color gradient which red means high velocity and dark blue means low velocity. For the case where the holes were linearly distributed (Figure 35b) no strong gradient could be observed. There is a large area with a light green and then again dark blue close to the walls. It means that for the construction of effective baffle plates not just the amount and diameter of the holes are important but also their distribution. It is essential to have the holes distributed in a way that all the active area of the low-pressure chamber is covered. The constructor must also have in mind the desired working pressure to develop the suitable baffle plate. The working pressure is also one important parameter along to the gas precursor ratio and the supplied power to achieve the desired coating properties.

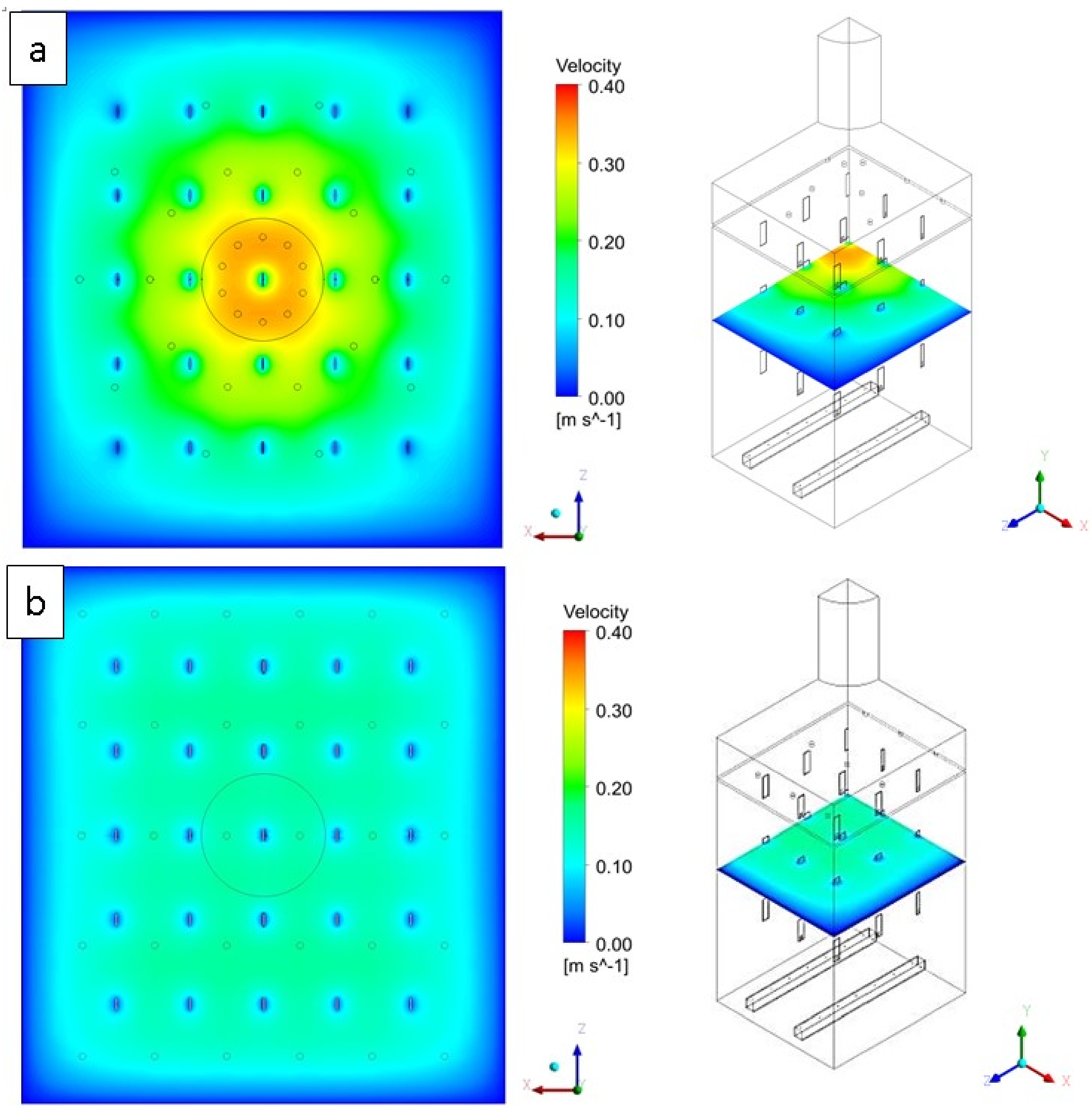

***Figure 35** Gas flow simulation results for two different baffle plates assembled (a) radial distribution of the holes (b) linear distribution of the holes*

To validate the calculated values, as it is not possible to measure the gas velocity inside the low-pressure plasma chamber, pressure measurements were done varying the gas flow from 100sccm to 600sccm and the measured data were compared to the calculated ones. For these measurements, the empty chamber was used, i.e. no samples inside.

Figure 36a show the pressure contour for 200sccm gas flow. It can be observed that the highest pressure is inside the gas feed-in pipe (~50Pa) and the lowest is above the baffle plate (~1Pa). Moreover, the pressure inside the chamber is very homogeneous (1.4Pa). This is the reason why the gas flow was more homogenous with the baffle plate installed (Figure 35b). The pressure measurements were done in the two points as depicted in Figure 36b, one in the gas exhaustion and the other one from a flange in the back of the chamber.

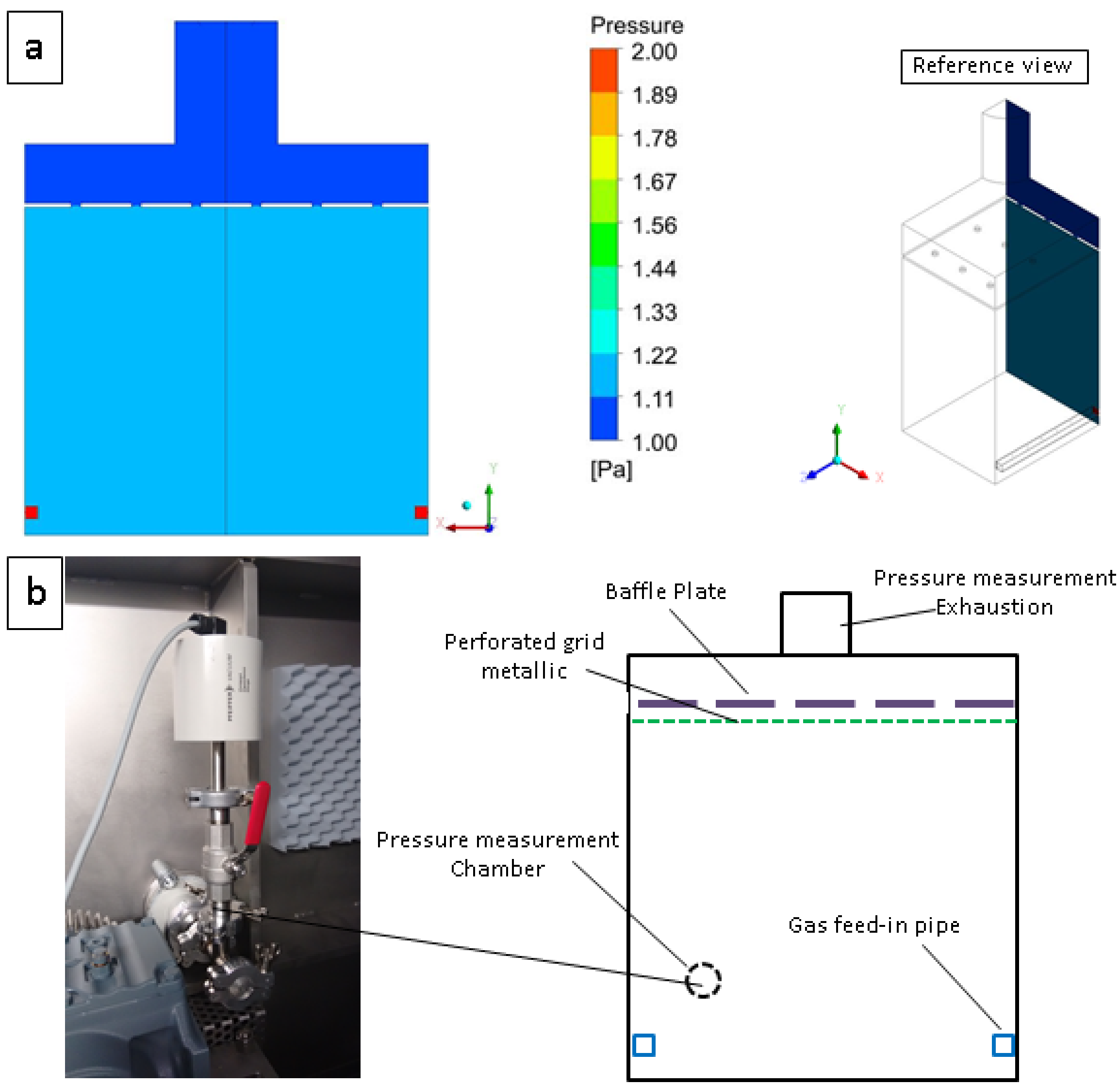

Figure 36 *(a) Pressure contour [simulation] (b) Scheme of the low-pressure chamber showing the positions where the pressure was measured*

The comparison of calculated (CALC) and measured (EXP) pressure can be seen in Figure 37. Because for the simulations the perforated grid was not considered, the pressure values obtained through the measurements are higher than the calculated ones as exhibited in Figure 37a. Nevertheless, both show a pressure increase by increasing the gas flow. Regarding the pressure in the exhaustion system (Figure 37b), the measured values increase by increasing the gas flow, although the calculated one remains constant. This difference might be related to the fact that the simulation considers a perfect pumping system, where the desired pressure can be achieved. In practice, there is the limitation of the pumps. Even though the butterfly valve was 100% open, the desired pressure could not be reached. For this thesis, the simulations results are still valuable because the pressure difference (Figure 37c) between inside chamber and the gas exhaustion were very similar and therefore it is expected that the gas flow would behave in the same way.

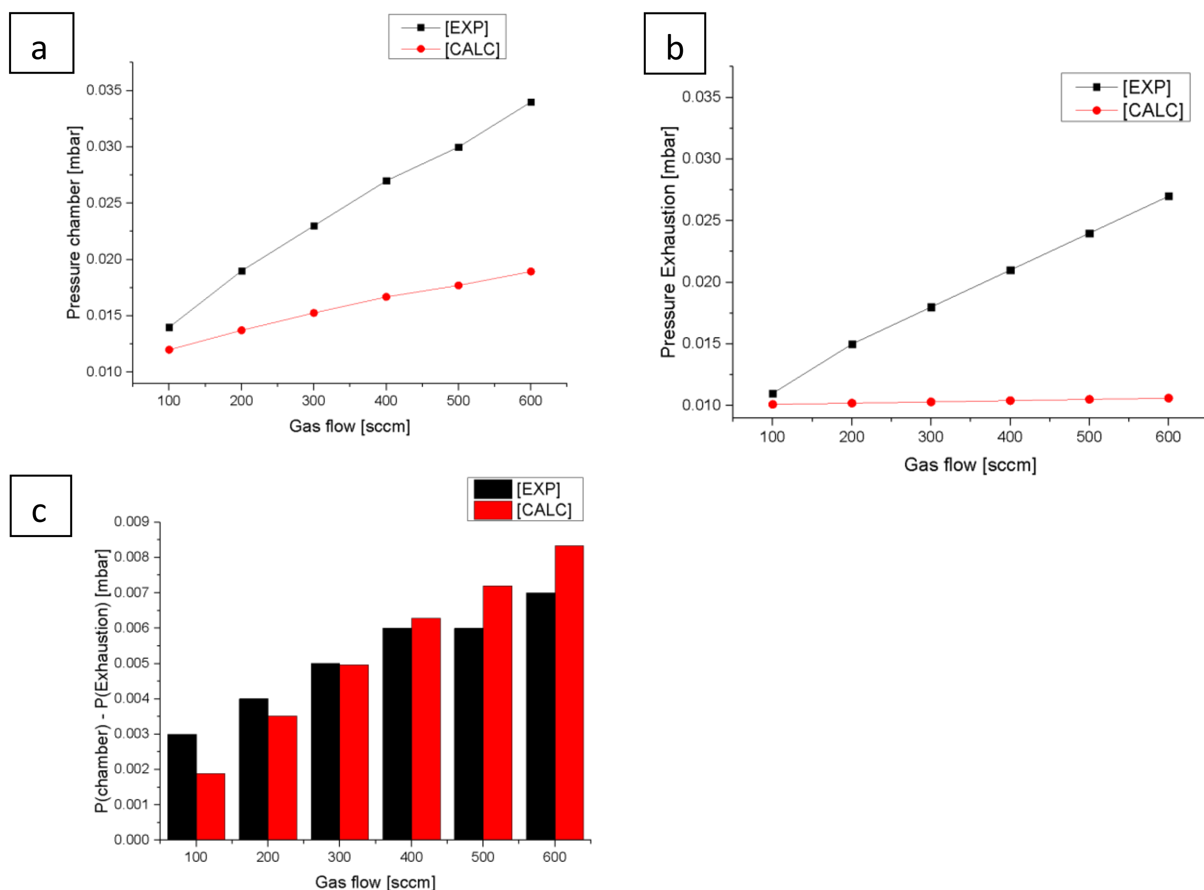

***Figure 37** Comparative of calculated and measured pressure values*
(a) Pressure inside the low-pressure chamber (b) Pressure in the gas exhaustion
(c) Pressure difference between the inside chamber and the gas exhaustion

The curves generated by the measurement and/or calculation of the pressure inside the chamber and over the Baffle Plate as showed in Figure 37 are important tools to keep the working pressure under control and consequently to avoid powder formation during deposition.

With the aim of create guidelines for the construction of Baffle Plates additional gas flow simulations were accomplished. Bayazit and coauthors [107] showed that for laminar flow regime the larger pressure drop occurred for larger plate thickness $\left(\frac{t}{D} = 1\right)$, where “t” is the plate thickness and “D” the hole diameter. Therefore, for this thesis a thin plate $\left(t = 3mm, \frac{t}{D} = 0.17\right)$ was used to avoid high pressure drop. The starting point was the simulation for five distinct distances between the Baffle Plate and the top of the chamber (Figure 38), keeping constant other reference parameters as presented in Table 8, the resulting curve was named as reference curve. Afterwards, the CFD simulations were performed varying the values of some parameters as shown in Table 8 under the changed parameters column. For each simulation one parameter was varied while the others were kept constant.

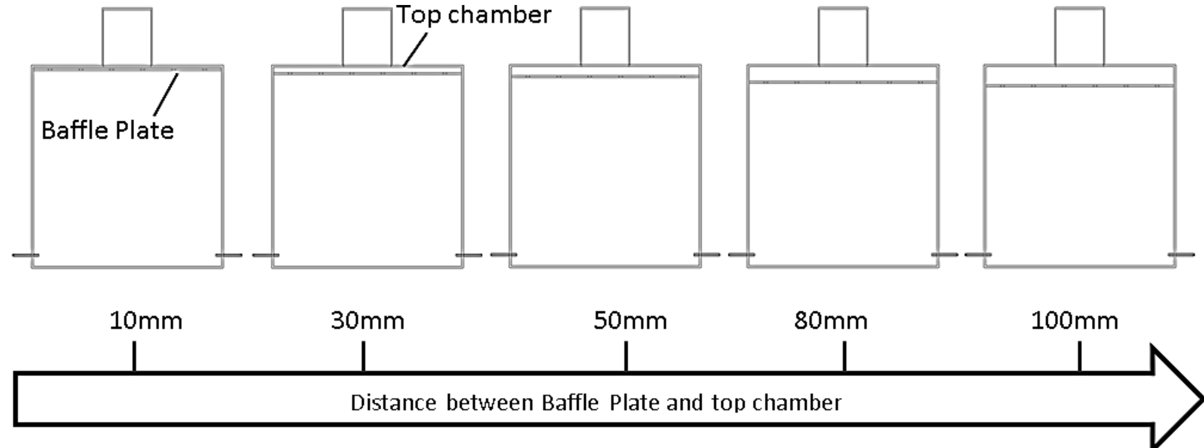

Figure 38 *Representation of the low-pressure plasma chamber with different distances between the Baffle Plate and the top chamber*

Table 8 *Baffle Plate technical layout under simulation analysis*

		Changed parameters			
***Distance to the top [mm]**	Reference parameters	Flow rate [sccm]	Number of holes	Hole Diameter [mm]	**Chamber volume
10		300	-	-	-
30	Flow rate [sccm] → 145				
		-	54	-	-
50	Number of holes → 30				
		-	-	30	-
80	Hole diameter [mm] → 18				
100		-	-	-	2/3

*Distance from the baffle plate to the top of the low-pressure plasma chamber
**Two thirds of the original model volume were used

Figure 39 are the calculated non-uniformity coefficient for the five distinct distances between the Baffle Plate and the top of the chamber. The non-uniformity coefficient was calculated in the same way as presented in section 3.1.3. It can be observed that the non-uniformity coefficient increases slightly from 100 mm to 50 mm distance and from 50 mm toward 10 mm it increases reasonably. This scenario is quite like the gas feed-in pipe construction described in section 3.1.1, where lower pipe section area led to higher non-uniformity coefficient.

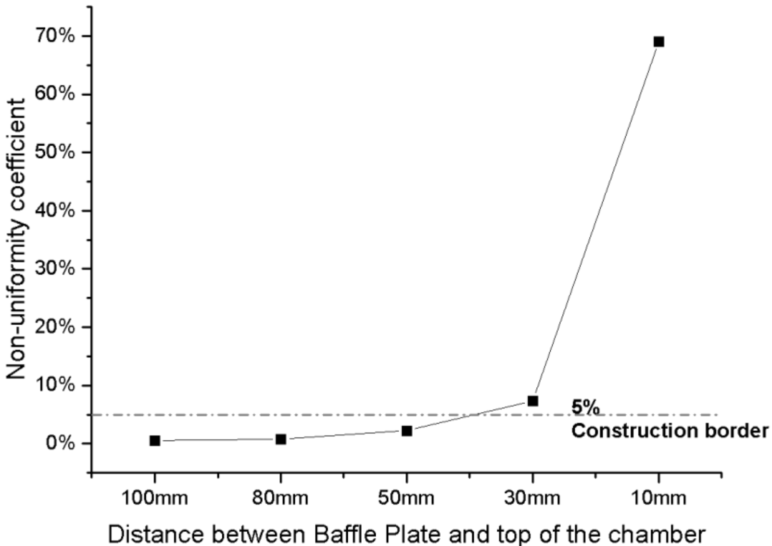

Figure 39 *Influence of the distance from the Baffle Plate to the top of the chamber on the non-uniformity coefficient. The results are shown via the points; the lines connecting the points in the plot are only to support guiding the eyes and are not modelled fits.*

Figure 40 displays the velocity and pressure plot contour for two different distances between Baffle Plate and top of the chamber. Left side shows the plots for 100 mm distance and right side for 10 mm distance. Comparing the two pressure contour plots, by 100 mm (top left) there is no pressure gradient (overall blue) over the Baffle Plate unlike the case with 10 mm distance (top right) where a gradient is seen represented by the transition from green color on the sides to blue color in the middle. Due to this pressure gradient, it can be observed in the velocity plot contour for 10mm distance case (bottom right) that the gas velocity is higher in the middle holes in comparison to the holes localized in the sides. For the case with 100 mm distance (bottom left) the gas velocity is the same in all exhibited holes.

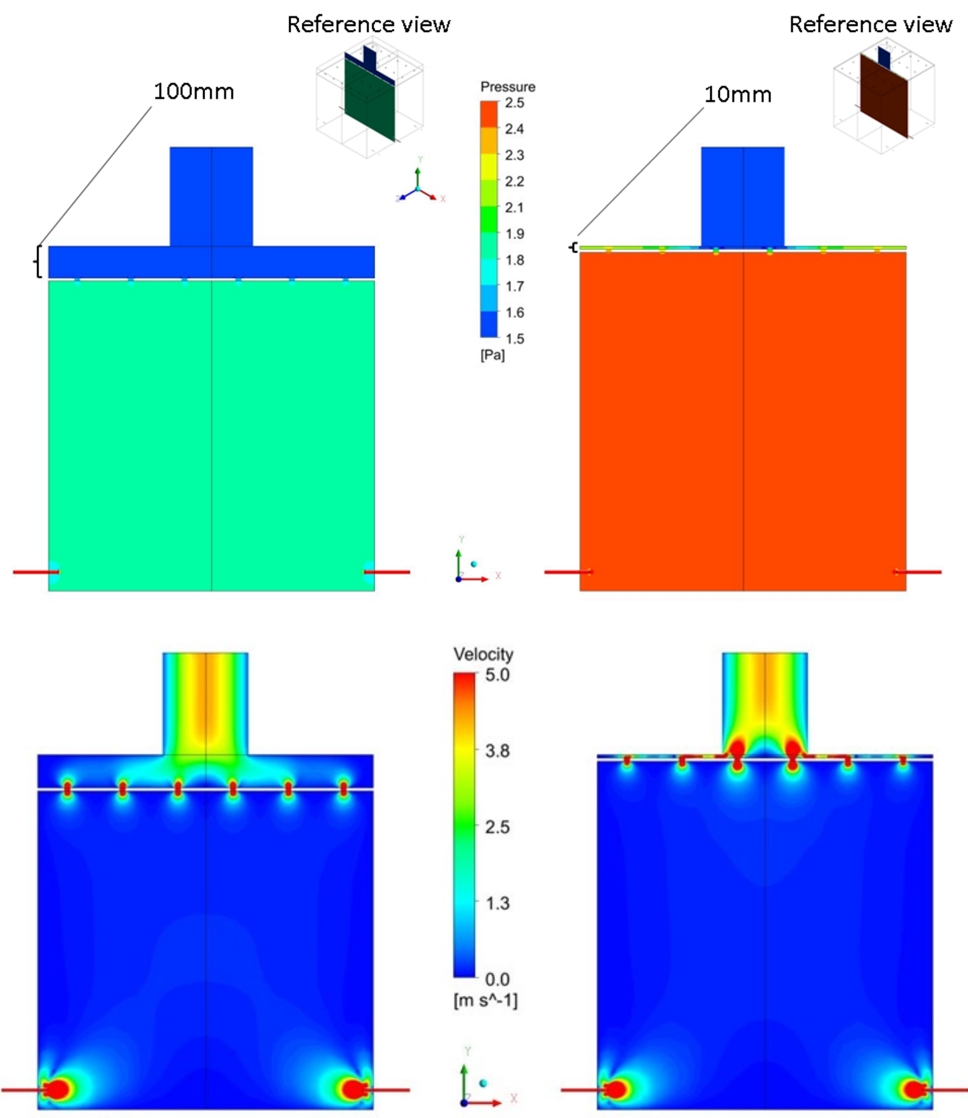

Figure 40 *Gas flow simulation results showing pressure contour and velocity contour for two different distances between Baffle Plate and top of the chamber*

Figure 41 shows the nonuniformity coefficient in a logarithmic scale for five different distances between Baffle Plate and top of chamber: 100 mm, 80 mm, 50 mm, 30 mm and 10 mm in diverse parameters arrangement. In each circumstance one parameter was changed keeping the others constant. The parameters varied were: flow rate, number of holes, hole diameter and aspect ratio of the chamber. In all cases the parameter was increased except the aspect ratio where two thirds of the initial chamber volume was considered. It is observed with an increase of the gas flow rate and the number of holes did not lead to a significant impact in the gas exhaustion homogeneity as well as by reducing the volume of the chamber. Increasing on the holes diameter decreases the homogeneity of the gas exhaustion. Thus, the influence of the distance between the Baffle Plate and the top chamber on the homogeneity of the gas exhaustion is more relevant. The installation of the Baffle Plate must keep a minimum distance of 80 mm from the top of the chamber to be in a safe area regarding to homogeneous of gas exhaustion, i.e. under the Φ based construction border.

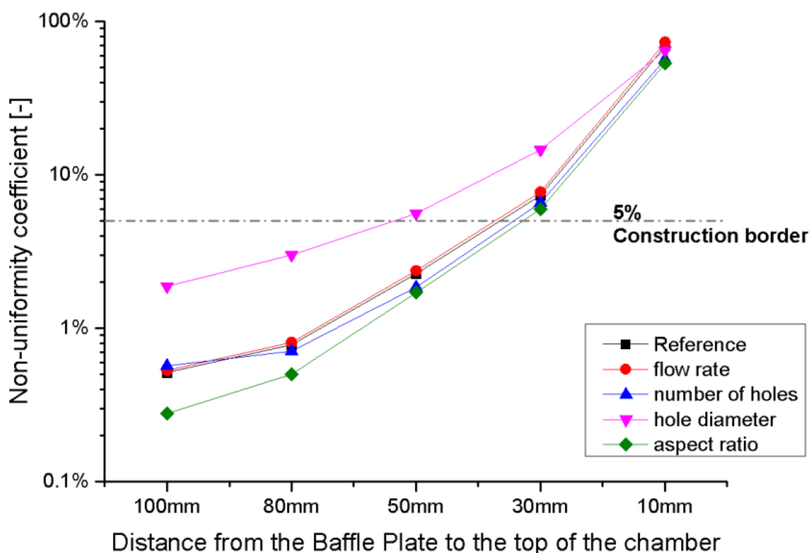

Figure 41 *Influence of different parameters in the homogeneity of the gas exhaustion through the holes of Baffle Plate The results are shown via the points; the lines connecting the points in the plot are only to support guiding the eyes and are not modelled fits.*

The main conclusions extracted from the results are:

a) From the analyzed parameters the distance between Baffle-Plate and top chamber was the most relevant one influencing the homogeneity of gas exhaustion.

b) By decreasing the distance between Baffle-Plate and top chamber, the pressure gradient in this region increases resulting in nonhomogeneous gas exhaustion through the holes. For instance, the nonuniformity coefficient for 100 mm distance is 0.5% and for 10 mm distance is 69%.

c) Taking the construction border (Φ <5%) into consideration the results showed that the installation of the Baffle-Plate with a distance above 80 mm to the top chamber is in a safety area regarding the homogeneity of gas exhaustion for low-pressure applica-tion.

d) From the analyzed values, flow rate and number of holes do not have a consid-erable influence in the homogeneity of gas exhaustion through the holes. However, it is recommended to start the layout with hole diameter in the order of 15 mm.

e) The hole diameter strongly influences the homogeneity of gas exhaustion through the holes, especially with high distances between Baffle-Plate and top of the chamber

f) The chamber volume has an influence in the homogeneity of gas exhaustion, es-pecially with high distances between Baffle-Plate and the top of the chamber

g) The Baffle-Plate is an effective solution to improve the homogeneity of coating deposition rate for plasma polymerization processes

3.2.2. **Experiment with installed Baffle Plate**

With the intention to identify the practical influence of the Baffle Plate in respect to the homogeneity of the coating deposition rate, the same experiment as shown in Figure 28 was performed. However, now with the Baffle plate installed as depicted in Figure 42.

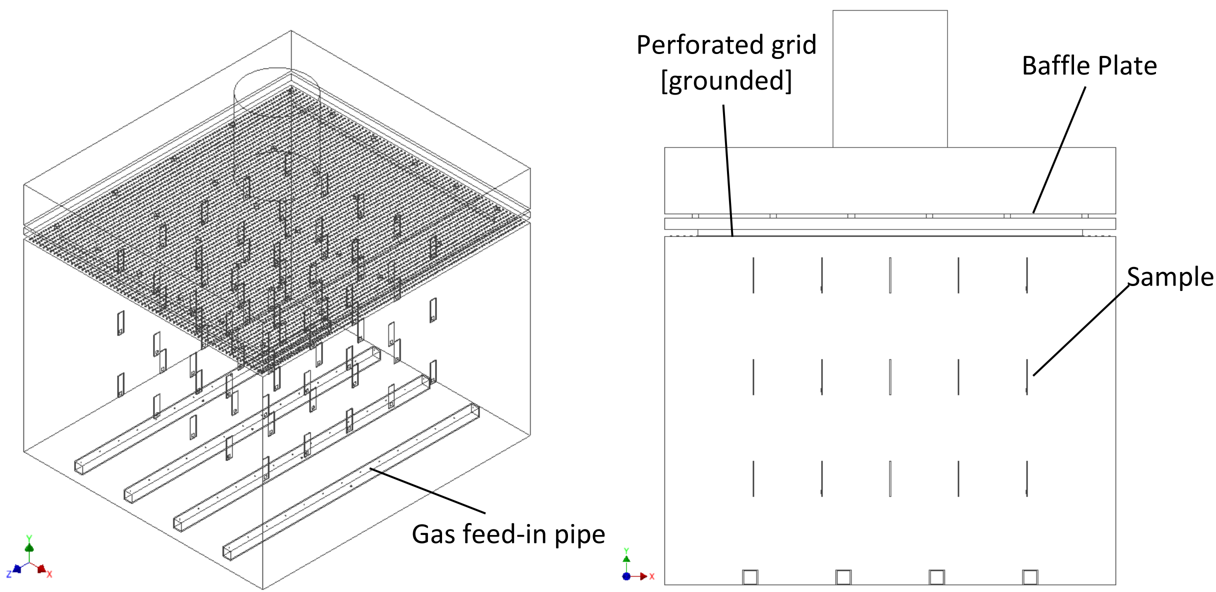

Figure 42 *Scheme of the experiment setup with the baffle plate installed*

The Baffle Plate was installed with 25 mm distance from the perforated grid to reduce the pressure loss through the holes. If the Baffle Plate is installed direct in contact with the perforated grid the pressure loss would drastically increase, increasing the work pressure, requiring more pump efforts to achieve the desired pressure. This happens due to the enlargement of the gas contact surface, in the case where the perforated grid is direct in contact with the baffle plate (Figure 43b) due to the small holes from the perforated grid in comparison to the case where the Baffle Plate is not direct in contact (Figure 43a).

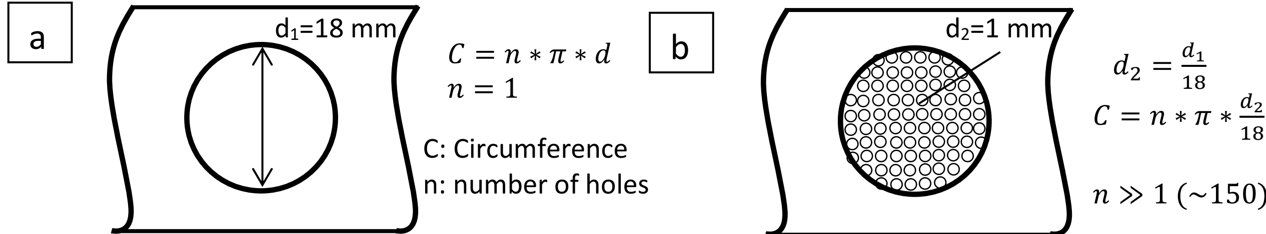

Figure 43 *Detail of one hole of the Baffle Plate*
a) just the Baffle Plate b) Baffle Plate direct in contact with the perforated grid

Due to the installation of the Baffle Plate is expected that the coating deposition rate will be more homogeneously distributed inside the chamber thanks to the achieved even gas flow as exhibited in Figure 44. In all three planes the gas velocity over most of the area is homogeneous (~0.2m/s) and close to the walls is lower, tending to 0 m/s.

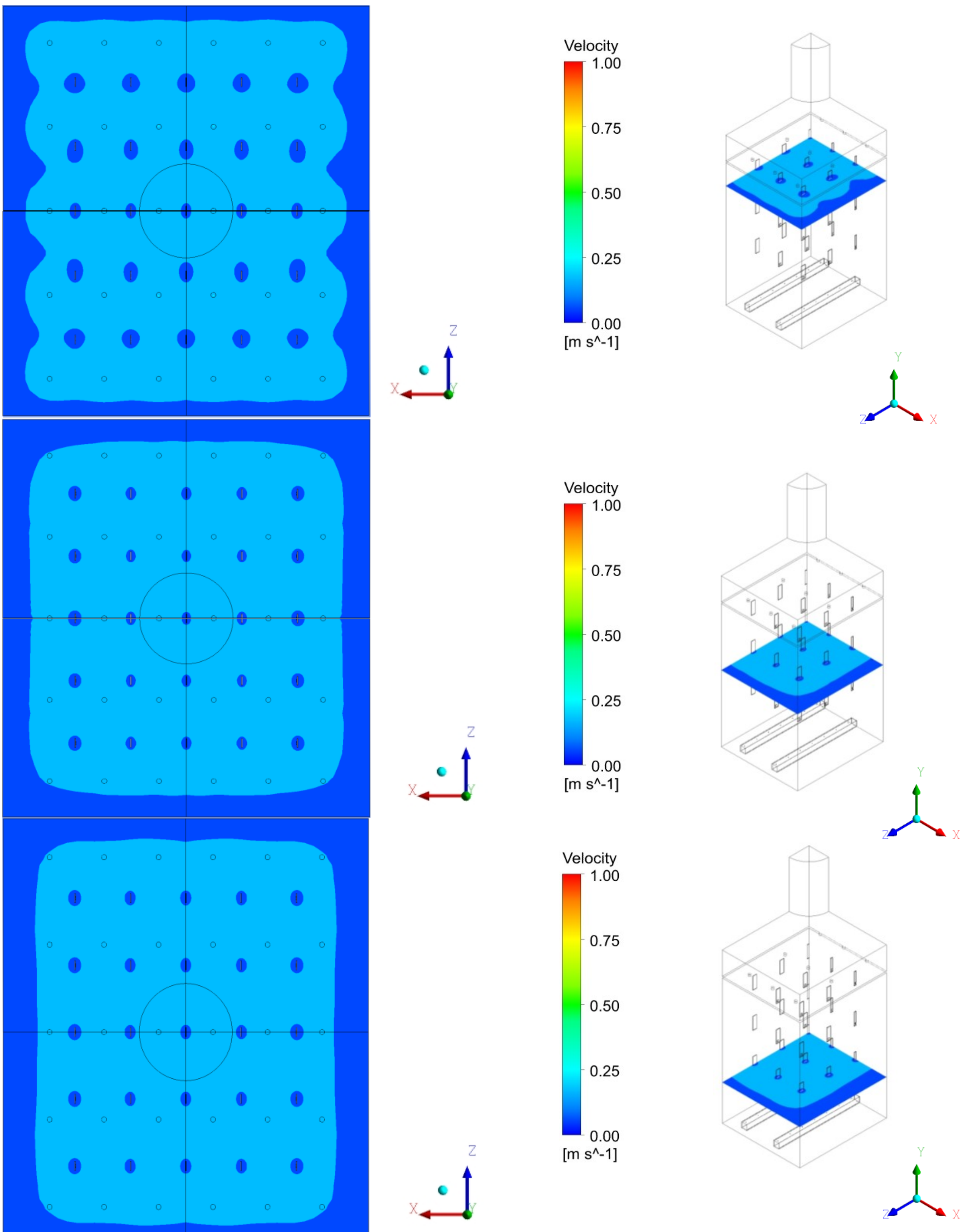

Figure 44 *Gas simulation results of the experiment- Current setup with Baffle Plate installed*

With the intention of make the comparison of the coating deposition rate homogeneity, obtained through the experiment with current setup and obtained through

the experiment with the Baffle Plate installed, easier, both color contour graphic of the distribution of the calculated deposition rate are showed in Figure 45. The results are divided in three planes: top plane (Figure 45a), middle plane (Figure 45b) and bottom plane (Figure 45c). Each plane contains 25 samples which positions are represented by the black dot points in each image. The results were organized in two columns where the left one represents the results without Baffle Plate installed and the right one represents the results with the Baffle Plate installed. All images were generated using the same scale bar, varying from 3nm/min to 30nm/min.

Figure 45 shows that the deposition rates are still higher close to the walls in comparison to the middle. Nevertheless, the color gradient in the right column, which represents the experiment with the Baffle Plate installed, are weaker than the color gradient in the left column (without the Baffle Plate). Like in the experiment without the Baffle Plate, the images from the right column (with Baffle Plate) show also higher deposition rate in average (dark green) in the top plane in comparison to the bottom and middle plane. Nonetheless, this difference is not as big as in the case without the Baffle Plate as showed in Figure 46. The improvement in the coating homogeneity due to the installation of the Baffle Plate is clearly visible in Figure 46. It shows a reduction in 50% of the standard deviation for the process with Baffle Plate installed (23%) in comparison to the previous one without Baffle Plate installed (47%) considering all samples. Moreover, the average of deposition rates considering all 75 samples in both experiments were the same. It gives a hint that the Baffle Plate do not influence the deposition rate itself, in fact just work in a way to homogenize it.

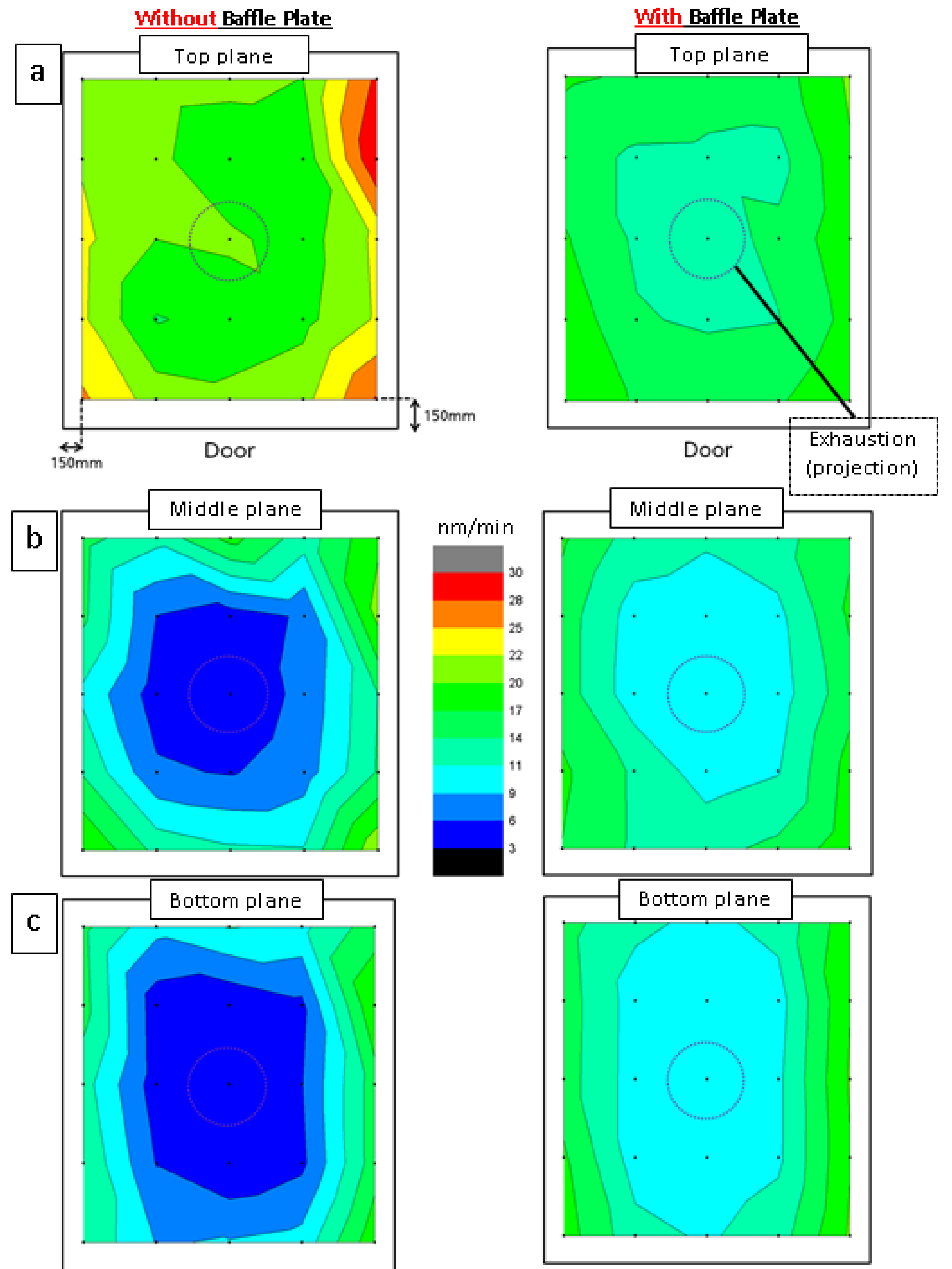

Figure 45 *Comparative of coating deposition rate with and without the Baffle Plate installed*

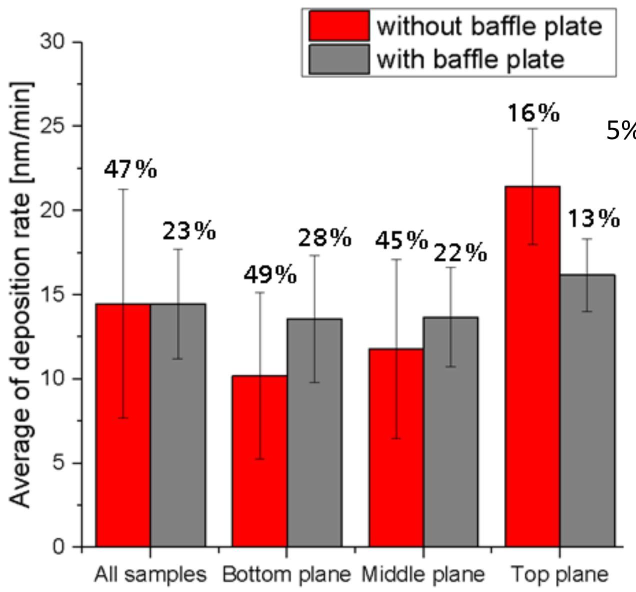

Figure 46 *Comparative of the average of deposition rate - Experiment current setup and with Baffle Plate installed*

Regarding the properties of the obtained coating, Figure 47 shows that both experiments exhibited a similar surface energy (low standard deviations) and there are no big differences among all three planes. As the surface energy is related to the chemical composition of the coating, it indicates that by the installation of the Baffle Plate no influence was generated in a way that could lead to different coating chemistry in different regions, which is an expected and positive signal.

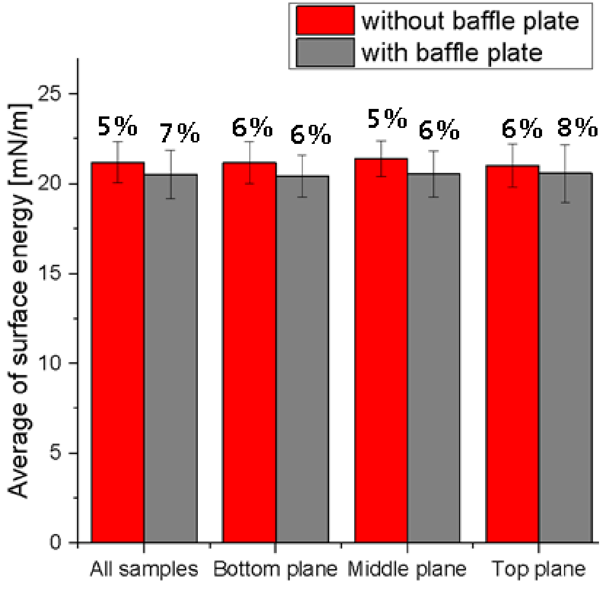

Figure 47 *Comparative average of the surface energy [Wu method] – With and without Baffle Plate*

The results suggest that the use of a Baffle-Plate do not influence the properties of the coating (surface energy), but it increase the homogeneity of the coating deposition rate since the only difference between both experiments was the change in the gas flow behavior due to its installation. Nevertheless, the deposition rate pattern does not match exactly with the gas flow pattern calculated through simulation and showed previously in Figure 44. Therefore, additional simulations were performed regarding not the gas flow but the electric field.

3.2.3. Electric field Simulation

The Electric field simulations were performed applying the software package Ansys Maxwell 16.0®. The calculations were done using Electrostatics solver described as follow [108]:

- The Electrostatic solver solves for the static electric fields resulting from stationary charge distribution or applied potentials
- Electric Field (E) and Electric Flux Density (D) are automatically calculated from the scalar potential (ø)
- All fields inside conductors are assumed to be perfect and equipotential in an electrostatic equilibrium (no current flow), therefore Joule losses are zero everywhere
- The Electrostatic solver utilizes an automatic adaptive mesh refinement technique to achieve an accurate and efficient mesh required to meet defined accuracy level (energy error)

For the present thesis, considering the current low-pressure plasma chamber setup, the following boundary conditions were applied:

- Powered electrodes potential: 30V
- Grounded electrodes potential: 0V
- Materials selection: Aluminum

The results of the electric field calculation for the current setup are shown in Figure 48. Black bars represent the powered electrode and orange bars represent grounded electrodes. The bottom plane shows a stronger electric field close to the left and right grounded electrode. The same plane by the coating deposition rate distribution (Figure 45c) showed also high deposition rates close to the grounded electrodes. The middle plane image from Figure 48, shows a very low electric field (radial) exactly in the middle of the plane, i.e. center of the chamber, and the coating deposition rate distribution by Figure 45b displays also a radial tendency. Regarding the top plane, the electric field pattern depicted in Figure 48 is rotated 90° in relation to the bottom plane – the higher electric field is closer to the powered electrodes. Nevertheless, by the same plane in Figure 45a, even though it showed lower deposition rate in the middle, there is not a visible higher deposition rate close to the powered electrodes.

The experimental results (Figure 45) in combination with the gas flow simulation (Figure 44) and electric field simulation (Figure 48) showed that the coating deposition rate distribution might be a compromise between gas flow and electric field. It is important to keep these findings in mind when a new chamber/electrode will be developed.

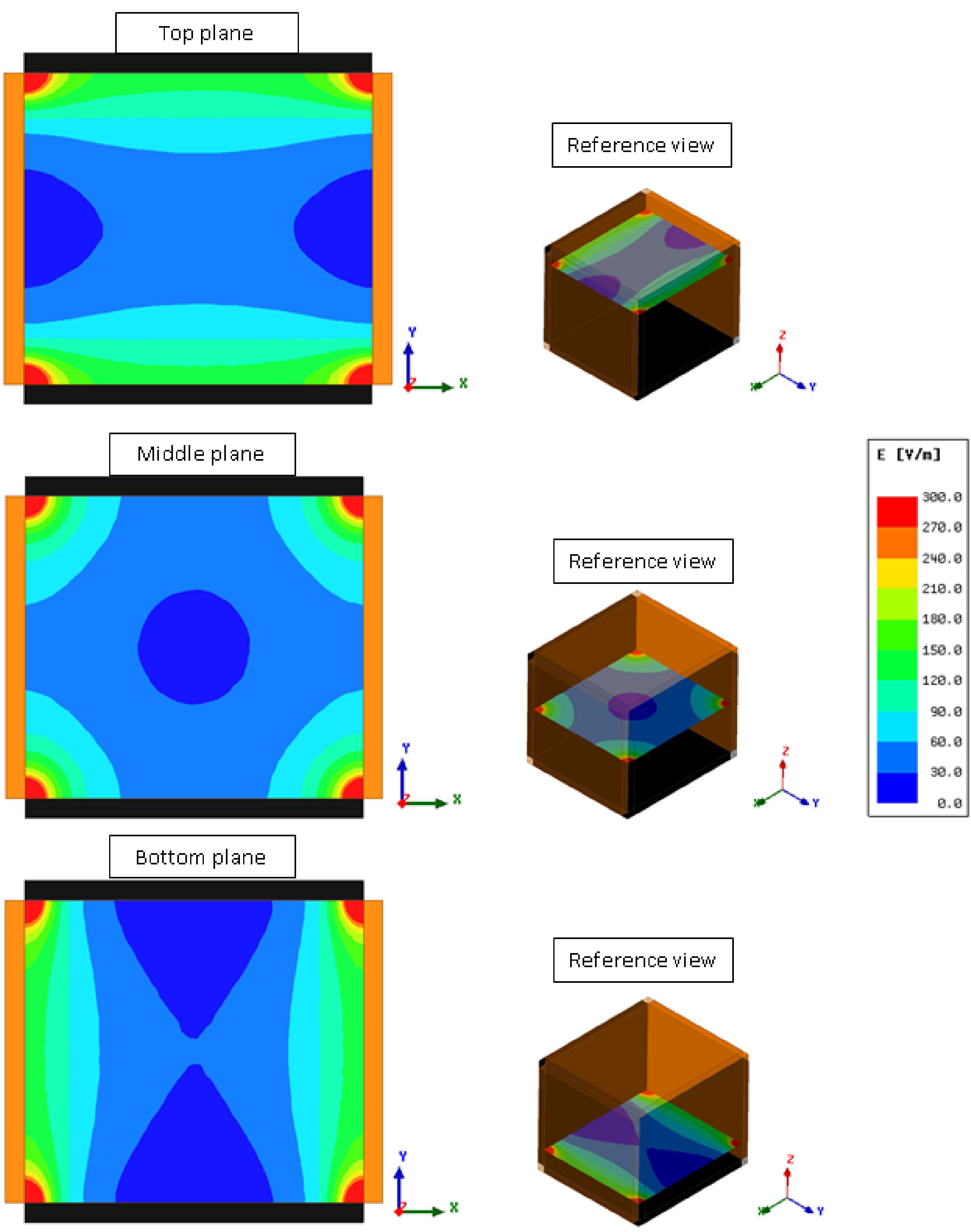

***Figure 48** Electric field calculation results for the current setup*

3.3. Electrode assembly

From the previous sections, it was observed and described the influence of the gas flow distribution and electric field distribution in respect to the local deposition rate as well as in the coating properties for an electrode setup with a “U-form”. In this connection it could be shown the benefits of a Baffle Plate to achieve a good coating homogeneity. The idea now is to keep the “U-form” electrode along with the Baffle Plate installed and just add a metallic plate connected with the bottom electrode. This metallic plate will act as an additional RF-electrode and could be used, for example, to place samples to be coated. In this case, the objective is to understand the effect of the assembly of additional electrode in the homogeneity of the coating deposition rate for the situation where there is a small distance between the metallic plate and the side of the “U-form” electrode. This is one desired construction from the point of view of scaling up the process. If there is an idea to place more electrode areas inside the plasma coaters, small distance between them will be generated and therefore this investigation is helpful. It is expected to see the local influence of the gas flow as well as from the electric field on the coating deposition rate distribution.

To evaluate the effect of the electrode assembly in the homogeneity of the coating deposition rate the experiment in Figure 49 was planned.

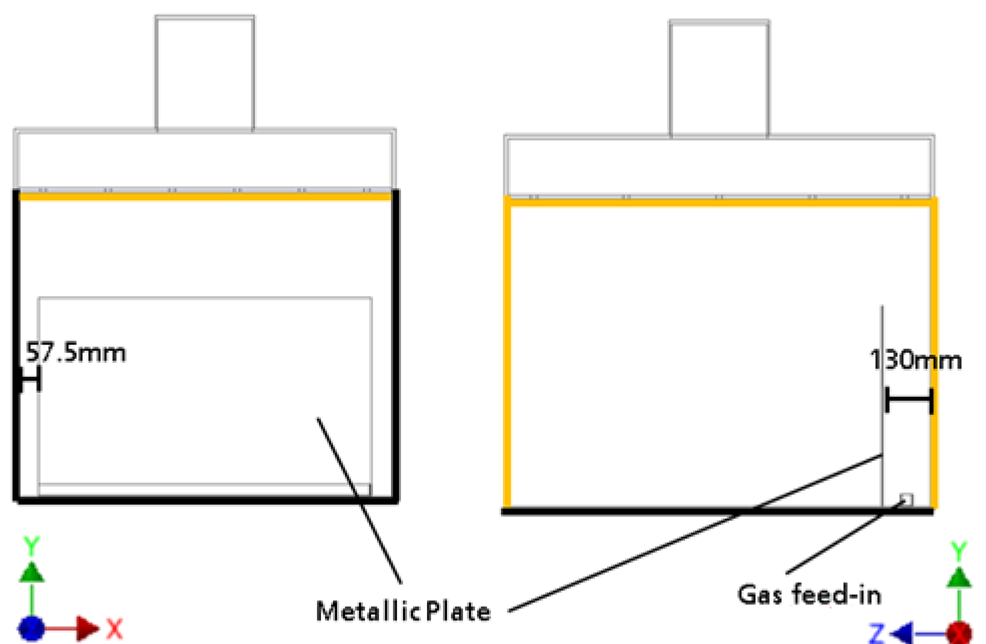

Figure 49 *Scheme of the experiment with one additional electrode (sides open)*

Figure 49 shows to different views of the experiment, XY plane (left) and ZY plane (right). The “U-Electrode” is represented by the thick black line and the grounded electrode is represented by the thick orange line. For this experiment, one additionally metallic plate (90 mm x 54 mm) was placed 130 mm from the back of the chamber (grounded). With this setup, the sides of the metallic plate were 57.5 mm distance from the powered electrode. As the metallic plate was direct in contact with the RF-electrode (“U-Electrode”), it will also work as an RF-electrode. The gas feed-in pipe was placed between the metallic plate and the grounded electrode. It is important to observe that for this case; the sides of the electrode are completely open. It means that the gas can flow to the sides as well as direct toward the exhaustion system. The surface of the metallic plate under analysis is the one facing the grounded electrode.

The second experiment, represented by the scheme in Figure 50, aimed to see the influence in the coating deposition rate distribution due to the installation of a polycarbonate plate, in each side of the metallic plate, to close both sides. There is 20 mm height difference between the metallic plate and the polycarbonate plate. This was let on purpose to force one pathway for the gas and due to that it is expected to see one influence in the coating deposition rate distribution.

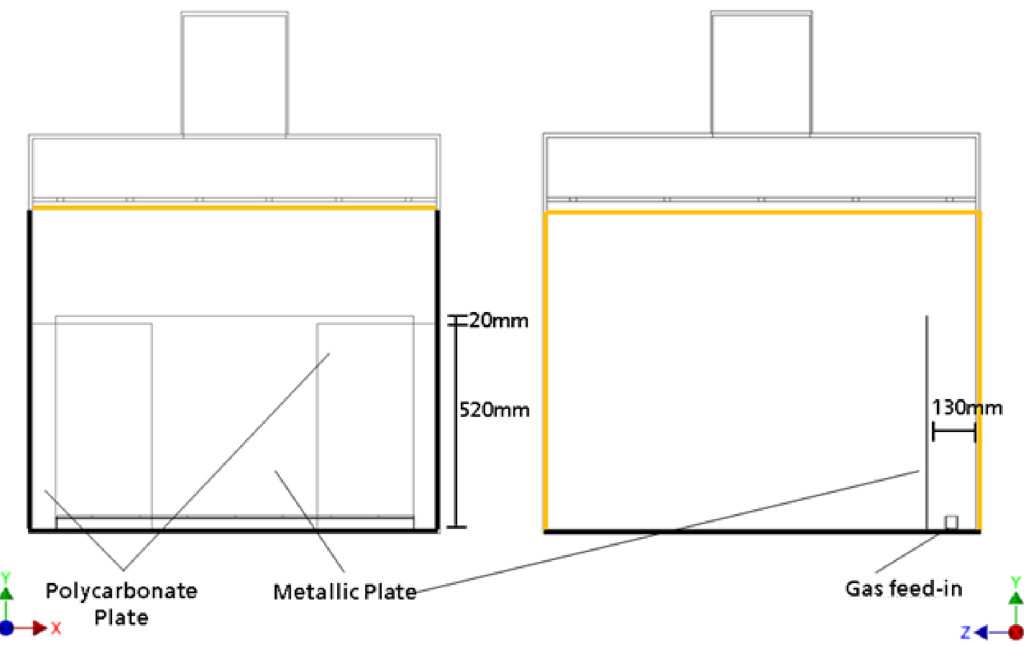

Figure 50 *Scheme of the experiment with one additional electrode (sides closed)*

Defined the experiments, the first step was to run the gas flow simulation as well as the electric field simulation for both cases.

3.3.1. CFD simulation

The CFD simulations were performed using the same boundary conditions showed in Table 7. From Figure 51a can be observed that due to the open sides, the gas tends to flow to the smallest pathway (sides), which imposes fewer obstacles to the flow. It shows also higher velocities (red) close to the bottom sides of the metallic plate. This scenario can be better understood with Figure 51b, where the streamlines are clear moving to the sides of the plate. Based on this statement, it can be expected that a higher density of gas, or reactive particles from the precursor gas, will be available in the bottom sides of the metallic plate and therefore higher deposition rate is expected in these regions.

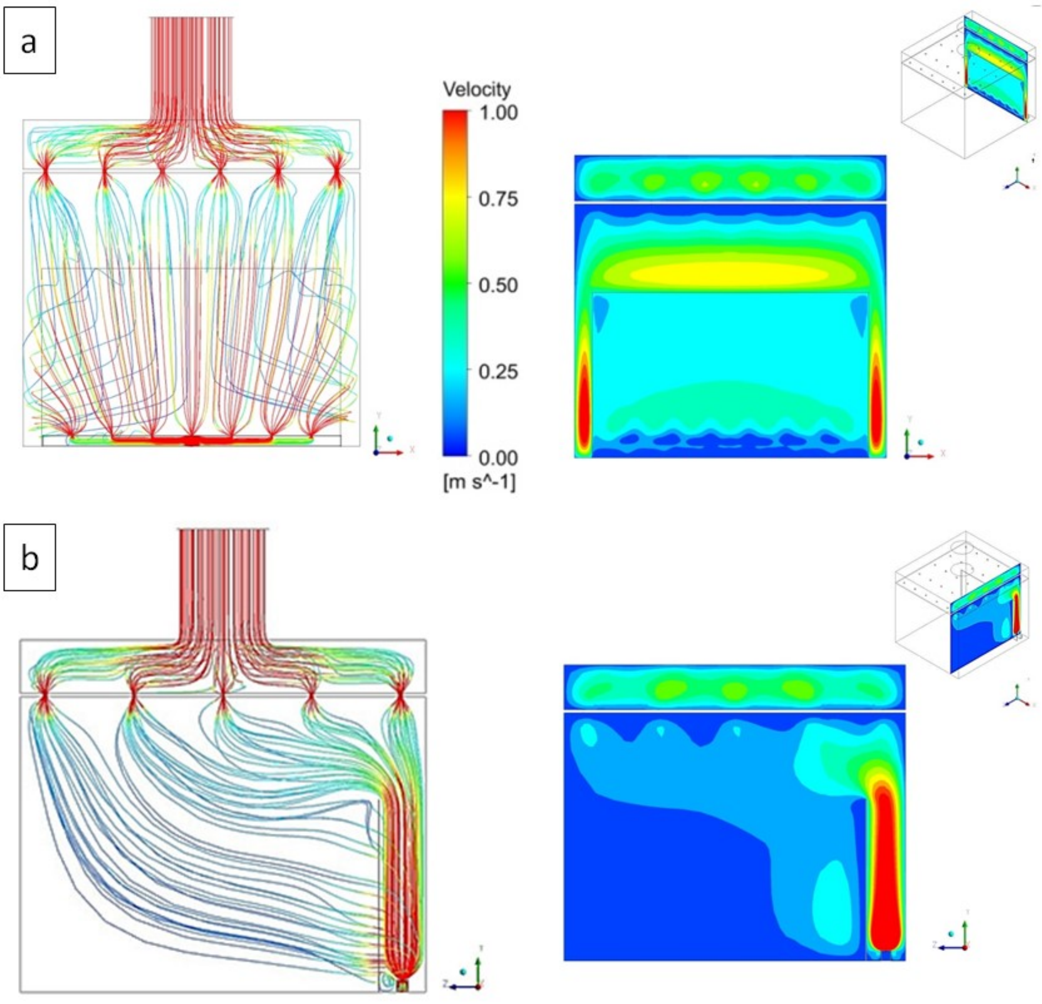

Figure 51 *Gas flow simulation results – Experiment Metallic Plate open sides (a) XY plane (b) ZY plane*

To see if it is possible to move the influence of the concentration of streamlines, as they represent the preferentially path which the gas will go through, for the same experiment construction new gas flow simulations were done with the polycarbonate plate installed to close the sides of the metallic plate but leaving on purpose 20 mm height difference between them. The idea is to let one pathway for the gas on the top sides and see if the streamlines will concentrate in this region.

Figure 52a show the streamlines moving straight from bottom to top and the higher velocities is close to the top of the metallic plate. Additionally, close to the top sides of the metallic plate the velocity is higher (yellow) as compared to the velocity over the plate (green). From this point of view, it would be expected that higher deposition rate will be find in the top sides of the metallic plate.

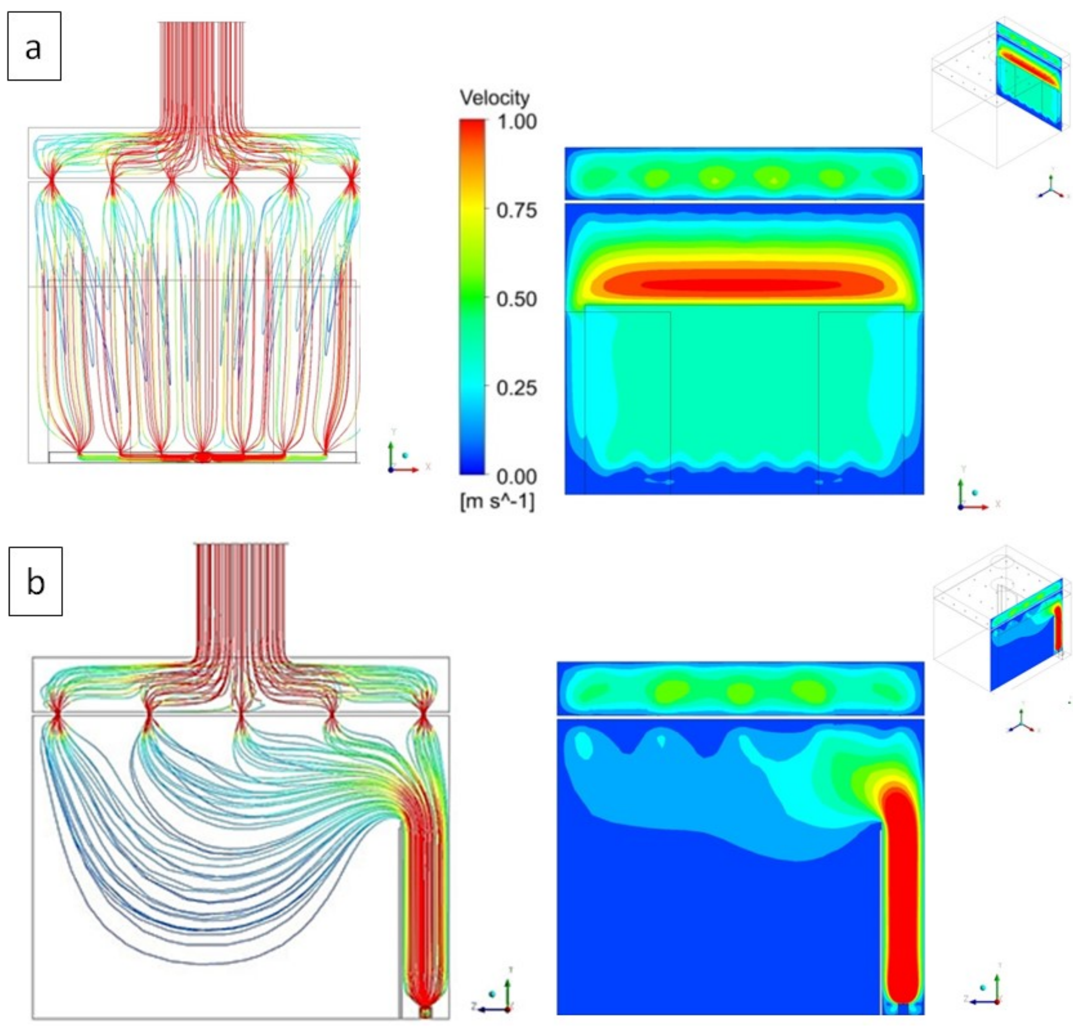

***Figure 52** Gas flow simulation results – Experiment Metallic Plate closed sides (a) XY plane (b) ZY plane*

Looking forward acquire more information about the coating deposition rate distribution over the metallic plate in both setups, electric field simulations were performed.

3.3.2. Electric field simulation

The electric field simulations were done in the same way as explained in section 3.2.3 and the results are depicted in Figure 53.

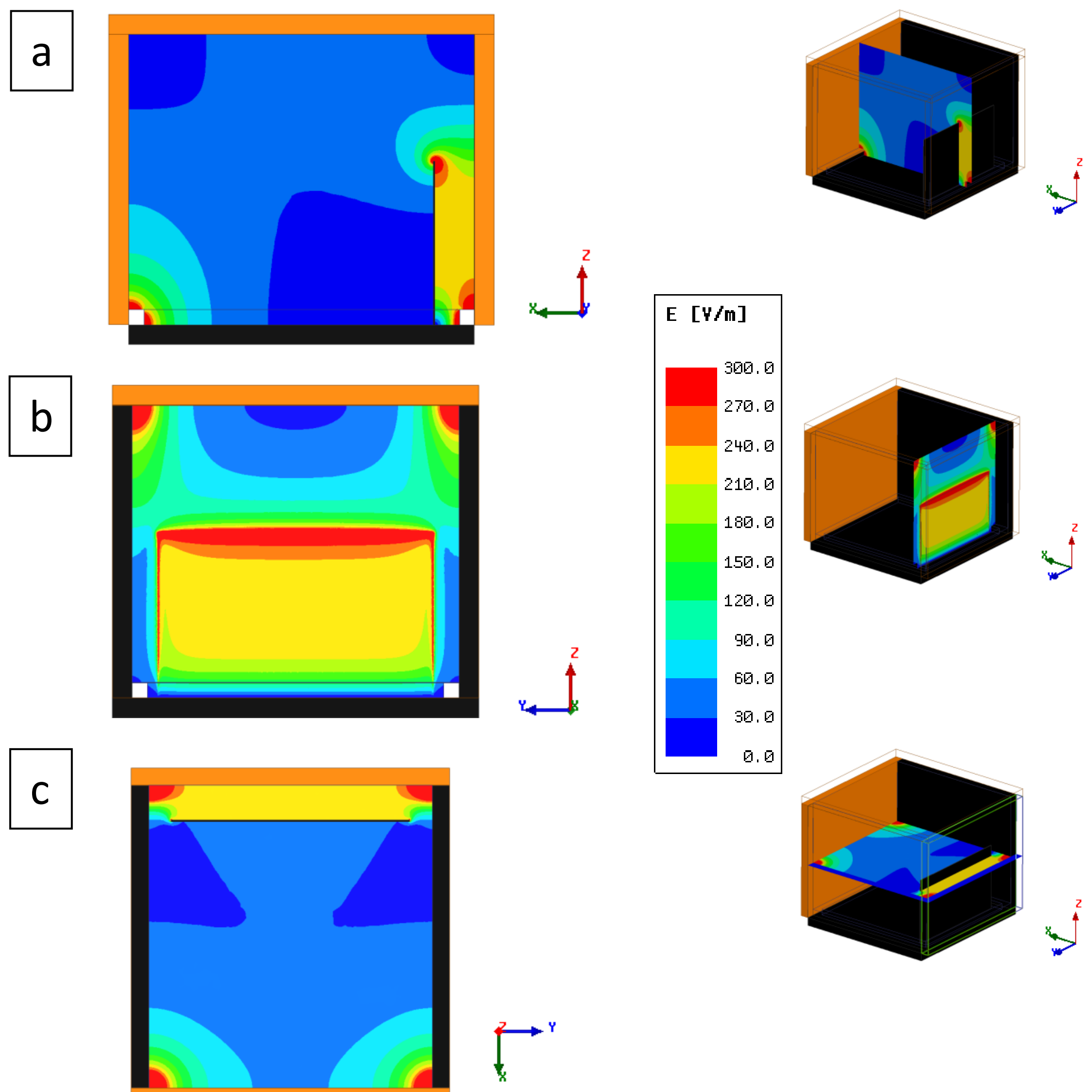

Figure 53 *Electric field calculation results for the Experiment - Metallic Plate (a) Plane XZ (side view) (b) Plane YZ (front view) (c) Plane XY (top view)*

The "U-Electrode" as well as the metallic plate is represented by the black color and the grounded electrode is represented by orange color. Figure 53a shows stronger electric field in the regions where a powered electrode is close to a grounded electrode. It can be

observed that the bottom of the metallic plate is close to a region with low electric field and the top of the metallic plate shows stronger electric field (red). Moreover, Figure 53b shows clearly the edge effect over the plate especially on the top. Additionally, the bottom of the plate shows lower electric field (blue and light blue). Furthermore, Figure 53b shows that in the four corners the electric field displays the highest values. The electric field simulation was showed just for the case with the metallic plate with open sides because the installation of the polycarbonate plate to close the sides of the plate did not have considerable influence. From the point of view of the electric field simulation results, the higher deposition rates are expected to be on the edges and on the top area of the plate because those are the regions where stronger electric fields are formed.

With the intention of understand the influence of the additional RF-Electrode (metallic plate), especially the installation itself, coating experiments were done for both cases: metallic plate with open sides and closed sides. The focus was just on the deposition rate distribution over the plate.

3.3.3. **Experiments**

The coating experiments were done using the same steps showed in Table 1. Figure 54a presents the experiment setup for the case with metallic plate with open sides (picture left). The blue dots in the picture in the top right represent the holes of the gas feed-in pipe through where the gas will be supplied to the chamber from bottom to top direction (sketch bottom right from Figure 54a). Part b of Figure 54 shows the setup for the experiment with the polycarbonate plate installed to close the sides of the metallic plate. It is important to keep in mind that for these experiments the baffle plate developed, as described in 3.1.1, was installed in the low-pressure plasma chamber to reduce the effect from the gas exhaustion system.

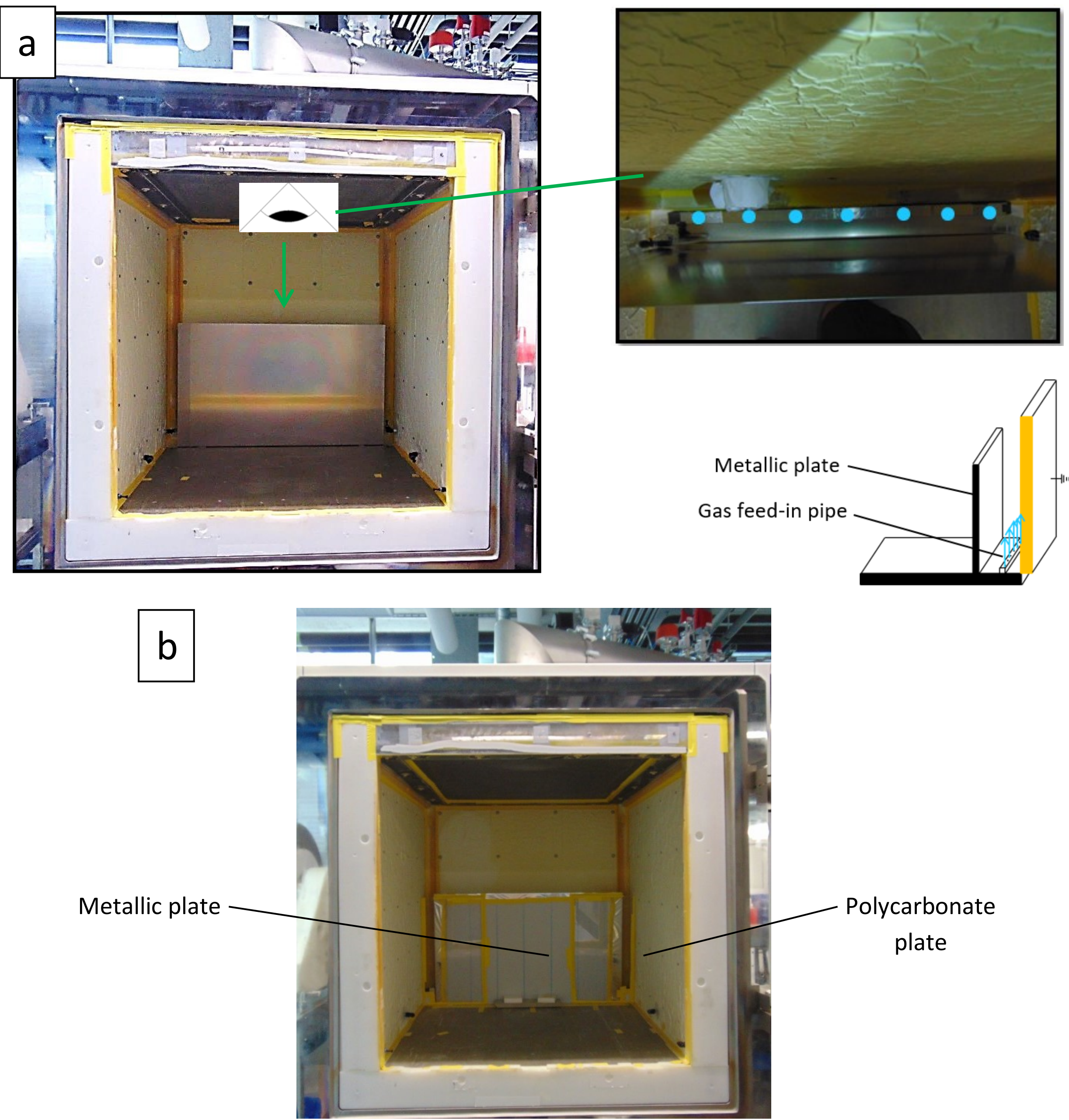

Figure 54 *Setup of the experiment - Metallic Plate (a) open sides (b) closed sides*

The calculated deposition rates were plotted using a color contour graphic and are depicted in Figure 55. This kind of plot was used to make easier the understanding, in a way that a 3D experiment is showed in a 2D graphic. In this case, blue color means low deposition rate and red color high deposition rate. The black dots represent the positions where the coating thicknesses were measured. The measurements started 25 mm for each edge of the plate.

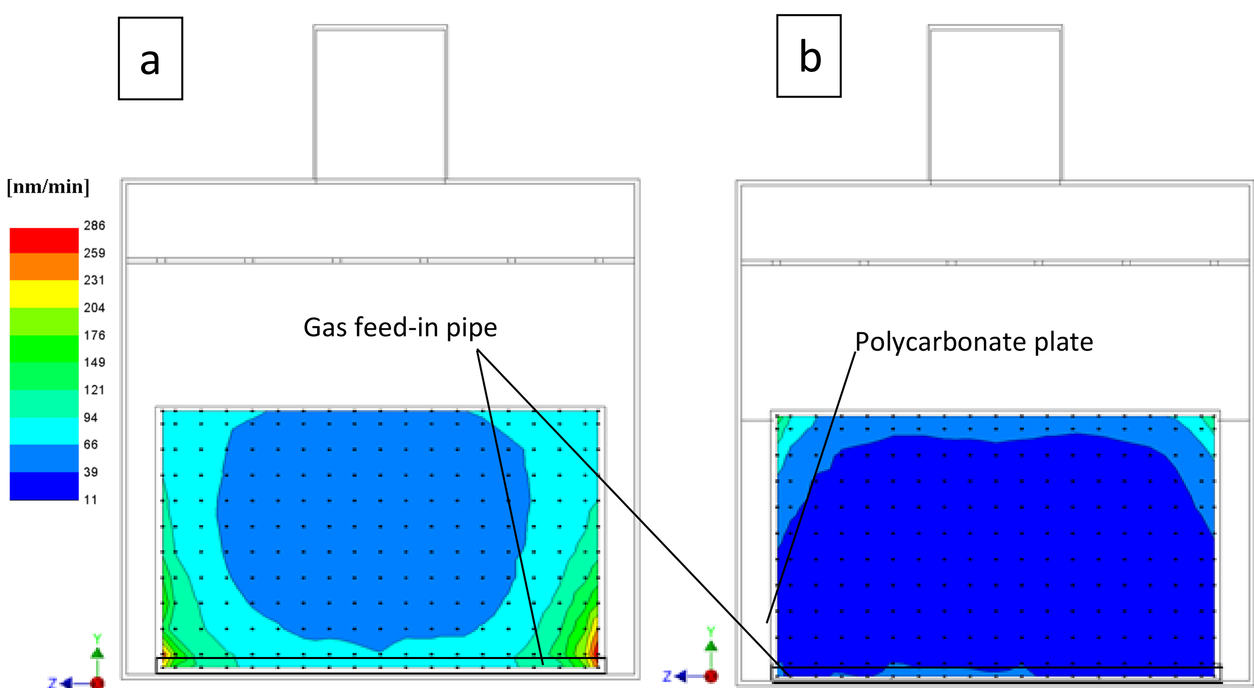

Figure 55 *Coating deposition rate distribution (a) open sides (b) closed sides*

Part "a" from Figure 55 shows the coating deposition rate distribution for the case where the sides of the metallic plate were open. It can be observed that the higher deposition rates were concentrated in the bottom corners and the lowest deposition rates were in the center of the plate. Figure 55b shows the deposition rate distribution for the experiment with the polycarbonate plate installed to close the sides of the metallic plate. For this case, the higher deposition rates were in the top corners. If we compare the pattern of the coating deposition rate from the two experiments, the action to close the sides of the metallic plate and leaving on purpose a gas pathway in the top corners, practically mirrored, in respect to the ZX plane, the results from the setup with open sides. This is a hint that the gas pathway, represented by the streamlines, played a major role in these experiments. This influence can also be seen in Figure 56, where a brighter plasma is seen in the top corners of the metallic plate in comparison to the hole volume of the low-pressure plasma chamber. The influence of the created gas pathway (metallic plate 20 mm higher than the polycarbonate plate) was higher than the electric field since from the electric field simulations results, it would be expected higher deposition rates all over the edges.

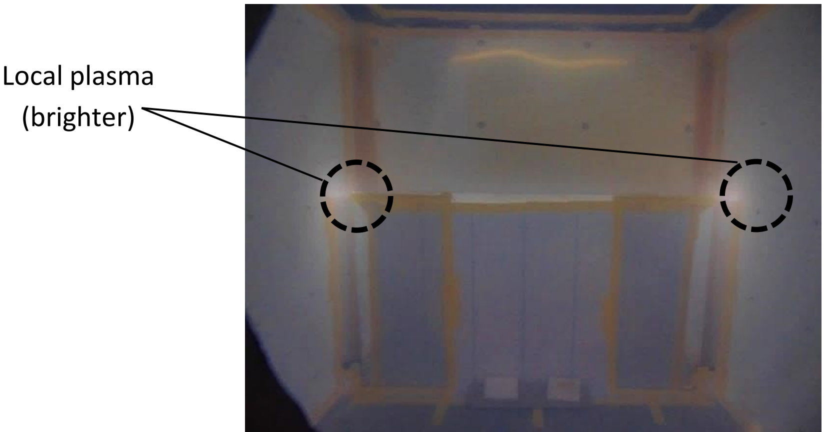

Figure 56 *Image of the coating process – Metallic plate with closed sides, showing local plasma concentration on the top corners*

The averages of coating deposition rate for both experiments are showed in Figure 57a. The experiment with closed sides presented lower values in average; however, the standard deviation was slightly lower than the experiment with open sides. The lower deposition rate in average for the case with closed sides can be attributed to the fact that the gas velocity was higher in this setup as compared to the open sides experiment as already showed in Figure 52a and Figure 51a respectively. From the coating properties point of view, both experiments displayed similar values of surface energy as depicted in Figure 57b. The higher standard deviations for both cases might be related to the local influence of the gas streamlines due to the open sides in the first experiment and due to the opening left on purpose on the top corners of the metallic plate in the second experiment. If these areas are removed from the analyzed data, the standard deviations would clearly decrease. Furthermore, from the experiments showed in the section 3.2, it is recommended to keep at least 200 mm distance from the electrodes to mitigate the influence of the walls in the gas flow and the region with stronger electric field.

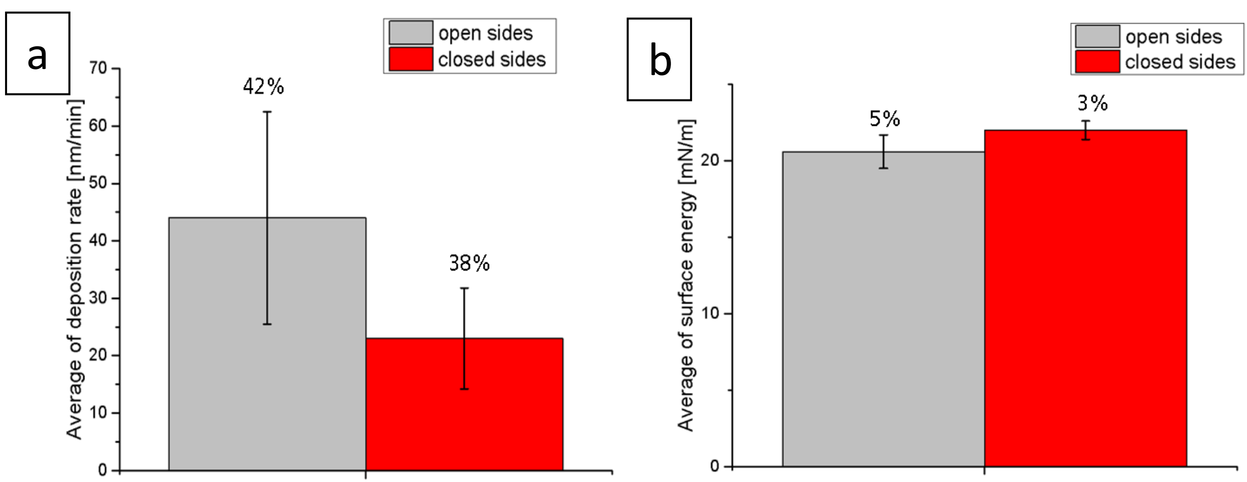

Figure 57 *Comparative average (a) deposition rate (b) surface energy*

From these experiments the following knowledge were acquired:

a) The gas streamlines indicate the coating deposition rate distribution as they represent the preferentially path which the gas will go through.

b) It is important to avoid local plasmas

c) The asymmetry might have influenced in the gas flow distribution as well as in the electric field distribution and consequently influence the homogeneity of the coating deposition rate

d) It is important to keep at least 200 mm distance from the electrodes to avoid the region where the gas velocity is influenced (reduced) and where the electric field is much stronger

4. Construction of a new low-pressure plasma chamber

In the three previous chapters (3.1,3.2,3.3) special attention were done for the construction of gas feed-in systems, gas exhaustion systems and construction of RF-Electrodes respectively. The idea was to create construction guidelines for scientists and constructors with higher probability to achieve homogenous coating deposition rate, in further applications of this low-pressure plasma technology, with less rework. It will consequently improve the time plan and costs for future developments. Moreover, it will at least reduce the risk significantly.

In this context, a new low-pressure plasma chamber was constructed using the knowledge acquired through this research work with the objective to deposit plasma polymeric coating over flat surfaces, for example over two plain metallic products (Figure 58) with 1 m^2 area each. This coating must show a homogeneous easy to clean functionality and at least over the plain a constant deposition rate.

Figure 58 *Plain metallic product placed on a Polycarbonate-holder*

Therefore an electrode with flat surfaces and large dimensions is required. The dimensions of the electrode must be larger than the ones from the plain metallic product to allow the placement of the products in an area distant from the chamber walls, where local influences on the coating deposition rate due to gradient in the gas flow as well as strong electric field are detected as showed in the previous chapter. The low-pressure plasma chamber has a volume of 3 m^3 and the working principle is the same as the previous one described in the end of the chapter 2.2.2.

The first step for this development was to define the gas feed-in system, gas exhaustion system and RF-Electrode geometry, since the coating parameters are already established (Table 1).

Regarding the gas feed in system, a square pipe (A=30 mm x 30 mm) with sides closed were selected. On the top plane of this pipe, 14 holes (D=1.5 mm) were equally distributed as depicted in Figure 59. This geometry was selected based on the guidelines showed previously in section 3.1.3.

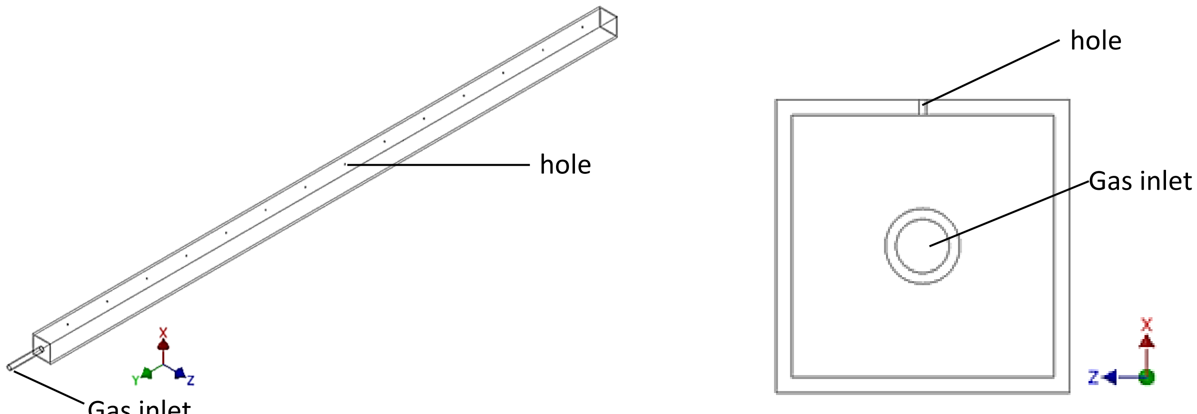

Figure 59 *Model of the gas feed-in system*

The next step was to define the geometry of the RF-Electrode. Since plain metallic products are desired to coat, the electrode must have flat and inclined sides to make easier the fixing of the product and consequently to enable of a fast preparation step for the next coating process. One first idea was to have a triangular shape RF-electrode as showed in Figure 60a. It has the two inclined sides and from this point of view it would be suitable to coat two plain metallic products per batch. However, the triangle shape implies in a very sharp edge on the top. The electric field calculations show that the electric field strongly concentrates in this region (Figure 60b).

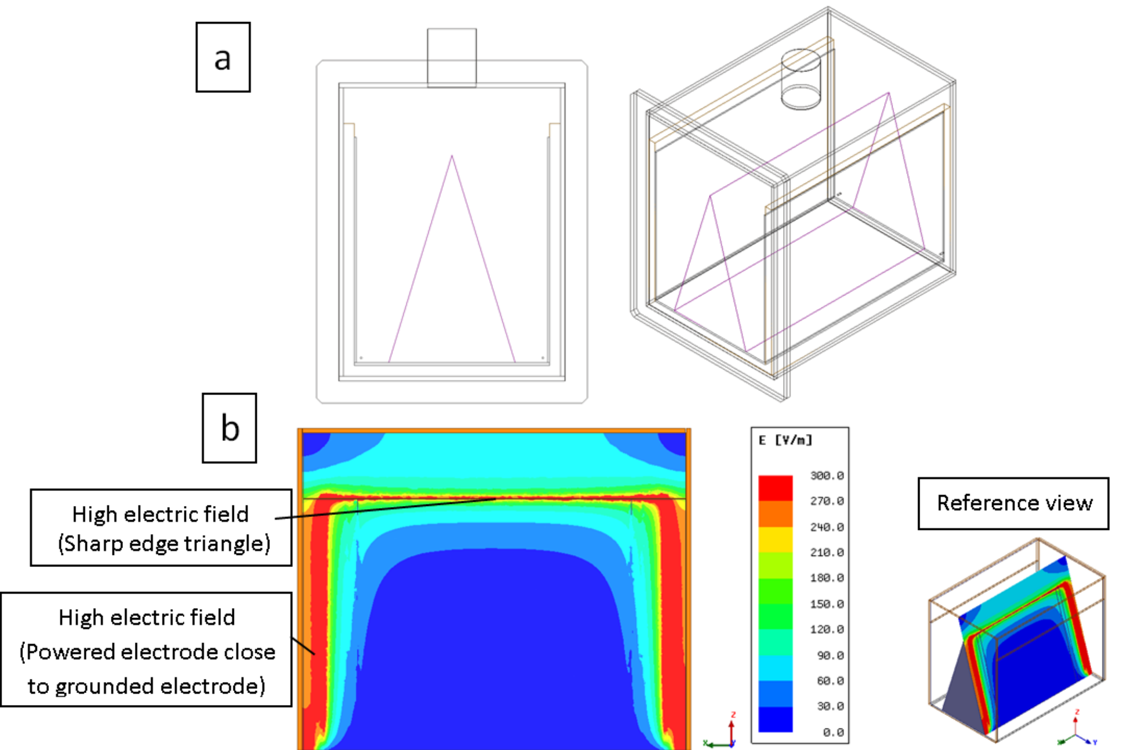

Figure 60 *(a) Model of the low-pressure plasma chamber with triangular shape RF-Electrode (b) Electric field simulation for the triangular shape RF-electrode*

For this reason, a new solution came substituting the triangular shape RF-Electrode to a trapeze shape RF-electrode. It will allow in the same way the coating of two plain metallic products per batch but without a sharp edge on the top. The model of this trapeze RF-electrode can be seen in Figure 61. Figure 65 shows the corresponding electrical field calculation.

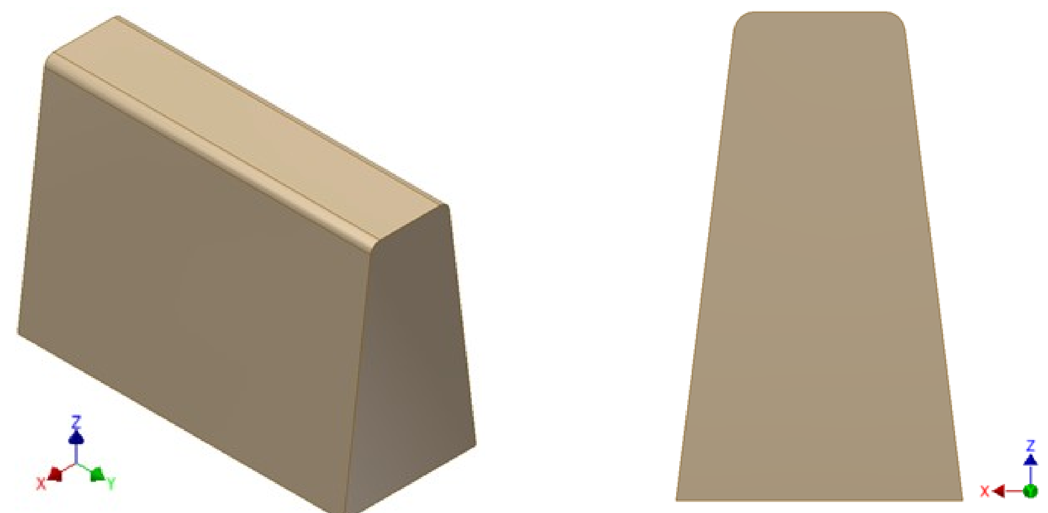

Figure 61 *Model of the trapeze RF-electrode*

The last step to define the low-pressure plasma chamber is related to the gas exhaustion system. In chapter 3.2, it was described the importance to install a Baffle Plate to reduce the effects from the central gas exhaustion system and thereby be able to increase the homogeneity of the coating distribution over the substrate surface. In this way, also a Baffle Plate was designed to this application as depicted in Figure 62. It has 30 holes (D=18 mm) evenly distributed. The holes distribution was done in a way that one row of holes would be placed exactly in the middle of the chamber and consequently in the middle of the trapeze electrode with the aim of keep the gas streamlines in contact all over the side electrode surfaces as can be seen in Figure 64a.

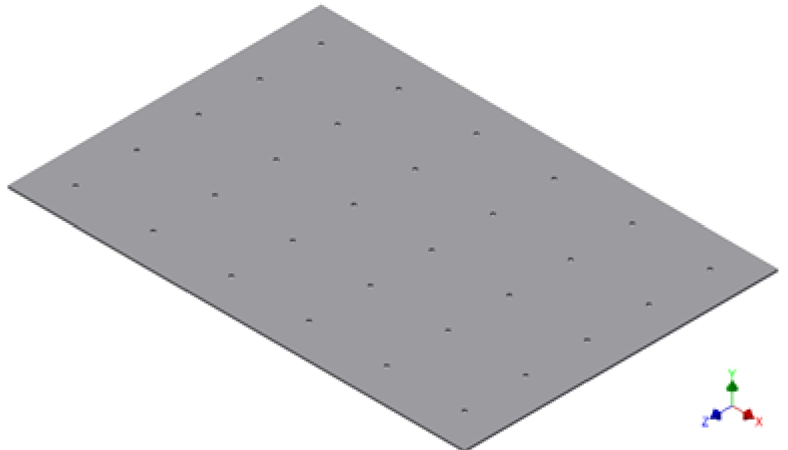

Figure 62 *Model of the Baffle Plate*

After the definition of the gas feed-in system, RF-electrode geometry and gas exhaustion system, the complete model of the low-pressure plasma chamber was completed and can be seen in Figure 63.

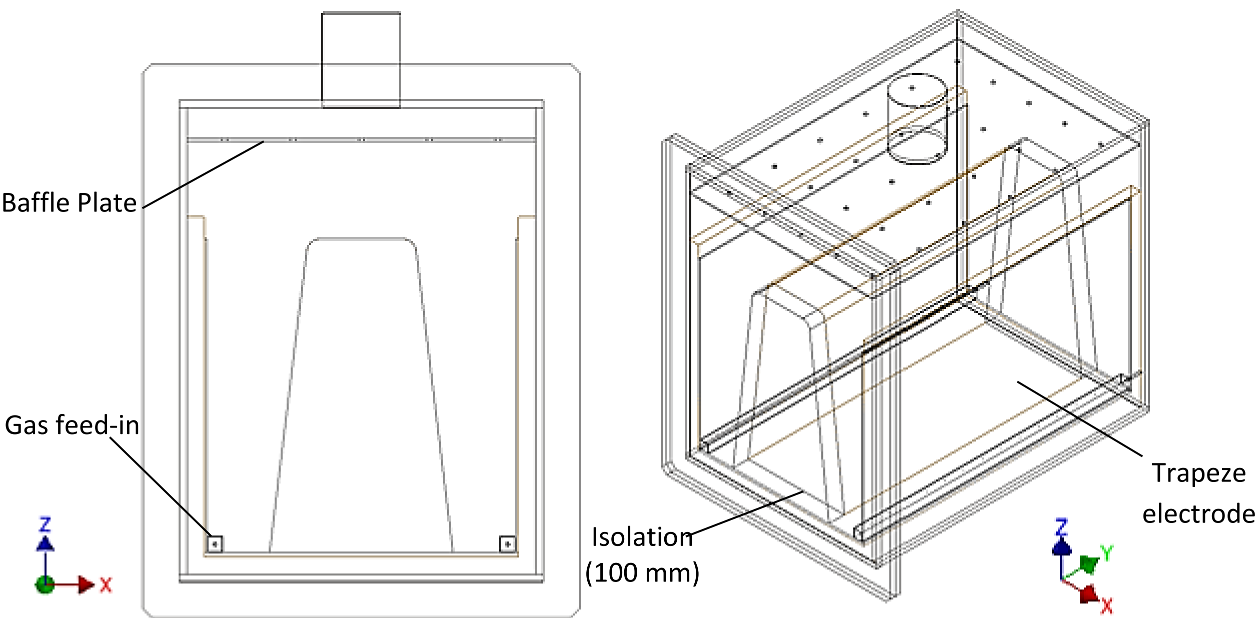

Figure 63 *Model of the complete low-pressure plasma chamber*

With the aim of be sure that the developed model will work, CFD simulation were done to have a picture of the gas flow behavior inside the developed low-pressure plasma chamber.

4.1.1. **CFD simulation**

The CFD simulations were performed using the same boundary conditions showed in Table 7 and the results are depicted in Figure 64. Part “a” from Figure 64 shows the gas streamlines. There is a recirculation zone in the bottom part of the trapeze electrode and it extends for approximately 70 mm in height from the bottom of the chamber. This might imply in higher deposition rate in this region due to the higher residence time of the gas, and consequently from its fragments. Moreover, the existence of a line of holes exactly in the middle of the Baffle Plate seems to work in a way that keeps the gas streamlines in contact with all the extension of the lateral sides of the trapeze electrodes. This effect is very important since this is the place where the plain metallic product will be placed and in fact where the coating deposition is expected. Part “b” from Figure 64 shows an equal gas velocity pattern in both sides of the electrodes and Figure 64c shows the gas velocity pattern over the plane close to the electrode surface. It shows a region of small velocities (dark blue) which extends for about 120 mm from the walls. Nevertheless, the gas velocity is homogeneous (light blue) in most of the electrode surface area.

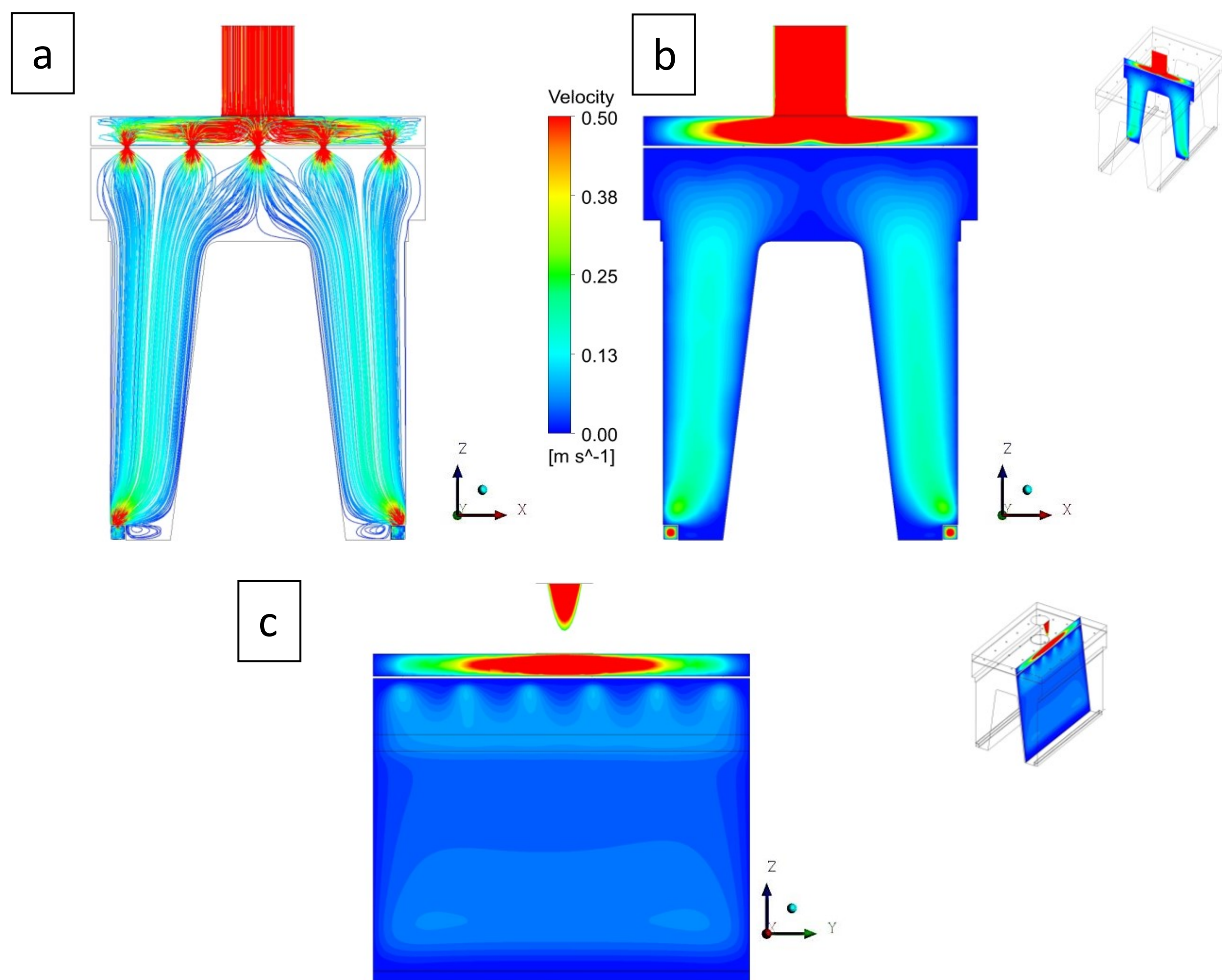

Figure 64 *Gas flow simulation – New low-pressure plasma chamber (a) gas streamlines b) velocity contour (middle plane) (c) velocity contour on product plane*

To have more information about the expected coating deposition rate distribution over the plain product for this planned setup, electric field simulations were performed.

4.1.2. Electric field simulation

The electric field simulations were done in the same way as explained in section 3.2.3 and the results are depicted in Figure 65.

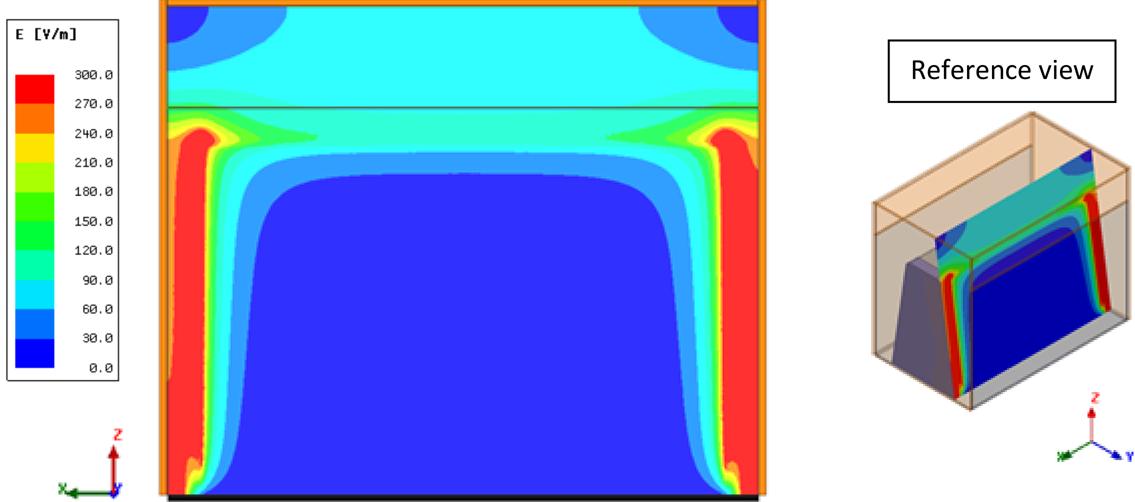

Figure 65 *Electric field simulation results for the new low-pressure plasma chamber model*

Figure 65 displays still a higher electric field on the sides of the electrode due to the proximity from the powered electrode (Trapeze) and the grounded electrode (represented by orange). Nevertheless, the electric field was strongly reduced in the top of the trapeze electrode due to the mitigation of sharp edge in this region (unlike the triangular electrode). Moreover, there is a large area (blue) on the surface of the trapeze electrode with homogeneous electric field which can contribute to a homogenous coating deposition rate.

4.1.3. Experiment

The results from the gas flow simulation and electric field simulation presented a very laminar and homogeneous gas flow as well as a large area with homogeneous electric field respectively. It is the confirmation that the way the low-pressure chamber was planned should be right and homogenous coating deposition rate can be achieved.

In this context, the low-pressure plasma chamber was constructed, and a practical experiment was performed. The coating experiment was done using the same steps showed in Table 1. Figure 66 illustrates the setup of the experiment. The plain product is fixed on

each side of the trapeze electrode (left and right) keeping 70 mm distance from the bottom of the chamber and 180 mm from the edge of the electrode.

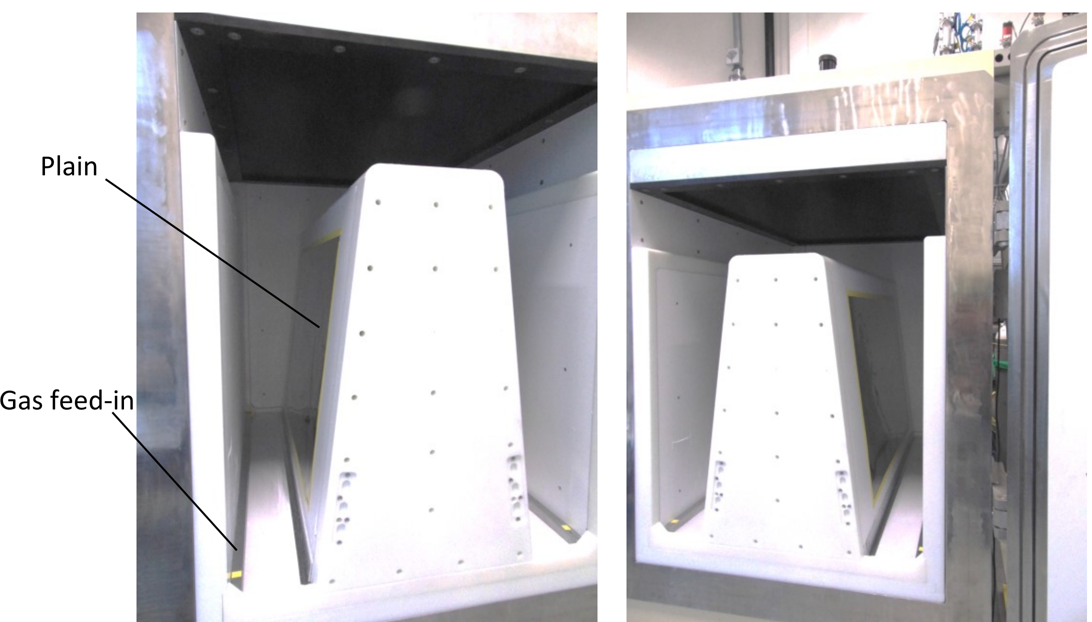

Figure 66 *Setup of the experiment – One product for each side of the trapeze electrode*

The calculated deposition rates were plotted using a color contour graphic and are depicted in Figure 67. This kind of plot was used to make easier the understanding, in a way that a 3D experiment is showed in 2D graphic. In this case, blue color means low deposition rate and red color high deposition rate. The black dots represent the positions where the coating thicknesses were measured. The measurements started 50 mm from each edge of the plain metallic product.

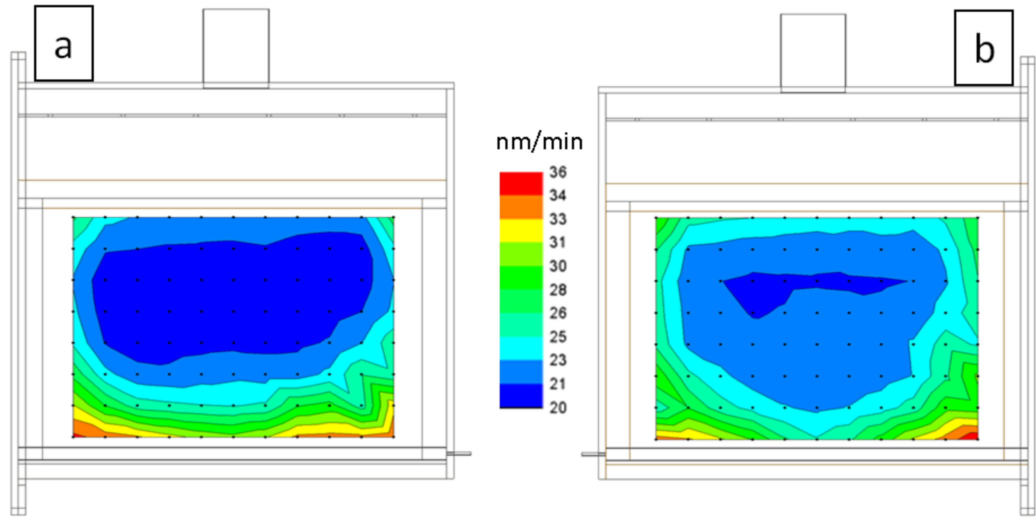

Figure 67 *Coating deposition rate distribution (a) left side (b) right side*

The results from Figure 67 show a symmetrically coating deposition rate pattern even though on the left side the deposition rate was slightly lower than the right side. Furthermore, in both sides the maximum values were in the bottom region. This can be related to the low gas velocity in this region, which increased the gas residence time. Consequently, higher deposition rates are realized. This is not a huge problem, once the product can be placed a little bit higher than 70 mm from the bottom to avoid this low gas velocity region. Regarding the higher deposition rate on the sides of the product, it seems that influences from the electrical field additively superpose those ones of lower gas velocity. It might be overcome through more distance to the side walls and a higher trapeze electrode. Figure 68 shows the average of the coating thickness measured on both plain products. The average value for both cases is in average 15%. This value is a successful result and corresponds to a reduction of 67% in the standard deviation value obtained for the standard equipment with the conditions described in chapter 3.2.

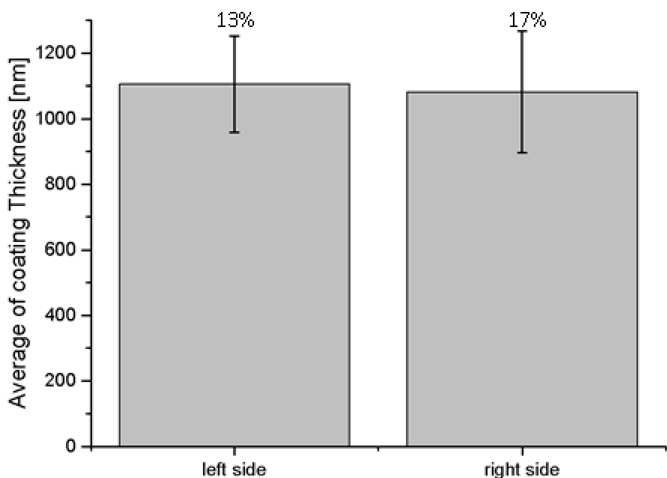

Figure 68 *Coating thickness results for both plain products*

Regarding coating properties, Figure 69 and Figure 70 shows a very homogeneous surface free energy and elastic modulus in both sides (left and right) which confirms the good development/construction of this low-pressure plasma chamber based on the construction guidelines developed in the previous chapter.

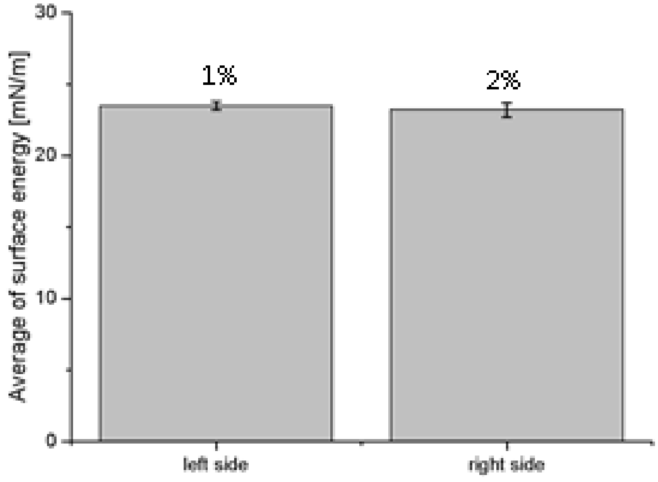

Figure 69 *Surface energy results for both plain products*

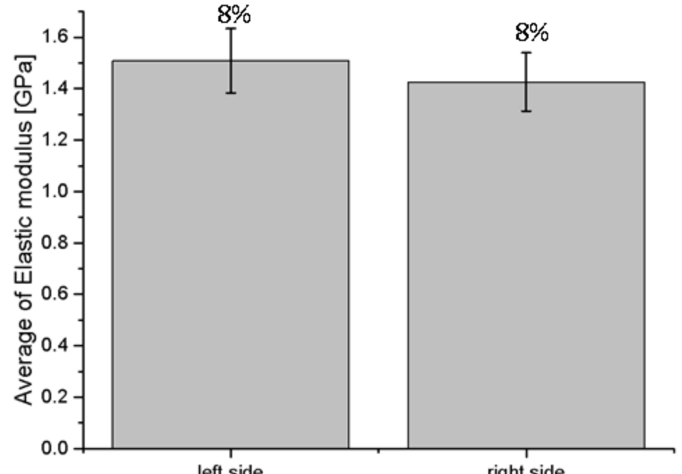

Figure 70 *Elastic modulus results for both plain products*

5. Conclusions

Plasma polymerization is a technique used to deposit thin film coatings (nanometer until some micrometer thickness) on different materials surface. This thin film coating technology offers the advantage to provide additional functions to multi-material surfaces. Some of the practical applications of this technique are the possibility to transform hydrophilic/adhesive surfaces in hydrophobic/non-sticking ones or vice versa, it allows the protection of surfaces against corrosion and permits also the enhancement of wear resistance. Therefore, this is a technique which can be applied in a broad range of industrial sectors. Additionally, it is an eco-friendly technology. The employed chemicals are used in very small quantities. Furthermore, if it is compared to the wet techniques applied in the textile industry it offers many advantages. There are no harmful chemicals, wet processes, waste water and mechanical hazards to textiles. Besides, it has specific action on the surface [109].

The thin film coating is deposited onto the surface of the substrate, which is placed in a low-pressure plasma chamber, from a partially ionized precursor gas subjected to the effect of the plasma. This coating process regarding the achievement of the desired properties is in general well developed. The challenge is the scaling-up of the deposition process. To realize attractive costs, it is necessary to coat very fast a smaller number of articles or to coat a lot of them at once. The decision, which may yield to the best economic results, depends among other things to the coating process itself. Processes which use a high Self-Bias are predicted for small chambers because they show a high deposition rate and the scale up is restricted by the RF-system. In the case of low Self-Bias processes there are strong limitations concerning the deposition rate because it is not possible to use higher RF-powers without changing the coating properties. For those processes the scale up in chamber volume is essential.

In this context, there are very few information available for scientists or constructors in respect to construction of large volume low-pressure plasma-coaters with the aim of achieve homogeneous coating deposition rate as well as homogeneous coating properties over all the products surfaces in contact with the plasma. Large volume plasma-activation chambers are common up to a volume of about 30m³. But those processes are quite easy in comparison to a coating process. They make no great demands on the process know-how.

The lack of information regarding large low-pressure plasma-coaters led to this research thesis. The general research question is:

- How to construct large volume low-pressure plasma-coaters focusing on homogeneous coating deposition rate as well as homogeneous coating properties?

Having this general question in mind, the next logical step was to identify the potential systems which could direct influence in the homogeneity of the deposition process. Starting from the principle that the coating process needs essentially a precursor gas, which is the material source for the coating. Analyzing the coating process, one can easily see that two main systems are involved directly to the gas flow: 1) gas feed-in system and 2) gas exhaustion system. The objective of this research was to create construction guidelines in a way that researchers or constructors could use them in an easy and efficient way. They must be generalized, so that they can be used for different chamber constructions.

Gas feed-in system

In the context of this work, a flexible and easy to build solution was developed. The solution needed to be flexible, to be suitable for different chamber and electrode configurations, to be built easily and to be feasible regarding time and cost. The solution consists in a square section pipe with closed sides and some equally distributed holes over one of the surfaces. The gas inlet is situated on the opposite surface in the middle or at one end of the pipe. The idea was to achieve a higher and homogeneous pressure along the pipe axis in comparison to the pressure inside the plasma chamber, to supply the gas evenly through the holes to the chamber volume. On the other hand it was necessary not to disturb the working conditions of the gas flow-meter. This idea could be achieved with other geometries like a ring, showerhead or a perforated plate (even integrated into the electrode system) but it would require higher investments and would be more time consuming. Furthermore, the flexibility to adapt the pipe for different electrode system in the same plasma-coater is much higher than in those possible solutions.

Because it is not possible to measure the local gas velocity inside of low-pressure plasma chamber a validation of the CFD results is only possible by using a pressure measurement. There are limited positions where the local pressure can be measured. The

goal was to identify the important technical layout parameters which influence the pressure gradient distribution inside the pipe and consequently the homogeneity of the gas supply through the holes and thereby to create guidelines for construction of gas feed-in systems.

During the development process, the following technical parameters were evaluated:

- Pipe section area;
- Gas flow rate;
- Pipe length;
- Hole diameter;
- Amount of holes;
- Aspect ratio of the pipe.

The main conclusions extracted from the results are:

a) From the analyzed parameters the pipe section area was the most relevant one influencing the homogeneity of gas distribution.

b) By decreasing the pipe section area, the pressure gradient increases inside the pipe resulting in a nonhomogeneous gas distribution through the holes. For instance, the nonuniformity coefficient for the 30 mm x 30 mm pipe section area is 0.1% and for the 6 mm x 6 mm one 45%.

c) Taking the construction border (Φ <5%) into consideration the results showed that the pipe section area above 20 mm x 20 mm is in a safety region regarding the homogeneity of gas distribution.

d) The pressure values from the CFD simulations were in good agreement with the obtained experimental data.

e) The gas feed-in has a main influence zone over a distance of about 50 mm from the holes. It means that one must respect this distance to avoid any direct gas effects on the coating deposition distribution over the substrate.

f) No limitations are observed through the gas feed-in system toward the capability of the flow meters, especially not for the pressure sensitive one for HMDSO.

The knowledge acquired with the CFD calculations in agreement with experimental pressure measurements are very helpful for researchers or constructors to develop new gas feed-in systems for low-pressure plasma chambers.

Gas exhaustion system

Regarding the gas exhaustion system, initially through experimental results and afterwards through simulations, its influence on the homogeneity of coating deposition rate was revealed. Therefore, a pretty new solution to reduce the influence of the gas exhaustion system in a low-pressure plasma system was developed. The idea consisted in a polymeric perforated plate (sealed towards the plasma chamber), which under the frame of this work was named as “Baffle Plate”. In this case, the knowledge was applied acquired with the construction of gas feed-in system but in an inverse way, instead of to feed-in the gas, to remove the gas from the chamber. To accomplish this objective, it would be necessary to develop this Baffle plate in a way that all the holes will show the same pressure difference between the regions under and above the holes what will imply in homogenous gas exhaustion from each hole.

In this scenario, again the support of a CFD tool was used to get access to the gas velocity distribution as well as pressure distribution inside the chamber volume. Important technical parameters were taken into consideration with the aim of create guidelines for the construction of Baffle Plates as follows:

- Distance from the Baffle Plate to the top of the chamber
- Distribution of the holes over the Baffle Plate
- Amount of holes
- Diameter of the holes
- Gas flow
- Volume of the chamber

The main conclusions extracted from the results are:

a) From the analyzed parameters the distance between Baffle-Plate and top chamber was the most relevant one influencing the homogeneity of gas exhaustion.

b) By decreasing the distance between Baffle-Plate and top chamber, the pressure gradient in this region increases resulting in nonhomogeneous gas exhaustion through the holes. For instance, the nonuniformity coefficient for 100 mm distance is 0.5% and for 10 mm distance is 69%.

c) Taking the construction border (Φ <5%) into consideration the results showed that the installation of the Baffle-Plate with a distance above 80 mm to the top chamber is in a safety area regarding the homogeneity of gas exhaustion for low-pressure applica-tion.

d) From the analyzed values, flow rate and number of holes do not have a consid-erable influence in the homogeneity of gas exhaustion through the holes. However, it is recommended to start the layout with hole diameter in the order of 15 mm.

e) The hole diameter strongly influences the homogeneity of gas exhaustion through the holes, especially with high distances between Baffle-Plate and top of the chamber

f) The chamber volume has an influence in the homogeneity of gas exhaustion, es-pecially with high distances between Baffle-Plate and the top of the chamber

g) The Baffle-Plate is an effective solution to improve the homogeneity of coating deposition rate for plasma polymerization processes

In this investigation it was not possible to run the gas flow simulations with the metallic perforated grid installed due to limited computer processing capacity. This is the reason why the absolute calculated pressure values were not in total agreement with the measured ones (especially for high gas flows). Nevertheless, for this thesis, the simulations results are still valuable because the calculated pressure difference between inside chamber and the gas exhaustion were very similar and therefore it is expected that the gas flow would behave in the same way.

The layout and the installation of a Baffle Plate for the described plasma-coater showed through practical coating experiments that the non-uniformity coefficient was enhanced from 47% (without Baffle Plate) to 23%. Low values from the nonuniformity coefficient mean more homogeneous coating distribution. Better values of the non-uniformity coefficient could be achieved with new RF-Electrode geometry as described in

chapter 4. Taking this into account for the construction of a new low-pressure plasma-chamber a non-uniformity coefficient of about 15% could be achieved for an area of 2 m^2, which are very good results for an industrial application.

The construction guidelines for the use of a Baffle-Plate solution for large volume PECVD chambers developed in this thesis showed to be very effective in terms of achieve homogenous coating deposition rate. Basically, the person in charge should start with hole diameter in the order of 15 mm and distribute them in a proper manner aiming to avoid concentration of gas suction in small areas. Optimal is to distribute the holes in a way to cover the section area of the chamber. Furthermore, it is important to keep a distance, for instance 25 mm, between the Baffle-Plate and the perforated grid to reduce pressure loss through the holes. After done the first layout, the next step is to assemble the Baffle-Plate and measure the pressure difference. If the desired working pressure is not reached, then the holes can be enlarged and proceed with measurements again until the desired working pressure is reached.

Like for the gas feed-in system, the support of CFD tool was very successful to understand the influence of the gas exhaustion system, to study and to propose solution to enhance the homogeneity of coating deposition.

Electrode assembly

For some industrial applications it is important to install more electrodes/product holders in the low-pressure plasma chamber. Therefore, it is important to understand the influence of its assembly from the point of view of the gas flow along with the electric field. Under the frame of this work it was found out that some points must be taken into consideration to achieve a proper homogeneity in the coating deposition as follows:

a) It is important to keep symmetry in the construction

b) It is mandatory to avoid opening areas close to the region of interest where the coating is desired.

c) It is recommended to keep the product to be coated at least 200 mm away from the walls to avoid the gas deceleration region as well as to avoid the sheath formed close to the electrodes.

Construction of a new low-pressure plasma chamber

The complete knowledge acquired through this research thesis was applied for the construction of a new low-pressure plasma-chamber that will be industrially used to coat plain metallic products. With this, the transfer of the results to a new chamber with new challenges are tested.

The gas feed-in system was selected based on the construction guidelines developed in section 3.1. It is a square section pipe (30 mm x 30 mm) with 14 holes equally spaced over its top surface. As well the Baffle Plate was constructed following the construction guidelines described in section 3.2. The holes have 18mm diameter and a total amount of 30 holes equally spaced distributed in a way to cover all the section area of the low-pressure plasma chamber. The Baffle Plate was installed 90 mm away from the top of the chamber which is a safety distance following the construction guidelines.

An electrode with trapeze geometry was selected because of its possibility to handle two products at once. Furthermore, it avoids sharp edges reducing the probability to develop local/concentrated electric field. It was assembled in a symmetrically way as well as avoiding opening regions close to the place where the product will be fixed.

The coating experiment showed symmetry in the coating deposition pattern distribution on both sides of the trapeze electrode and the non-uniformity coefficient was very positive: 15% for both sides. This is clear a successful result once in the beginning of the thesis, the standard low-pressure plasma chamber showed a standard deviation of 46% and now, with this new low-pressure plasma chamber construction based on the created guidelines, presented 15% as standard deviation value. Moreover, the coating properties (surface free energy and elastic modulus) were homogenous over the area of both products.

The objectives proposed to this work were well accomplished and the results of the knowledge acquired about gas feed-in system, electrode geometry and gas exhaustion system which led to the formulation of construction guidelines. They are already used for the construction of new low-pressure plasma-chamber focusing on good coating homogeneity as well as good homogeneity of coating properties. From this point of view, the knowledge acquired and described in this research thesis represents an advance in the state of the art.

6. Outlook

The framework provided by the presented research work precede to the creation of construction guidelines for gas feed-in-, gas exhaustion systems and electrodes applied to low-pressure plasma coating processes, could be used for future investigations dealing with the aim of coat lots of small products in one batch or a single huge product keeping the same coating properties regardless of the installed electrode area. To coat a big amount of small products, parts holders (connected or not with the RF generator) are required. Depending on the case, three scenarios can happen:

1) Less RF-electrode area than grounded one which leads to negative Self-Bias;
2) Equal area of RF- and grounded electrode which leads to a Self-Bias near zero;
3) More RF-electrode area than grounded one which leads to positive Self-Bias.

With all three aforementioned scenarios, using apart from that the same coating conditions, three different coating properties can be achieved [110,111]. The different coating properties are directly related to the Self-Bias signal as well as to its absolute value. In this sense, future investigations could focus on techniques to manipulate electronically the Self-Bias for different ratio of electrode area (powered/grounded) looking toward to the same coating properties. Similar effect occurs for the case where a single metallic massive product (in contact with the RF-Electrode) is desired to coat. In this case, the large surface area of the product will contribute to increase the powered electrode area influencing the Self-Bias and consequently leading to different coating properties.

Furthermore, it could be helpful to investigate techniques which allow the measurement/control of plasma potential, floating potential, sheath potential and Self-Bias during the coating process. There are some techniques available, for example the Langmuir Probe [112] associated with thermal probes [113], which work very fine for activation or etching processes. However, it is still challenging to apply these techniques looking toward to acquire the real potential values for plasma-coaters since the tip of the measuring device will be covered and therefore the acquired signal will change.

Regarding the gas feed-in system, further investigation would be interesting using a kind of perforated plate instead of a square section pipe. This perforated plate could be part of the RF-electrode or made with plastic material like the Baffle Plate. This solution offer more flexibility for different electrode configurations using the same plasma-coater.

Additional investigation can be done regarding the meshing process for the CFD model, since for this thesis it was a restriction in the case of the perforated grid which is installed under the Baffle Plate keeping 25 mm distance. As the perforated grid contains a huge quantity of very small holes, it requires lots of computational efforts to do the mesh and afterwards to calculate. Therefore, would be interesting to search for alternatives in the CFD community ways to overcome this barrier.

Not of less importance is the investigation of software or codes which allows the calculation of the precursor gas flow along with the chemical reactions (coating formation) under the influence of plasma generated by an RF-generator source. Modelling of reactive plasma process is quite complex due to a variety of reasons. For instance, there are countless reactions among charged particles and neutral species with mostly unknown rate constants.

These future investigations would contribute to widen the present guidelines for development of new low-pressure plasma coating processes.

Besides, the methodology developed in this thesis to construct gas feed-in systems, gas exhaustion systems and electrodes for low-pressure plasma process can similarly be tailored to new developments in the atmospheric plasma applications.

7. Acknowledgements

Foremost, I would like to express my sincere gratitude to Prof. Dr. Bernd Mayer for his assessment and that he thereby enabled me to carry out my research at Fraunhofer IFAM in cooperation with the University of Bremen. Besides my advisor, I would like to thank Prof. Dr. Jürgen Meichsner for his involvement as second evaluator.

Special thanks to Dr. Welchy Leite Cavalcanti. She believed on me and opened the doors to do this research thesis.

My sincere thanks also go to Dr. Ralph Wilken, my head of department, for his affable reception and for the acceptance of the elaboration of this thesis in the department “Plasma Technology and Surfaces” at Fraunhofer Institute IFAM.

I am truly grateful to Dr. Klaus Vissing for all the time spent on discussions and sharing ideas as well as his constant motivation, permanent guidance and endless patience, without which, this work would not have been possible. I could not have imagined having better help and advice during my thesis. For their aid and scientific inputs, I am grateful to the technicians and researchers of the OE413. Special thanks to my “ND-Plasma” colleagues always helping me with German and making me feel at home.

Thanks a lot to all IFAM colleagues, which I have the pleasure to meet, for their friendly atmosphere.

I would like to thank my beloved wife, Lays, for her patience and comprehension during the realization and writing of my thesis. She has always tried to make my PhD time easier. My infinite gratitude to my parents, Leila and Nocleci, for giving me all the tools I needed to become a responsible man, especially to keep believing in my dreams; to my sisters Ana Paula and Simone and my nephew Joaquim for pushing me up always when I needed and to believe on me.

A particular gratitude to all my friends in Brazil, especially to Cadu Palumbo and Sheila Costa, for the right words in the right time which motivated me to move on.

Finally, I would like to thank the financial support of the Brazilian Government (Brazilian National Council of Technological and Scientific Development - CNPq) in the frame of the Science without Borders Program (201387/2014-0).

8. References

[1] H. Yasuda. Plasma Polymerization. Orlando,Florida: Academic Press,Inc; 1985.

[2] Dominik Paulkowski, Stefanie Karpinski, Klaus Vissing. Friction and wear resistance of plasmapolymeric coatings applied on elastomers. *Tribologia: Finnish Journal of Tribology* 2014;32(2):12–9.

[3] Yong Tae Kim, Suk-Ki Min, Jong Sung Hong, Choong-Ki Kim. Highly Conductive Tungsten Thin Films Prepared by the Plasma-Assisted Silane Reduction Process. *Japanese Journal of Applied Physics* 1991;30(4):820–6.

[4] Vogel K, Westphal N, Salz D, Thiel K, Wittig L, Ciacchi LC et al. Dental implants coated with a durable and antibacterial film. *Surface Innovations* 2015;3(1):27–38.

[5] Paulkowski D, Vissing K. Tribological improvement of elastomers using plasmapolymeric coatings. *Proceedings of Tribologie Fachtagung* 2011;1:15/1-15/14.

[6] Gürsoy M, Karaman M. Hydrophobic coating of expanded perlite particles by plasma polymerization. *Chemical Engineering Journal* 2016;284:343–50.

[7] Milton Ohring. The Materials Science of Thin Films. San Diego, California: Academic Press; 1992.

[8] Martinu L, Poitras D. Plasma deposition of optical films and coatings: A review. *Journal of Vacuum Science & Technology A Vacuum Surfaces and Films* 2000;18(6):2619–45.

[9] Harald Herchen, Walter Merry, William Brown. Etch enhancement using an improved gas distribution plate(US 5819434 A); 1998.

[10] Kyung Cheol Jeong. Gas distribution system and method for chemical vapor deposition apparatus(US 5853484 A); 1998.

[11] Ramprakash Sankarakrishnan, Ganesh Balasubramanian, Juan Carlos Rocha-Alvarez, Dale R. Du Bois, Mark Fodor, Jianhua Zhou et al. Confined process volume PECVD chamber(US 8778813 B2); 2014.

[12] Qunhua Wang, Li Hou, Sanjay Yadav, Gaku Furuta, Kenji Omori, Soo Young Choi et al. Gas distribution uniformity improvement by baffle plate with multi-size holes for large size pecvd systems(US 20080178807 A1); 2008.

[13] Eric Breitung, George Dalakos, Peter Codella, Manisha Tinani-Mendleson. Delivery system for PECVD powered electrode(US20050022735 A1); 2005.

[14] Alan D. Rose, Robert M. Kennedy. Gas dispersion disk for use in plasma enhanced chemical vapor deposition reactor(US 4792378 A); 1988.

[15] Kulkarni AV, Roy SS, Joshi JB. Pressure and flow distribution in pipe and ring spargers: Experimental measurements and CFD simulation. *Chemical Engineering Journal* 2007;133(1-3):173–86.

[16] Michelmore A, Steele DA, Whittle JD, Bradley JW, Short RD. Nanoscale deposition of chemically functionalised films via plasma polymerisation. *RSC Adv.* 2013;3(33):13540–57.

[17] Michelmore A, Whittle JD, Short RD. The importance of ions in low pressure PECVD plasmas. *Front. Phys.* 2015;3:1–5.

[18] Michelmore A, Charles C, Boswell RW, Short RD, Whittle JD. Defining plasma polymerization: new insight into what we should be measuring. *ACS Appl Mater Interfaces* 2013;5(12):5387–91.

[19] Hiroji Hanawa, Kyawwin Maung, Hua Chung. Gas distribution showerhead and method of cleaning(US 20110052833 A1); 2011.

[20] Yuh-Jia Su. Gas distribution plate for semiconductor wafer processing apparatus with means for inhibiting arcing(US5589002 A); 1996.

[21] Jelil RA. A review of low-temperature plasma treatment of textile materials. *J Mater Sci* 2015;50(18):5913–43.

[22] Kang MS, Chung TH, Kim Y. Plasma enhanced chemical vapor deposition of nitrogen-incorporated silicon oxide films using TMOS/N2O gas. *Thin Solid Films* 2006;506-507:45–9.

[23] Carlos E. Viana, Ana N. R. da Silva, Nilton I. Morimoto. Analysis of SiO2 thin films deposited by PECVD using an Oxygen-TEOS-Argon mixture. *Brazilian Journal of Physics* 2001;31(2):299–303.

[24] Barni R, Zanini S, Riccardi C. Characterization of the Chemical Kinetics in an O 2 /HMDSO RF Plasma for Material Processing. *Advances in Physical Chemistry* 2012;2012(6):1–6.

[25] S. Gaur and G. Vergason. Plasma Polymerization:Theory and Practice. *Society of Vacuum Coaters* 2000:267–71.

[26] Petit-Etienne C, Tatoulian M, Mabille I, Sutter E, Arefi-Khonsari F. Deposition of SiOχ-Like Thin Films from a Mixture of HMDSO and Oxygen by Low Pressure and DBD

Discharges to Improve the Corrosion Behaviour of Steel. *Plasma Process. Polym.* 2007;4(S1):S562-S567.

[27] Bewilogua K, Bräuer G, Dietz A, Gäbler J, Goch G, Karpuschewski B et al. Surface technology for automotive engineering. *CIRP Annals - Manufacturing Technology* 2009;58(2):608–27.

[28] Noborisaka M, Kodama H, Nagashima S, Shirakura A, Horiuchi T, Suzuki T. Synthesis of transparent and hard SiOC(−H) thin films on polycarbonate substrates by PECVD method. *Surface and Coatings Technology* 2012;206(8-9):2581–4.

[29] R. Lamendola, R. d'Agostino, and F. Fracassi. Thin film deposition from hexamethyldisiloxane fed glow discharges. *Plasmas and Polymers* 1997;2:147–64.

[30] F. Fracassi, R. d'Agostino, F. Fanelli, A. Fornelli, and F. Palumbo. GC-MS Investigation of Hexamethyldisiloxane-Oxygen Fed Plasmas. *Plasmas and Polymers* 2003;8:259–69.

[31] Lutz Körner. Diffusion Barrier Coatings for Polymer Diffusion Barrier Coatings for Polymer Containers processed by Plasma Enhanced Chemical Vapor Deposition (Doctoral dissertation); 2010, Retrieved from http://e-collection.library.ethz.ch/eserv/eth:1657/eth-1657-02.pdf.

[32] Bernd Jacoby. Abscheidung und Charakterisierung von Plasmapolymerschichten auf Fluorkohlenstoffund Siloxan-Basis (Doctoral dissertation); 2008, Retrieved from https://www.deutsche-digitale-bibliothek.de/binary/7CVTT726IQBBCOQWC4DXNDB3D55B7XY3/full/1.pdf.

[33] H. Conrads, M. Schmidt. Plasma generation and plasma sources. *Plasma Sources Sci. Technol.* 2000;9:441–54.

[34] Li C, Liang C, Huang C. Tailoring surface properties of polyethylene separator by low pressure 13.56 MHz RF oxygen plasma glow discharge. *Jpn. J. Appl. Phys.* 2016;55(1S):01AF04.

[35] Tanışlı M, Şahin N, Demir S. An investigation on optical properties of capacitive coupled radio-frequency mixture plasma with Langmuir probe. *Optik - International Journal for Light and Electron Optics* 2017;142:153–62.

[36] Vladimir Danilov. Plasma Modification of Polydimethylsiloxane in a hydrogen CCRF low-pressure discharge (Doctoral dissertation); 2013, Retrieved from http://d-nb.info/1047137178/34.

[37] Bohm D. Minimum ionic kinetic energy for a stable sheath: In: Guthrie A and Wakerling RK,editors. The Characteristics of Electrical Discharges in Magnetic Fields. NewYork, London: McGrawHill; 1949.

[38] Prof. A. von Keudell. Vorlesungsskript: Einführung in die Plasmaphysik II: Niedertemperaturplasmen: Wintersemester 2010/11. Ruhr-Universität Bochum; 2013.

[39] Advanced Energy Industries Inc. Impedance Matching. [June,2017]; Available from: Retrieved from: http://www.advanced-energy.com/upload/file/white_papers/eng-white18-270-02.pdf.

[40] University of Bristol - School of Chemistry. Plasma Diagnostics: Electron Temperatures and Ion Energy Distributions. [June, 2017]; Available from: http://www.chm.bris.ac.uk/~paulmay/misc/msc/msc4.htm.

[41] F. Fracassi. Architecture of Plasma Reactors: In R. D'Agostino, P. Favia, and F. Fracassi, editors. Plasma Processing of Polymers, pages 47-64. Kluwer Academic Publishers, Dordrecht; 1997.

[42] Kohler K, Cobum JW, Home DE, Kay E, Keller JH. Plasma potentials of 13.56-MHz rf argon glow discharges in a planar system. *Journal of Applied Physics* 1985:59–66.

[43] Enrico Malatesta, Dennis Tee Xian Yang. The Importance of DC Self-Bias Voltage in Plasma Applications. [June,2017]; Available from: http://www.palomartechnologies.com/blog/the-importance-of-dc-self-bias-voltage-in-plasma-applications.

[44] Giessler S, Just E, Störger R. Easy-to-clean properties–Just a temporary appearance? *Thin Solid Films* 2006;502(1-2):252–6.

[45] Vissing K, Klyszcz-Nasko H. Permanente plasmapolymere Trennschichten. *VIP* 2006;18(1):12–4.

[46] Thorben Brenner. Struktureigenschaftsbeziehung von chemisch gleichartigen plasmapolymeren Trennschichten mit stark variierendem Elastizitätsmodul (Master thesis); 2017.

[47] Oxford Instruments Asylum Research, Inc. AFM Characterization of Thin Films: AFM Characterization of Thin Films: High-Resolution Topography and Functional Properties. [July/2017]; Available from: https://www.asylumresearch.com/Applications/ThinFilms/Thin-Films-Characterization-AFM.pdf.

[48] Baturin AS, Bormashov VS, Gavrilenko VP, Zablotskii AB, Zaitsev SA, Kuzin AY et al. Ellipsometric Technique for Estimating the Thickness Nonuniformity of Thin-Film Coatings. *Meas Tech* 2014;56(11):1224–32.

[49] Nie H, McIntyre NS, Lau WM, Feng JM. Optical properties of an octadecylphosphonic acid self-assembled monolayer on a silicon wafer. *Thin Solid Films* 2008;517(2):814–8.

[50] Lei X, Kane S, Cogan S, Lorach H, Galambos L, Huie P et al. SiC protective coating for photovoltaic retinal prosthesis. *J Neural Eng* 2016;13(4):1–12.

[51] Wolfgang Jacob, Achim von Keudell, and Thomas Schwarz-Selinger. Infrared Analysis of Thin Films: Amorphous, Hydrogenated Carbon on Silicon. *Brazilian Journal of Physics* 2000;30(3):508–16.

[52] Wojcieszak D, Mazur M, Indyka J, Jurkowska A, Kalisz M, Domanowski P et al. Mechanical and structural properties of titanium dioxide deposited by innovative magnetron sputtering process. *Materials Science-Poland* 2015;33(3):660–8.

[53] Bruno P, Cicala G, Losacco A, Decuzzi P. Mechanical properties of PECVD hydrogenated amorphous carbon coatings via nanoindentation and nanoscratching techniques. *Surface and Coatings Technology* 2004;180-181:259–64.

[54] Sarkar DK, Farzaneh M, Paynter RW. Wetting and superhydrophobic properties of PECVD grown hydrocarbon and fluorinated-hydrocarbon coatings. *Applied Surface Science* 2010;256(11):3698–701.

[55] Subhash Latthe S, Basavraj Gurav A, Shridhar Maruti C, Shrikant Vhatkar R. Recent Progress in Preparation of Superhydrophobic Surfaces: A Review. *JSEMAT* 2012;02(02):76–94.

[56] PLASMAtech I. Plasma Polymerized Thin Films for Surface Engineering. [July,2017]; Available from: http://www.plasmatechnology.com/pdf/PECVDCoatingsv2.pdf.

[57] Houta F, Quinten M. Layer Thickness Determination: The influence of the aperture of a measuring head. *Optik & Photonik* 2015;10(4):54–6.

[58] Ocean Optics. Thickness Measurement. [July,2017]; Available from: https://oceanoptics.com//application/thickness-measurement/.

[59] W.C. Oliver, G.M. Pharr. Measurement of hardness and elastic modulus by instrumented indentation: Advances in understanding and refinements to methodology. *Journal of Materials Research* 2004;19(1):3–20.

[60] Cech V, Lukes J, Palesch E, Lasota T. Elastic Modulus and Hardness of Plasma-Polymerized Organosilicones Evaluated by Nanoindentation Techniques. *Plasma Process. Polym.* 2015;12(9):864–81.

[61] W.C. Oliver, G. M. Pharr. An improved technique for determining hardness and elastic modulus using load and displacement sensing indentation experiments. *Journal of Materials Research* 1992;7(6):1564–83.

[62] Zhang M, Feng S, Wang L, Zheng Y. Lotus effect in wetting and self-cleaning. *Biotribology* 2016;5:31–43.

[63] Lafuma A, Quéré D. Superhydrophobic states. *Nat Mater* 2003;2(7):457–60.

[64] Yuan Y, Lee TR. Contact Angle and Wetting Properties. In: Bracco G, Holst B, editors. Surface Science Techniques. Berlin, Heidelberg: Springer Berlin Heidelberg; 2013, p. 3–34.

[65] Snoeijer JH, Andreotti B. A microscopic view on contact angle selection. *Physics of Fluids* 2008;20(5):57101.

[66] Young T. An Essay on the Cohesion of Fluids. *Philosophical Transactions of the Royal Society of London* 1805;95(0):65–87.

[67] Kaelble DH. Dispersion-Polar Surface Tension Properties of Organic Solids. *The Journal of Adhesion* 2008;2(2):66–81.

[68] D. Owens, R. Wendt. Estimation of the surface free energy of polymers. *J. Appl. Polym. Sci* 1969;13:1741–7.

[69] Wu S. Polar and Nonpolar Interactions in Adhesion. *The Journal of Adhesion* 1973;5(1):39–55.

[70] KRÜSS GmbH. Method according to Wu. [September 08, 2017]; Available from: https://www.kruss.de/services/education-theory/glossary/method-according-to-wu/.

[71] Mohr, Sebastian. Simulation und Modellierung von CCRF-Entladungen in molekularen Gasen; 2014, Retrieved from: http://www-brs.ub.ruhr-uni-bochum.de/netahtml/HSS/Diss/MohrSebastian/diss.pdf.

[72] Cheng J, Ji L, Wang K, Han C, Shi Y. Two-dimensional simulation of inductively coupled plasma based on COMSOL and comparison with experimental data. *J. Semicond.* 2013;34(6):66004.

[73] Krzhizhanovskaya VV, Sloot PM, Gorbachev YE. Grid-Based Simulation of Industrial Thin-Film Production. *SIMULATION* 2016;81(1):77–85.

[74] Son S, Yi K, Mahrholz J, Rie K. Numerical studies on up scaling of metal organic PACVD processes used for tribological coating in automotive industry. *Surface and Coatings Technology* 2007;201(16-17):7318–26.

[75] Murley DT, Gibson R, Dunnett B, Goodyear A, French ID. Influence of gas residence time on the deposition of nitrogen-rich amorphous silicon nitride. *Journal of Non-Crystalline Solids* 1995;187:324–8.

[76] Collins DJ, Strojwas AJ, White DD. A CFD model for the PECVD of silicon nitride. *IEEE Trans. Semicond. Manufact.* 1994;7(2):176–83.

[77] Crose M, Tran A, Christofides P. Multiscale Computational Fluid Dynamics: Methodology and Application to PECVD of Thin Film Solar Cells. *Coatings* 2017;7(2):22.

[78] Da Silva A, Morimoto N. Gas flow simulation in a PECVD reactor. *In Proceedings of the 2002 International Conference on Computational Nanoscience and Nanotechnology,San Juan, Puerto Rico,22–25 April 2002*.

[79] ANSYS Inc. ANSYS Fluent Theory Guide 16.0;. ANSYS Inc.:Canonsburg,PA, USA; 2015.

[80] Xu SY, Cai JS, Li J. Modeling and simulation of plasma gas flow driven by a single nanosecond-pulsed dielectric barrier discharge. *Physics of Plasmas* 2016;23(10):103510.

[81] Kim HJ, Lee HJ. 2D fluid model analysis for the effect of 3D gas flow on a capacitively coupled plasma deposition reactor. *Plasma Sources Sci. Technol.* 2016;25(3):35006.

[82] Barber RW, Emerson DR. The influence of Knudsen number on the hydrodynamic development length within parallel plate micro-channels. *Advances in fluid mechanics IV* 2002;32:207–16.

[83] Gad-el-Hak M. The MEMS handbook. 2nd ed. Boca Raton, Florida: CRC Taylor & Francis; 2006.

[84] Jeerasak Pitakarnnop RW. Rarefied gas flow in pressure and vacuum measurements. *ACTA IMEKO* 2014;3(2):60–3.

[85] Yasuda HK. Some Important Aspects of Plasma Polymerization. *Plasma Processes and Polymers* 2005;2:293–304.

[86] Prabhakara S, Deshpande MD. The no-slip boundary condition in fluid mechanics. *Reson*:61–71.

[87] Harvard University - Materials Research Science and Engineering Center. Fabrication techniques II: Deposition; Available from:

http://www.mrsec.harvard.edu/education/ap298r2004/Erli%20chenFabrication%20II%20-%20Deposition-1.pdf.

[88] Pfeiffer Vacuum GmbH. Vacuum Technology - Know How; 2009.

[89] Brandisky, Kostadin, et al. Electrostatic field simulations in the analysis and design of electrical capacitance tomography sensors. *Automatyka/Akademia Górniczo-Hutnicza im. Stanisława Staszica w Krakowie* 2010;14:655–69.

[90] Fleisch DA (ed.). A student's guide to Maxwell's equations. 14th ed. Cambridge: Cambridge University Press; 2014, cop. 2008.

[91] Tinck S, Boullart W, Bogaerts A. Investigation of etching and deposition processes of Cl 2 /O 2 /Ar inductively coupled plasmas on silicon by means of plasma–surface simulations and experiments. *J. Phys. D: Appl. Phys.* 2009;42(9):95204.

[92] Cunge G, Pelissier B, Joubert O, Ramos R, Maurice C. New chamber walls conditioning and cleaning strategies to improve the stability of plasma processes. *Plasma Sources Sci. Technol.* 2005;14(3):599–609.

[93] Moriya T, Nakayama H, Nagaike H, Kobayashi Y, Shimada M, Okuyama K. Particle Reduction and Control in Plasma Etching Equipment. *IEEE Trans. Semicond. Manufact.* 2005;18(4):477–86.

[94] Guensuk Lee, Suhong Kim, Seunghyun Seok, Junsung Lee, Jinseok Lee, Sangjin Choi, Taeyang Yoon, Juhwan Park, Han Seo Ko. A Study on Film Thickness Control of vertical Flow Showerhead Reactor for RF Plasma Deposition. *28th Annual SEMI Advanced Semiconductor Manufacturing Conference (ASMC),15-18 May 2017* 2017:217–21.

[95] L. Sansonnens, A. A. Howling, Ch. Hollenstein. Gas flow uniformity study in large-area showerhead reactors for RF plasma deposition. *Plasma Sources Science and Technology* 2000;9(2):205–9.

[96] Applied Materials I. Centura® POLYgen™ LPCVD. [October,2017]; Available from: http://www.appliedmaterials.com/products/centura-polygen-lpcvd.

[97] Kulkarni AV, Joshi JB. Design and selection of sparger for bubble column reactor. Part I: Performance of different spargers. *Chemical Engineering Research and Design* 2011.

[98] Kulkarni AV, Joshi JB. Design and selection of sparger for bubble column reactor. Part II: Optimum sparger type and design. *Chemical Engineering Research and Design* 2011.

[99] Bahroun K, Behm H, Dahlmann R, Hopmann C. Plasmagestützte Flascheninnenbeschichtung. *Vakuum in Forschung und Praxis* 2013;25(4):17–23.

[100] Reis R, Dumee LF, Tardy BL, Dagastine R, Orbell JD, Schutz JA et al. Towards Enhanced Performance Thin-film Composite Membranes via Surface Plasma Modification. *Sci Rep* 2016;6:1–13.

[101] Barbosa, Gustavo Simiema de Freitas, Vissing K, Mayer B. Creation and Evaluation of Construction Guidelines Using CFD for Low Pressure Plasma Gas Feed-in Systems to Homogenize the Precursor Gas Flow. *OJFD* 2016;06(04):391–405.

[102] Heehak Ahn, Sunghyuk Lee, Sehyun Shin. Flow Distribution in Manifolds for Low Reynolds Number Flow. *KSME International Journal* 1998;12:87–95.

[103] Kim Y, Boo J, Hong B, Kim YJ. Effects of showerhead shapes on the flowfields in a RF-PECVD reactor. *Surface and Coatings Technology* 2005;193(1-3):88–93.

[104] Caquineau H, Despax B. Influence of the reactor design in the case of silicon nitride PECVD. *Chemical Engineering Science* 1997;52(17):2901–14.

[105] Hassan JM, Mohamed TA, Mohammed WS, Alawee WH. Modeling the Uniformity of Manifold with Various Configurations. *Journal of Fluids* 2014;2014(11):1–8.

[106] Malavasi S, Messa G, Fratino U, Pagano A. On the pressure losses through perforated plates. *Flow Measurement and Instrumentation* 2012;28:57–66.

[107] Bayazit Y, Sparrow EM, Joseph DD. Perforated plates for fluid management: Plate geometry effects and flow regimes. *International Journal of Thermal Sciences* 2014;85:104–11.

[108] ANSYS Inc. Ansys Maxwell V16 - Training Manual: Lecture4: Static Electric Solver. ANSYS Inc.:Canonsburg,PA, USA; 2013.

[109] Gorjanc M, Gorensek M, Jovancic P, Mozetic M. Multifunctional Textiles – Modification by Plasma, Dyeing and Nanoparticles. In: Gunay M, editor. Eco-Friendly Textile Dyeing and Finishing. InTech; 2013.

[110] L. Zajickova, J. Janca, V. Perina. Characterization of silicon oxide thin films deposited by plasma enhanced chemical vapour deposition from octamethylcyclotetrasiloxane/oxygen feeds. *Thin Solid Films* 1999;338:49–59.

[111] Hegemann D, Brunner H, Oehr C. Deposition rate and three-dimensional uniformity of RF plasma deposited SiOx films. *Surface and Coatings Technology* 2001;142-144:849–55.

[112] Hansen AB. Langmuir Probe Measurements of an Argon Plasma. *Macalester Journal of Physics and Astronomy* 2014;Vol. 2: Iss. 1, Article 5.

[113] Stamate E. Status and challenges in electrical diagnostics of processing plasmas. *Surface and Coatings Technology* 2014;260:401–10.